


8-2010

MODELING SPORADIC TUMOR FORMATION DRIVEN BY TELOMERE DYSFUNCTION IN THE GASTROINTESTINAL TRACT

Suzanne S. Chan

Follow this and additional works at: https://digitalcommons.library.tmc.edu/utgsbs_dissertations

 Part of the [Biology Commons](#), [Disease Modeling Commons](#), [Genetics and Genomics Commons](#), [Laboratory and Basic Science Research Commons](#), and the [Neoplasms Commons](#)

Recommended Citation

Chan, Suzanne S., "MODELING SPORADIC TUMOR FORMATION DRIVEN BY TELOMERE DYSFUNCTION IN THE GASTROINTESTINAL TRACT" (2010). *The University of Texas MD Anderson Cancer Center UTHealth Graduate School of Biomedical Sciences Dissertations and Theses (Open Access)*. 75.
https://digitalcommons.library.tmc.edu/utgsbs_dissertations/75

This Dissertation (PhD) is brought to you for free and open access by the The University of Texas MD Anderson Cancer Center UTHealth Graduate School of Biomedical Sciences at DigitalCommons@TMC. It has been accepted for inclusion in The University of Texas MD Anderson Cancer Center UTHealth Graduate School of Biomedical Sciences Dissertations and Theses (Open Access) by an authorized administrator of DigitalCommons@TMC. For more information, please contact digitalcommons@library.tmc.edu.

MODELING SPORADIC TUMOR FORMATION DRIVEN BY TELOMERE
DYSFUNCTION IN THE GASTROINTESTINAL TRACT

By

Suzanne Sea-Wan Chan, B.S.

APPROVED:

Sandy Chang, M.D., Ph.D.
Supervisory Advisor

Russell Broadus, M.D., Ph.D.

Elsa Flores, Ph.D.

Stanley Hamilton, M.D.

Guillermina Lozano, Ph.D.

APPROVED:

Dean, The University of Texas
Graduate School of Biomedical Sciences at Houston

**MODELING SPORADIC TUMOR FORMATION DRIVEN BY TELOMERE
DYSFUNCTION IN THE GASTROINTESTINAL TRACT**

A

DISSERTATION

Presented to the Faculty of
The University of Texas
Health Science Center at Houston
and
The University of Texas
M. D. Anderson Cancer Center
Graduate School of Biomedical Sciences

in Partial Fulfillment

of the Requirements

for the Degree of

DOCTOR OF PHILOSOPHY

by

Suzanne Sea-Wan Chan, B.S.
Houston, Texas

August 2010

DEDICATION

I'd like to dedicate this work to my parents, Paul and Anne, and to the memory of my grandmother, Suk-Ying Chan, for their unconditional love, support and inspiration during my many years of education.

ACKNOWLEDGEMENTS

There are many people who have helped me through the last four years. Without them, I could not have completed this project. First and foremost, I'd like to thank my advisor, Sandy Chang, for supporting me throughout this experience and for introducing this Boston girl to the opportunities available at the Texas Medical Center in Houston, especially at the MD Anderson Cancer Center.

I'd also like to thank the past and current members of my advisory, examining and supervisory committees: Drs. Russell Broadus, Elsa Flores, Stanley Hamilton, Guillermina Lozano, Richard Behringer, Chenming Zhu, Sharon Dent, and Randy Legerski. Special thanks to Dr. Broadus for taking the time to review slides for intestinal pathology with me, and for his advice and support throughout the MD/PhD process. I'd also like to extend my gratitude to Dr. Lozano, for sharing mouse lines that have been vital to the project: the Villin-Cre transgenic mice and the conditional p53 knockout mice; Dr. Zhu for providing the ATM mice; and Dr. Behringer for the Rosa26-LacZ mice.

Thank you to all my past and present colleagues in the Chang lab for their technical help, scientific discussion, support, advice and of course, friendship: Wilfredo Cosme-Blanco, Ruby Deng, Hua He, Ling Wu, Meifeng Shen, Rehka Rai, Mahira Zaheer, Carman Lam, Yibin Deng, Xiaolan Guo, Asha Multani, Jin Ma, Ying Luo, Peili Gu, Yang Wang, Waikin Chan, Tao Peng, Hong Xiang, Yang Xiao, and Puneeth Iyengar. In particular, I am grateful to my "benchmates": Hua, Ruby, and especially Wilfredo, who also paved the path for graduate students in the Chang lab. I am also indebted to Rehka, Mahira and Carmen, who have been my sounding board for issues both science and non-science related. Thank you to Meifeng, who has been an immense help with management the mouse colony; and

Ling, who taught me so much when I was just getting started in the lab. I'd also like to thank Alma Buena for her summer of hard work during her internship with the King Foundation. And finally, I am grateful to the wonderful support staff in the Genetics department: Pat Arubaleze, Elva Lopez, Cedric Thomas, Elisabeth Lindheim, Angela Lillie, Vicky Garza, and Linda Ricks.

Thank you to Hank Adams for his help with microscopy; the entire MD Anderson Histology core for their help processing the incredible amount of tissue samples I've generated; Nancy Otto and the Histology and Tissue Processing Facility Core at MDACC Science Park – Research Division in Smithville, Texas for their help with IHC staining; David Pollack and Dr. Mini Kapoor from the MD Anderson Microarray Core for their assistance with running the array CGH experiments; and Dr. Li Zhang from the Department of Bioinformatics for advice on data analysis.

Thank you to the UT-Houston MD/PhD program, who have given me this incredible opportunity to study in the Texas Medical Center, especially Dr. Broaddus and Dr. Dianna Milewicz. Thank you to Doris Thornton and Melissa Proll for helping me through the process.

I am forever grateful to my family, who has cheered me on from afar. My parents and my brother Jonathan, who thought I was crazy for choosing a combined program, have been nonetheless been most supportive throughout this long training process. And the rest of my large extended family have kept a steady flow encouragement and well wishes to help me stay motivated. Thank you for always keeping a place for me at the Chan Clan dinners.

And finally, I'd like to thank my Houston family: my medical school friends whom I've grown up with these last seven years: Roxanna Irani, Susan Cameron, Jamie Causey,

Susan Haley and Eric Mueller. Morgan Scarborough, thank you for your love and support, for being my rock and keeping me sane.

My thesis was partially supported by the MD Anderson Cancer Center Training Grant in the Molecular Genetics of Cancer (2006-2009) and the American Legion Auxiliary Fellowship for Cancer Research (2008-2010).

ABSTRACT

MODELING SPORADIC TUMOR FORMATION DRIVEN BY TELOMERE DYSFUNCTION IN THE GASTROINTESTINAL TRACT

Publication No._____

Suzanne S. Chan

Supervisory Professor: Sandy Chang, M.D., Ph.D.

Colorectal cancer is a complex disease that is thought to arise when cells accumulate mutations that allow for uncontrolled growth. There are several recognized mechanisms for generating such mutations in sporadic colon cancer; one of which is chromosomal instability (CIN). One hypothesized driver of CIN in cancer is the improper repair of dysfunctional telomeres. Telomeres comprise the linear ends of chromosomes and play a dual role in cancer. Its length is maintained by the ribonucleoprotein, telomerase, which is not a normally expressed in somatic cells and as cells divide, telomeres continuously shorten. Critically shortened telomeres are considered dysfunctional as they are recognized as sites of DNA damage and cells respond by entering into replicative senescence or apoptosis, a process that is p53-dependent and the mechanism for telomere-induced tumor suppression. Loss of this checkpoint and improper repair of dysfunctional telomeres can initiate a cycle of fusion, bridge and breakage that can lead to chromosomal changes and genomic instability, a process that can lead to transformation of normal cells to cancer cells. Mouse models of telomere dysfunction are currently based on knocking out the telomerase protein or RNA component; however, the naturally long telomeres of mice require multiple generational crosses of

telomerase null mice to achieve critically short telomeres. Shelterin is a complex of six core proteins that bind to telomeres specifically. Pot1a is a highly conserved member of this complex that specifically binds to the telomeric single-stranded 3' G-rich overhang. Previous work in our lab has shown that Pot1a is essential for chromosomal end protection as deletion of Pot1a in murine embryonic fibroblasts (MEFs) leads to open telomere ends that initiate a DNA damage response mediated by ATR, resulting in p53-dependent cellular senescence. Loss of Pot1a in the background of p53 deficiency results in increased aberrant homologous recombination at telomeres and elevated genomic instability, which allows Pot1a^{-/-}, p53^{-/-} MEFs to form tumors when injected into SCID mice. These phenotypes are similar to those seen in cells with critically shortened telomeres.

In this work, we created a mouse model of telomere dysfunction in the gastrointestinal tract through the conditional deletion of Pot1a that recapitulates the microscopic features seen in severe telomere attrition. Combined intestinal loss of Pot1a and p53 lead to formation of invasive adenocarcinomas in the small and large intestines. The tumors formed with long latency, low multiplicity and had complex genomes due to chromosomal instability, features similar to those seen in sporadic human colorectal cancers. Taken together, we have developed a novel mouse model of intestinal tumorigenesis based on genomic instability driven by telomere dysfunction.

TABLE OF CONTENTS

DEDICATION.....	III
ACKNOWLEDGEMENTS.....	IV
ABSTRACT.....	VII
TABLE OF CONTENTS.....	IX
LIST OF FIGURES.....	XI
LIST OF TABLES.....	XIII
INTRODUCTION.....	1
Colon cancer and chromosomal instability.....	1
The telomere-cancer paradox.....	3
The shelterin complex.....	7
How shelterin protects telomeres.....	13
Targeting Pot1a to model telomere dysfunction <i>in vivo</i>	14
GENERATION OF A MOUSE MODEL OF TELOMERE DYSFUNCTION	
IN THE GASTROINTESTINAL TRACT THROUGH LOSS OF POT1A..	17
Generation and validation of the Villin-Cre Pot1a mouse colony.....	17
Pot1a ^{intΔ} mice have normal intestinal morphology, but	
increased apoptosis and anaphase bridges.....	22
Pot1a deficiency leads to increased activation of p53 and p21	30
Loss of Pot1a leads to activation of a telomere-induced DNA	
damage response.....	32
Intestinal Pot1a deficiency does not affect response to irradiation.....	34
Discussion.....	38

THE EFFECT OF POT1A DEFICIENCY ON ESTABLISHED	
MOUSE MODELS OF GI TUMORS.....	43
The effect of loss of Pot1a on APC ^{min} genetic model of	
intestinal tumorigenesis.....	43
The effect of loss of Pot1a on a colitis-induced model of colorectal cancer...	54
COMBINED LOSS OF POT1A AND P53 LEADS TO	
TUMOR FORMATION.....	59
Apoptosis and p21 activation in Pot1a intestines is p53-dependent	60
p53 deficiency allows for more cells with telomere dysfunction to persist...	60
Mice with combined Pot1a and p53 loss develop invasive	
adenocarcinomas	64
Pot1a, p53 intestinal tumors shows signs of genomic instability	67
Discussion.....	72
THE EFFECT OF ATM ON POT1A-INDUCED TELOMERE	
DYSFUNCTION IN THE GI TRACT.....	79
Animals with combined loss of Pot1a and ATR in the intestinal	
tract are not viable.....	79
ATM loss results in decreased overall survival.....	81
ATM deficiency rescues p21 activation and apoptosis	81
Pot1a ATM+/- leads to rare tumor formation.....	84
Discussion	84
CONCLUSION AND FUTURE DIRECTIONS	88
MATERIALS AND METHODS.....	93
BIBLIOGRAPHY.....	100
VITA.....	113

LIST OF FIGURES

Figure 1. The Vogelstein model of colon cancer progression.....	2
Figure 2. The structure of telomeres.....	4
Figure 3. The shelterin complex.....	10
Figure 4. Consequences of telomere dysfunction.....	15
Figure 5. Pot1a is restricted to the intestines.....	19
Figure 6. Villin-Cre expression leads to decreased expression of Pot1a mRNA in the intestines.....	21
Figure 7. β -galactosidase activity is only detected in intestines when both VCre and R26R transgenes are present	23
Figure 8. Villin-Cre activity is specific to the intestinal epithelium.....	24
Figure 9: Intestinal deficiency of Pot1a does not affect overall survival.....	26
Figure 10: Loss of Pot1a does not affect the gross morphology of the Intestinal epithelium, but increases apoptosis in crypts.....	27
Figure 11. Pot1a deficiency leads to increased TUNEL positive cells in the intestinal crypts.....	28
Figure 12. Anaphase bridges are a hallmark of telomere dysfunction.....	29
Figure 13. Loss of Pot1a activates p53 in the intestinal crypts.....	31
Figure 14. Loss of Pot1a leads to upregulated p21 expression in the intestines.....	33
Figure 15: Loss of Pot1a activates a DNA damage response in the intestines.....	35
Figure 16: DNA damage is only observed in cells of the crypts.....	36
Figure 17: Pot1a deficiency in the intestines does not affect survival of 3-month old animals after irradiation.....	38

Figure 18: Pot1a deficiency does not affect intestinal response to irradiation.....	39
Figure 19: Loss of Pot1a does not affect the number or size of tumors in APC ^{min} ...	46
Figure 20: Pot1a loss does not affect the tumor type or grade in APC ^{min} mice.....	48
Figure 21: Intestinal depletion of Pot1a leads to decreased overall survival in APC ^{min} mice.....	50
Figure 22: Pot1a ^{intΔ} APC ^{min} animals form large tumors earlier than control mice.. ...	51
Figure 23: Pot1a ^{intΔ} APC ^{min} intestines have increased apoptosis and anaphase bridges	53
Figure 24: Protocol for AOM/DSS experiment.....	55
Figure 25: Tumor formation in mice treated with AOM/DSS at 15 weeks.....	58
Figure 26: Verification of Pot1a and p53 deletion in Pot1a ^{intΔ} p53 ^{F/F} mice.....	61
Figure 27: Apoptosis and p21 activation in Pot1a ^{intΔ} intestines is p53-dependent...	62
Figure 28: p53 deficiency leads to increased numbers of cells with telomere dysfunction.....	63
Figure 29: Combined loss of Pot1a and p53 leads to formation of invasive cancers in the GI tract.....	66
Figure 30: Tumors from Pot1a ^{intΔ} p53 ^{F/F} mice show genomic alterations	69
Figure 31: Tumors from Pot1a ^{intΔ} p53 ^{F/F} mice show genomic alterations	70
Figure 32: Summary of aCGH results for thirteen intestinal tumors	71
Figure 33: Distribution of copy number changes	73
Figure 34: ATM deficiency leads to early death in Pot1a deficient mice.....	82
Figure 35: ATM deficiency rescues apoptosis and p21 activation in Pot1 ^{intΔ} crypts.....	83

LIST OF TABLES

Table 1: Cohorts for study in the Villin-Cre, Pot1a colony and progeny distribution	18
Table 2: Shortened telomeres (mTerc ^{-/-}) reduce tumor incidence in mouse models of cancer.....	44
Table 3: Summary of average tumor burdens for Pot1a, APC mice	47
Table 4: Tumor formation in mice treated with AOM/DSS at 10-weeks.....	56
Table 5: Combined Pot1a and p53 deficiency leads to tumor formation	65
Table 6: Description of tumors used for aCGH experiments	68
Table 7: Results of VCre ⁺ Pot1a ^{F/F} ATR ^{F/+} x VCre ⁻ Pot1a ^{F/F} ATR ^{F/+}	80
Table 8: Pot1a ^{intΔ} ATM+/- mice occasionally form tumors.....	85
Table 9: Genotyping primers and conditions.....	99

INTRODUCTION

Colon cancer and chromosomal instability

Colon cancer is the third most common cause of cancer, as well as the third leading cause of cancer death in both men and women in the United States(ACS, 2010). Cancer is a complex disease that arises when cells accumulate mutations that allow for uncontrolled growth. The progression of colorectal tumorigenesis has been characterized as a step-wise progression from adenoma to carcinoma to metastatic disease(Fearon and Vogelstein, 1990) as these mutations accumulate (Figure 1). Some of the important genes involved in some of the transitions are well known, such as activation of the Wnt signaling pathway especially through loss of APC(Goss and Groden, 2000). However, recent work with cancer genomics have revealed that colorectal cancer cells harbor very complex genomes with a multitude of genetic changes, so there are may be many other genes important for cancer progression, especially the metastatic transition, that have yet to be elucidated.

There are several mechanisms that drive the accumulation of genetic alterations, which can fuel colon cancer formation and progression. Genetic alterations can include subtle sequence changes, alterations in chromosome numbers, chromosome translocations and gene amplifications(Lengauer et al., 1997). These types of changes can be a consequence of chromosomal instability or defects in the DNA repair pathways(Markowitz and Bertagnolli, 2009). The mismatch repair (MMR) pathway is one such DNA repair mechanism that is found in colon cancers. Inactivation of MMR genes, such as MLH1 or MSH2, leads to a phenotype called microsatellite instability (MSI), which targets simple repeat sequences in the genome(Rajagopalan et al., 2003). MSI is most associated with patients with hereditary

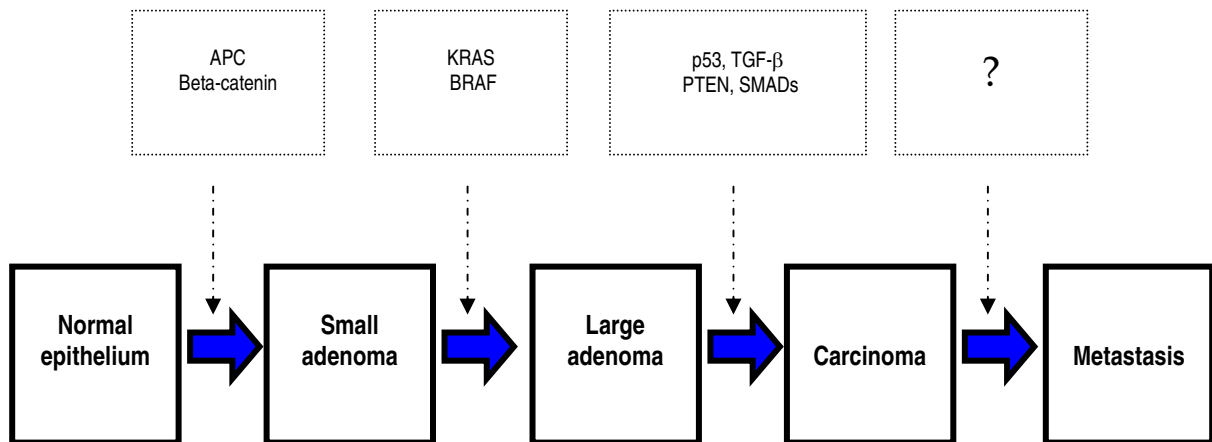


Figure 1: The Vogelstein model of colon cancer progression. Colorectal cancers develop first as small benign adenomas and follow a progression to malignant adenocarcinomas and finally to metastasis. Some of the genetic alterations associated with various steps of the pathway have been elucidated and are outlined above (dotted boxes).

non-polyposis colorectal cancer (HNPCC), but can also be seen in 15% of sporadic tumors (Markowitz and Bertagnolli, 2009; Rajagopalan et al., 2003).

On the other hand, chromosomal instability (CIN) is seen in 85% of sporadic colon cancers and is thought to be a major driver of genomic instability (Rajagopalan et al., 2003). CIN can cause cells to gain or lose large pieces or entire chromosomes leading to aneuploidy and gene copy number variations (CNV) (Lengauer et al., 1997; Rajagopalan et al., 2003). Here, we will explore one mechanism that may be involved in driving CIN during tumorigenesis: dysfunctional telomeres.

The telomere-cancer paradox

Telomeres are located at the terminal ends of chromosomes. They consist of tandem TTAGGG repeats and end with a 3' single stranded G-rich overhang (Figure 2). This overhang is thought to invade the upstream duplex telomere DNA to effectively hide the end and create a structure called a t-loop (Griffith et al., 1999). It is bound by a complex of telomere specific proteins called shelterin (de Lange, 2005). The main function of telomeres is to protect the chromosomal ends from being recognized as sites of DNA damage or being exposed to nuclease degradation with subsequent loss of genetic information (Verdun and Karlseder, 2007). The length of telomeres can be maintained by a ribonucleoprotein called telomerase, which consists of two main components: a reverse transcriptase protein (TERT) and a RNA component (TERC) that serves as a template for elongation.

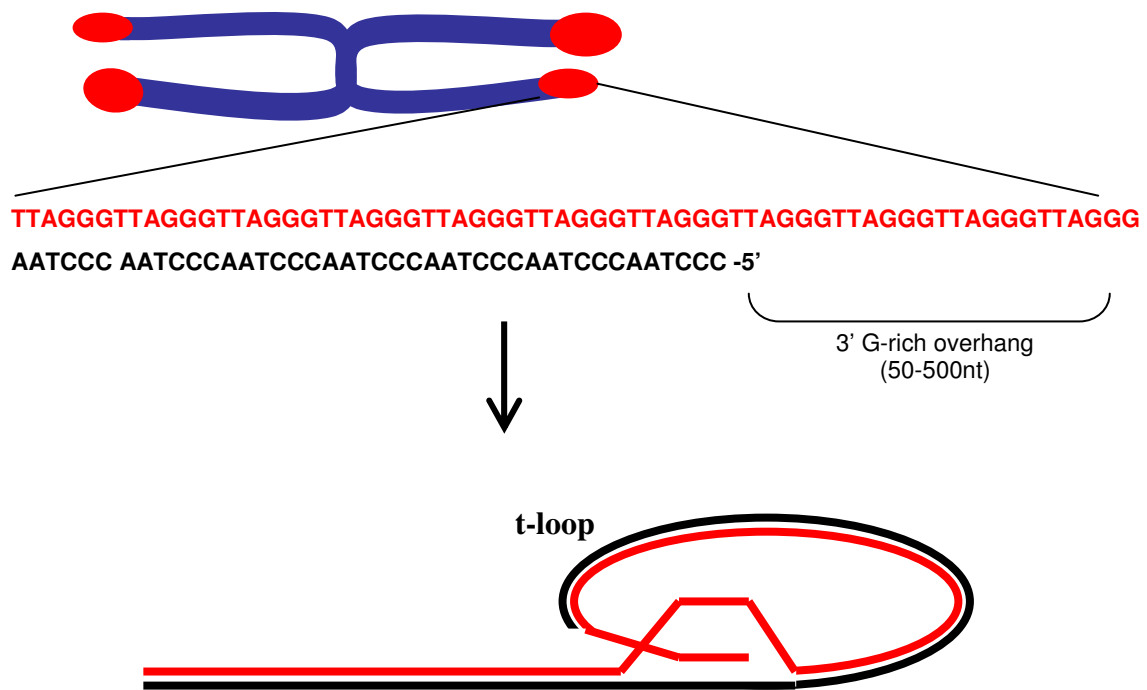


Figure 2: The structure of telomeres. Telomeres are located at the terminal ends of chromosomes. They consist of tandem TTAGGG repeats and end with a 3' single stranded G-rich overhang. This overhang is thought to invade the upstream duplex telomere DNA that effectively hides the end and creating a structure called a t-loop.

In humans, telomerase activity is limited to germ cells and stem cells, but absent in most somatic cells. Without telomerase maintenance, the overall length of telomeres shortens with each cell division due to the inability of DNA replication machinery to fully replicate the lagging strand DNA, a characteristic termed the end replication problem. It is estimated that humans lose between 2-4 kb of telomeric DNA in a lifetime. Considering human telomere lengths average 8-12kb, this amount of loss may be significant and might play a role in organismal aging(Blasco, 2007). Increasing age is the biggest risk factor for sporadic colon cancer formation, so it stands to reason that telomeres may provide the link between aging and cancer(DePinho, 2000). Accordingly, telomere length has been shown to correlate with age in normal intestinal mucosa(Rampazzo et al.). Furthermore, telomeres in colorectal tumor tissue are shorter than the surrounding normal mucosa(Rampazzo et al.). Therefore it is postulated that telomere erosion may be a key initiating event in the colon tumor formation.

Telomeres play a dual role in cancer (Artandi and DePinho; Deng et al., 2008). First, there is a limit to the amount of telomere attrition that a cell can tolerate. This phenomenon was originally described by Hayflick and Moorhead, who observed that primary human diploid fibroblasts cannot be cultured indefinitely(Hayflick and Moorhead, 1961). There is a limit to the number of population doublings that a culture can be passaged, after which the cells enter into a state of permanent cell cycle arrest termed replicative senescence. This checkpoint is the basis of the first half of the telomere-cancer paradox: telomere-dependent tumor suppression(Deng et al., 2008).

Replicative senescence is thought to be a consequence of the DNA damage response to telomere attrition. Senescent fibroblasts stained positively for markers of DNA damage, such as phosphorylated histone H2AX (γ -H2AX) and p53 binding protein 1 (53BP1)(d'Adda di Fagagna et al., 2003). Critically short telomeres also activate sensors of DNA damage such as the phosphatidylinositol 3-kinase (PIKKs): ataxia telangiectasia mutated (ATM) and ataxia telangiectasia- and Rad3- related protein (ATR)(d'Adda di Fagagna et al., 2003). These proteins in turn activate the downstream transducers, CHK1 and CHK2, which go on to activate p53(Gire et al., 2004), the protein that ultimately triggers cell cycle arrest/senescence through p21. While the Ink4a/Rb pathway may also play a role in this process that is less understood (Jacobs and de Lange, 2004; Kim and Sharpless, 2006), it is the p53-dependent senescence or apoptosis that is thought to mediate the first checkpoint in telomere-induced tumor suppression.

Inactivation of p53 or Rb can bypass this checkpoint and allow fibroblasts to continue to proliferate (Hara et al., 1991; Shay et al., 1991). Telomere attrition continues and the resulting dysfunctional telomeres lead to genomic instability. When the deprotected ends are recognized as double strand breaks, DNA repair mechanisms, such as non-homologous end joining (NHEJ) or homologous recombination (HR), are activated to produce fusions with other chromosomes resulting in a dicentric chromosome. When the dicentric chromosome is pulled to opposite poles during anaphase, a bridge is formed between the two cells, called an anaphase bridge. In order for cytokinesis to occur, the anaphase bridge must break to separate. This break is random and creates amplification in one cell and a corresponding deletion in the other cell. The new breaks must then be repaired through the same pathways, resulting in new fusions that will form another bridge and the process repeats. This cycle is

called the break-fusion-bridge (BFB) cycle and was first noticed by Barbara McClintock during her studies of maize (McClintock, 1941). Since the sites of breakage and repair are random, one can see how repeated cycles of BFB triggered by just a few fusions can lead to changes in the integrity of the genome, either through large losses or amplifications of genetic information. This rampant genomic instability can lead to the accumulation of oncogenic changes necessary for a cell to become transformed. Therefore, activation of the BFB cycle through dysfunctional telomeres represent the second half of the telomere-cancer paradox: dysfunctional telomere-induced genomic instability can promote tumor formation (Bailey and Murnane, 2006; DePinho and Polyak, 2004).

While there are many studies associating telomere length to human disease (Jiang et al., 2007), much of our direct knowledge of *in vivo* consequences of telomere dysfunction has come from the telomerase knockout mouse. In this model, gene targeting of the RNA component of telomerase (mTerc) efficiently disrupts the function of telomerase. However, owing to the differences in the length of laboratory mouse telomeres (40-80kb) compared to human telomeres (8-12kb), it takes successive intergenerational breeding of mTerc^{-/-} animals to reach critical shortening. It is only at later generations (G4 or beyond) that one begins to see the effects of shortened telomeres (Lee et al., 1998; Rudolph et al., 1999). We sought to avoid this process by approaching telomere dysfunction from a different angle: targeting the telomere binding complex, shelterin.

The shelterin complex

The term “dysfunctional telomeres” refers to a state of deprotected telomeres that can be caused by severe shortening or by uncapping due to disruption of the shelterin

components(Harrington and Robinson, 2002). Shelterin is composed of six proteins that bind specifically to telomeres, including: TRF1, TRF2, TIN2, RAP1, TPP1 and POT1(de Lange, 2005) (Figure 3). They are all essential to cell survival, as depletion of shelterin components either drives cells into cellular senescence or results in early embryonic lethality. Together, these six proteins form a complex that maintains telomeric length and structure, and protects chromosome ends from activating the DNA damage response and inappropriate repair mechanisms. However, each protein plays a unique role in telomere homeostasis.

The two main proteins that anchor the complex to the double stranded telomeric DNA are telomeric repeat-binding factors 1 and 2 (TRF1 and TRF2), which recognize duplex TTAGGG repeats and bind directly through their SANT/Myb domain(Broccoli et al., 1997). Although TRF1 and TRF2 have similar structure and protein binding domains, they recruit proteins to telomeres differently (Chen et al., 2008) and play distinct roles in protection of chromosome ends. TRF2 appears to be a vital component of shelterin as its loss is very toxic to cells. Depletion of TRF2 from cells initiates a potent DNA damage response, which leads to cellular senescence or very dramatic fusion phenotype indicative of improper activation of NHEJ (Karlseder et al., 1999; van Steensel et al., 1998). This response suggests that it plays a prominent role in suppressing both these processes at normal chromosome ends. While the exact method of repression of these pathways is still speculative, TRF2 has been shown to interact with other proteins, including the shelterin protein RAP1 (Li et al., 2000), as well as a variety of non-shelterin proteins, including ATM, the MRN complex, WRN, BLM, Ku86, ERCC1/XPF, PARP1 and PARP2 (Palm and de Lange, 2008). Many of these proteins are involved DNA damage sensing and repair processes, leading to the theory that TRF2 repression of these pathways is mediated by physical interactions with these factors. TRF2

may also play a role in stabilizing telomere secondary structure as it has been shown to facilitate t-loop formation *in vitro* (Stansel et al., 2001).

Although it can also bind double stranded telomeric DNA, TRF1 appears to play a minor role in repression of damage responses and repair. Its depletion also leads to cellular senescence (Karlseder et al., 2003; Martinez et al., 2009; Sfeir et al., 2009), but *in vitro* experiments show that TRF1 is unable to inhibit end-joining of telomeric substrates (Bae and Baumann, 2007). Instead, TRF1 may be more important in regulation of telomere length (Smogorzewska et al., 2000; van Steensel and de Lange, 1997). It can interact with non-shelterin telomere factors, including PINX1, Tankyrase 1 and Tankyrase 2 (Palm and de Lange, 2008). These factors can in turn interact with telomerase, suggesting telomere length regulation involves TRF1 recruitment of these factors to telomeres. There is emerging evidence that TRF1 may also be important for preventing telomere replication mistakes and protects telomeres against a fragile-telomere phenotype (Martinez et al., 2009; Sfeir et al., 2009).

The TRF1-interacting nuclear protein 2 (TIN2) has been called the linchpin of shelterin, as it is able to bind TRF1, TRF2 and TPP1, acting as a bridge between the double stranded and single stranded telomere binding proteins. While it can stabilize the six protein complex (O'Connor et al., 2006), TIN2 exists in stoichiometric quantities enough to bind each molecule of TRF1 or TRF2, suggesting that it may not always bind to both proteins simultaneously and that the shelterin complex may not always exist with all components (Takai et al.). It was recently discovered that TIN2 exists in two isoforms in human cells. One of these isoforms, TIN2L, was shown to bind tightly to nuclear matrix proteins suggesting a role in anchoring telomeres in the nucleus (Kaminker et al., 2009).

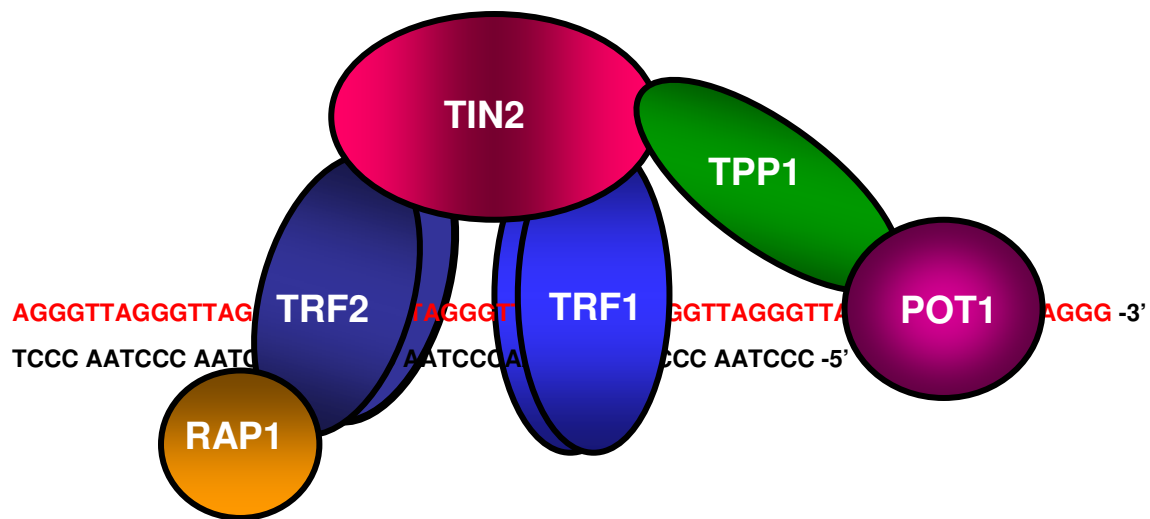


Figure 3: The shelterin complex. Telomeres are bound by a complex of telomere specific proteins called shelterin, which includes TRF1, TRF2, TIN2, TPP1, POT1 and RAP1. TRF1 and TRF2 bind directly to duplex telomeric DNA, while POT1 binds to the single stranded G-rich 3' overhang. TIN2 bridges TRF1 and TRF2, while connecting POT1 to these molecules through TPP1. RAP2 localizes to telomeres through its interaction with TRF2.

TPP1 can interact with TIN2 and POT1, providing the essential link for the recruitment of POT1 to telomeres(Hockemeyer et al., 2007). As with other members of shelterin, homozygous loss of TPP1 is incompatible with survival(Kibe et al.). Depletion of TPP1 through genetic ablation(Kibe et al.), RNA interference(Guo et al., 2007), or a mutant that abolishes POT1 interaction(Guo et al., 2007) leads to cellular consequences consistent with POT1 loss, suggesting its main role is the recruitment of POT1 to the chromosome ends. TPP1 can also interact with telomerase, suggesting that it may play role in telomere length maintenance(Xin et al., 2007).

Originally discovered in *S. pombe*, protection of telomeres (POT1) is the component that specifically binds to the single stranded G-rich overhang. It was found based on its similarity to the ciliate telomere binding protein TEBP α (Baumann and Cech, 2001). It is essential for the protection of telomeres in yeast as its loss leads to cell death, where the only surviving colonies have circularized their chromosomes eliminating the need for telomere protection(Baumann and Cech, 2001). It is one of the most highly conserved members of shelterin and has been studied in humans, chicken, mice, yeast and plants(Churikov and Price, 2008; He et al., 2006; Hockemeyer et al., 2006; Hockemeyer et al., 2007; Loayza and De Lange, 2003; Wang et al., 2007). All POT1 proteins have two highly conserved oligonucleotide/oligosaccharide binding folds (OB folds) that show specificity for telomeric sequences and are essential for binding the single stranded 3' overhang. Human POT1 associates with the rest of the shelterin complex through its interaction with TPP1, an interaction that appears essential for its function(Hockemeyer et al., 2007). It is also a vital

component in telomere protection as knockdown of POT1 also triggers a chromosomal aberrations and cell death(Wu et al., 2006).

Mice have two orthologs of the gene, named Pot1a and Pot1b(Hockemeyer et al., 2006; Wu et al., 2006). Pot1a is essential to cells as targeted deletion of this gene in the mouse leads to embryonic lethality very early during development (Hockemeyer et al., 2006; Wu et al., 2006). Pot1a is necessary for chromosomal end protection as deletion of Pot1a in murine embryonic fibroblasts (MEFs) promotes chromosomal fusions and a DNA damage response resulting in cellular senescence(Wu et al., 2006). On the other hand, Pot1b is not essential for survival as Pot1b^{-/-} mice are viable, and its deficiency in cells does not produce as severe of a phenotype as loss of Pot1a alone or deletion of both Pot1a and Pot1b(He et al., 2006; Hockemeyer et al., 2006). Recent studies have implicated Pot1b in telomeric length maintenance; in particular, the regulation of C-strand resection for the formation of the 3' overhang, which is greatly elongated following Pot1b loss(He et al., 2006; Hockemeyer et al., 2006; Hockemeyer et al., 2008).

RAP1 is one of the most evolutionarily conserved members of shelterin. However, its role in telomere biology seems to vary between species. For instance, in *S. cerevisiae*, rap1 binds directly to telomeric sequences, where it is involved in the negative regulation of telomere length, inhibition of fusions, and the recruitment of Sir proteins for silencing of genes near the telomeric region (Hardy et al., 1992). However, in mammalian cells, RAP1 cannot bind telomeric DNA and depends on TRF2 binding for recruitment to chromosome ends(Li et al., 2000). Biochemical assays have revealed that the TRF2/RAP1 complex can inhibit NHEJ-mediated fusions at telomeric ends(Bae and Baumann, 2007), but because of this dependence, the role of RAP1 alone remains unclear. *In vitro* studies in human cell lines

suggest overexpression of RAP1 may have an effect on telomere length regulation, which is independent of its ability to localize to telomeres(Li and de Lange, 2003). Recent generation of a fusion protein between RAP1 and the telomeric binding domain of a yeast protein allowed localization of RAP1 to telomeres independent of TRF2 binding(Sarthy et al., 2009). Using this fusion protein, localization of RAP1 to telomeres did not prevent DNA damage signaling, but was sufficient to inhibit NHEJ(Sarthy et al., 2009) suggesting that RAP1 plays more of a role in repression of repair rather than damage sensing.

How shelterin protects telomeres

The linear nature of eukaryotic chromosomes presents a difficult problem for cells: how can cellular DNA damage response machinery distinguish the normal ends of chromosomes from sites of DNA breaks? Or alternatively, how can chromosomes mask its ends from activating this response so that cells can propagate? This obstacle has been deemed the “end protection problem”(de Lange, 2009). Telomeres function to solve this problem, and as discussed above, severe erosion of telomeres exposes chromosome ends to a potent DNA damage response(d'Adda di Fagagna et al., 2003; Gire et al., 2004), resulting in p53-dependent senescence or apoptosis (Figure 4).

The role shelterin proteins play in suppressing this response at normal telomeres has been teased out through the use of mouse embryonic fibroblasts (MEFs) with genetic ablation of various combinations of these factors. First, TRF2 knockdown experiments show that cells respond to loss of TRF2 in a similar manner as IR-induced DSB, with the MRN complex required for the initial sensing of damage at dysfunctional telomeres(Deng et al., 2009; Dimitrova and de Lange, 2009), while ATM is necessary for propagation of the

signal(Denchi and de Lange, 2007; Guo et al., 2007). On the other hand, TPP1 or Pot1a/b disruption leads to a response that is dependent on the ATR pathway (Denchi and de Lange, 2007; Guo et al., 2007). These results reveal that TRF2 acts mainly to repress ATM-mediated DNA damage responses, while Pot1a and Pot1b are involved in repression of the ATR pathway (Figure 4). How TRF2 and POT1 act to inhibit these pathways is still unclear. Paradoxically, many components of DDR pathways can be found normally at telomeres without activating an apparent DNA damage response(Verdun et al., 2005). Given that TRF2 can interact with these non-shelterin telomeric factors, perhaps it directly suppresses their activation through physical inhibition. In fact, there is some evidence that the TRF2 interaction with ATM directly inhibit its activity(Karlseder et al., 2004). However, POT1 proteins are not known to interact with non-shelterin components. Instead, it is postulated that the binding of the POT1 proteins to the 3' overhang provides protection through competitive blockade of RPA binding to the single stranded protrusion, preventing the activation of the ATR pathway (Zou and Elledge, 2003).

Targeted deletion of Pot1a to model telomere dysfunction *in vivo*

Given the similarities the consequences of disruption of shelterin components have to severe telomere attrition (Figure 4), we decided to target Pot1a in this project to study telomere dysfunction *in vivo*. With the parallels seen between the responses of both types of dysfunctional telomeres, we believe that the *in vivo* consequences of loss of Pot1a will also mimic that of mice with critically short telomeres. We used the conditional Pot1a knockout mouse(Wu et al., 2006) to allow us to take advantage of the different models of tissue-specific expression of the Cre recombinase to focus on the affect of telomere dysfunction on

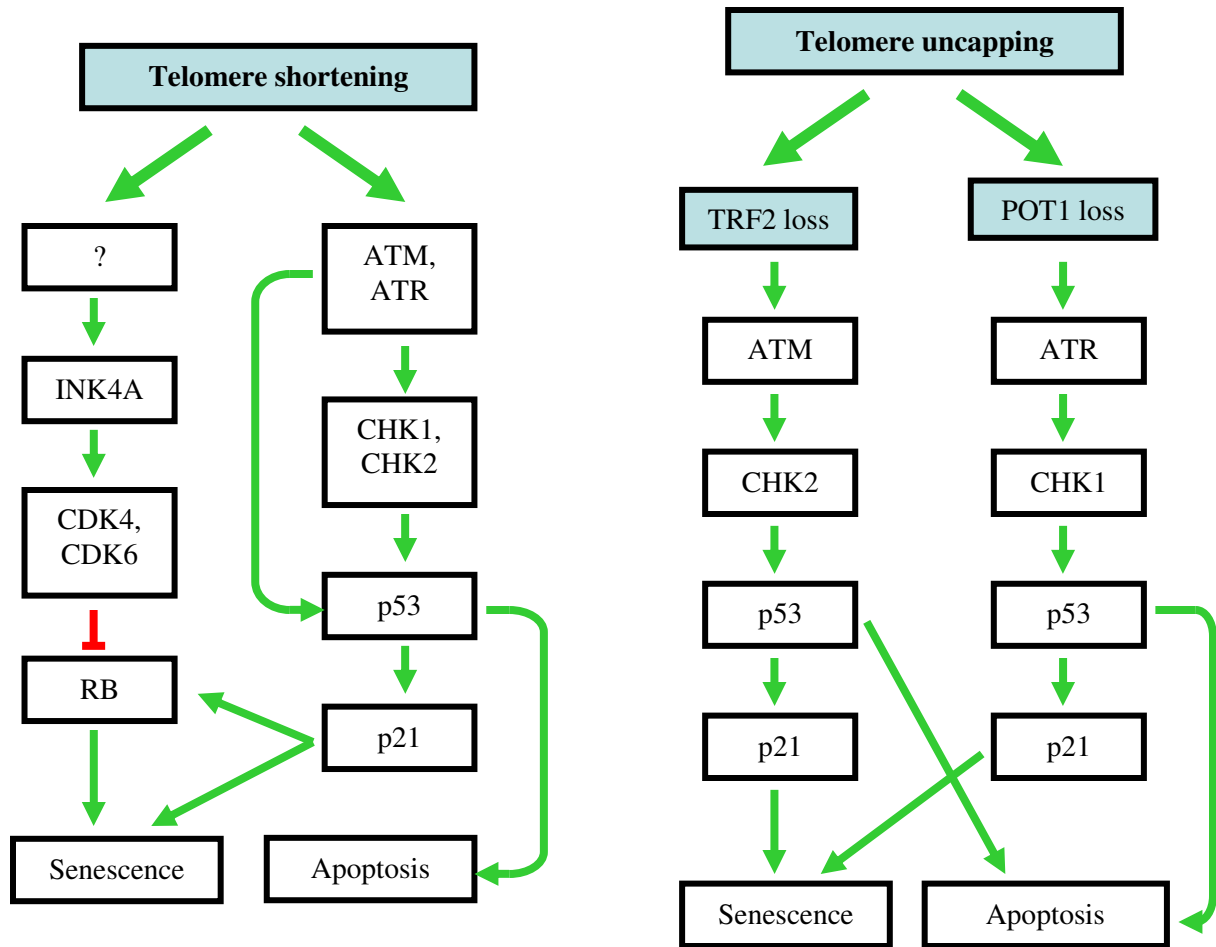


Figure 4. Consequences of telomere dysfunction. Work in human and mouse cells, as well as the telomerase null mouse models, have shown that telomere dysfunction caused by severe telomere shortening activates a DNA damage response (DDR) mainly mediated by the ATM/ATR pathway, which ultimately leads to p53-dependent apoptosis or senescence. Recent studies in mouse cells have shown that telomere dysfunction due to uncapping through loss of the shelterin proteins activate a similar response resulting in p53 activation and cellular senescence or apoptosis. TRF2 mainly suppresses an ATM-dependent response, while POT1 protects against ATR-dependent DDR.

one organ system at a time. This reduces the possibility of confounding factors that may arise with telomere dysfunction throughout the organism, such as the hematopoietic compromise that affects late generation telomerase null mice (Lee et al., 1998; Rudolph et al., 1999). In this project, we focused on the gastrointestinal system, which, as one of the body's most proliferative compartments, telomere dysfunction is postulated to play a role due to the multiple rounds of cell division necessary to maintain the level of tissue renewal.

Similar to results seen in cell culture experiments, our mice show that intestinal deletion of Pot1a leads to a DNA damage response in cells of the crypts of Lieberkuhn, which activates p53 leading to upregulation of p21 and increased apoptosis. These phenotypes are also seen in the gut of late generation telomerase null mice with severe telomere shortening (Rudolph et al., 1999). Loss of Pot1a in the background of p53 deficiency results in increased aberrant homologous recombination at telomeres and elevated genomic instability, which allows Pot1a^{-/-}, p53^{-/-} MEFs to form tumors when injected into SCID mice (Wu et al., 2006). Similarly, mice with combined Pot1a and p53 formed tumors in the small intestines and colon. The mouse model produced invasive adenocarcinomas with low multiplicity, long latency, but high penetrance. Analysis of these tumors showed complex genomes with heterogeneity in genetic alterations between tumors, indicative of genomic instability. Taken together, the data we present here demonstrate that intestinal deletion of Pot1a and p53 produced a mouse model sporadic gastrointestinal cancer driven by telomere-induced genomic instability.

RESULTS

GENERATION OF A MOUSE MODEL OF TELOMERE-DYSFUNCTION IN THE GASTROINTESTINAL TRACT THROUGH LOSS OF POT1A

Generation and validation of the Villin-Cre Pot1a mouse colony

Since homozygous loss of Pot1a leads to embryonic lethality, we used a conditional knockout mouse previously created in our lab, in which exons 4 and 5 of the Pot1a gene are flanked by loxP sites (Wu et al., 2006). Exon 4 contains the translational start site and exon 5 contains part of the first OB-fold. The gastrointestinal tract was targeted by crossing the conditional Pot1a mouse with a Villin-Cre (VCre) transgenic mouse, which specifically expresses the Cre recombinase in intestinal epithelia through the Villin promoter (Madison et al., 2002). These mice were mated to produce the three cohorts used for this study (Table 1): one group which does not possess the VCre transgene and should therefore have wild-type Pot1a in the intestines (VCre⁻); one consisting of VCre⁺ Pot1a^{+/+} or Pot1a^{F/+} mice, which express the Cre recombinase, but retain one or both wild-type alleles of Pot1a in the intestines (VCre⁺); and the mutant cohort of VCre⁺ Pot1a^{F/F} mice with both copies of Pot1a deleted in the intestines (Pot1a^{intΔ}). A mating set-up between VCre⁻ Pot1a^{F/+} and VCre⁺ Pot1a^{F/+} revealed that Pot1a^{intΔ} are viable and born at expected Mendelian ratio (Table 1).

Cre-mediated deletion of the Pot1a allele was determined indirectly through several different methods. First, we developed a PCR strategy that is able to detect the recombination event in which exons 4 and 5 are deleted. This method can distinguish between this “delta” allele and the intact “floxed” conditional allele (Figure 5A). Genomic DNA was isolated from various tissue samples harvested from Pot1a^{intΔ} mice and assayed for the presence of the delta band.

Table 1: Cohorts for study in the Villin-Cre, Pot1a colony and progeny distribution.

The table below lists the three main cohorts studied and the genotypes included in those cohorts. Results from a $\text{VCre}^- \text{Pot1a}^{F/+}$ x $\text{VCre}^+ \text{Pot1a}^{F/+}$ cross show that mice with homozygous deletion of Pot1a in the intestines ($\text{VCre}^+ \text{Pot1a}^{F/F}$) are viable and observed in approximately the expected Mendelian ratios.

Cohort name	Genotypes included	Expected	Observed
VCre^-	$\text{VCre}^- \text{Pot1a}^{+/+}$	1/8 (12.5%)	14 (13.2%)
	$\text{VCre}^- \text{Pot1a}^{F/+}$	1/4 (25%)	25 (23.5%)
	$\text{VCre}^- \text{Pot1a}^{F/F}$	1/8 (12.5%)	13 (12.3%)
VCre^+	* $\text{VCre}^+ \text{Pot1a}^{+/+}$	1/8 (12.5%)	12 (11.3%)
	* $\text{VCre}^+ \text{Pot1a}^{F/+}$	1/4 (25%)	27 (25.4%)
$\text{Pot1a}^{\text{int}\Delta}$	$\text{VCre}^+ \text{Pot1a}^{F/F}$	1/8 (12.5%)	15 (14.1%)
		Total:	106 mice

* These two cohorts of mice behave very similarly since heterozygous loss of Pot1a has no apparent affect on cells *in vitro* or *in vivo*.

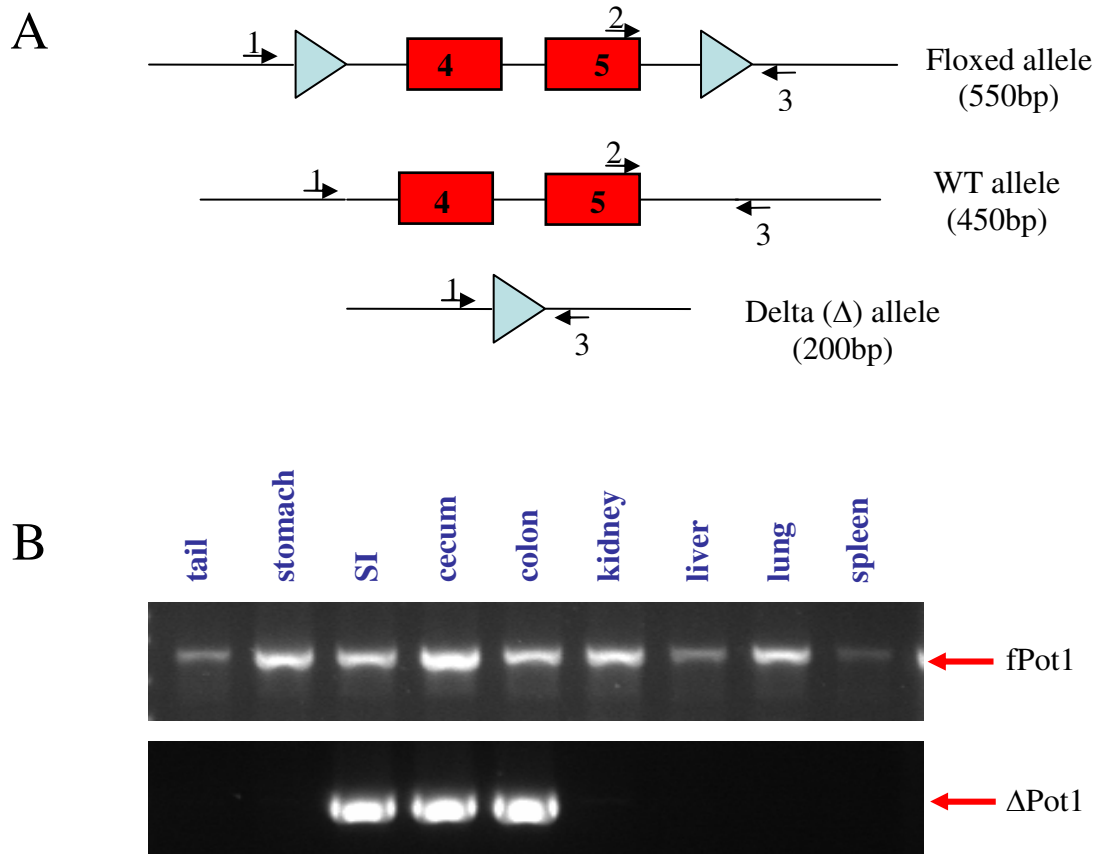


Figure 5: Pot1a deletion is restricted to the intestines. Panel A shows the PCR strategy for detecting Pot1a deletion from genomic PCR. Primers 1 & 3 are used to detect the null allele. Primers 2 & 3 are used to distinguish the floxed allele vs. the WT allele, and serve as an internal control for the PCR reaction. DNA was extracted from several different organs from a *Pot1a*^{int Δ} mouse. PCR analysis shows that the Δ Pot1a band is only amplified in genomic DNA harvested from the small intestine, cecum and colon; and not in other organs, including the stomach (Panel B).

The Villin-Cre transgene is only active in the intestinal epithelial cells and not in other tissues, including the liver and stomach (Madison et al., 2002). Accordingly, PCR results showed that the delta band was only amplified in samples harvested from the small intestine, cecum and colon, but not the stomach, kidney, liver, heart or spleen (Figure 5B). These results confirm that deletion of Pot1a occurs preferentially in the gastrointestinal tract.

To measure the expression of Pot1a mRNA, RT-PCR was performed using a Taqman Gene Expression Assay with probes specific for a region located in exon 4 of the Pot1a gene. RNA was isolated from liver tissue and scrapings of epithelial cells from the small intestine and colon. Analysis of tissues from VCre⁺ Pot1a^{F/+} mice demonstrated that loss of one allele of Pot1a leads to approximately 30% reduction in Pot1a expression in both the small intestine (0.720 ± 0.046 , t-test, $p = 0.022$) and colon (0.69 ± 0.096 , t-test, $p = 0.012$) (Figure 6). Intestines with both alleles of Pot1a deleted (Pot1a^{intΔ}) showed only a tenth of the expression seen in VCre- control small intestines (0.120 ± 0.072 , t-test, $p < 0.001$) and colon (0.183 ± 0.104 , t-test, $p < 0.001$) (Figure 6). These results confirm that conditional deletion of both Pot1a alleles leads to a dramatic reduction in Pot1a mRNA expression that is restricted to the small intestines and colon.

Finally, to determine the distribution of the Cre-mediated deletion, we crossed VCre, Pot1a mice with the Rosa26-LacZ reporter (R26R) strain (Soriano, 1999) to generate mice of all the genotypes of the above cohorts with an additional R26R gene. The R26R transgene consists of a loxP-flanked neomycin cassette in front of a lacZ reporter gene driven by the Rosa26 promoter, which under normal conditions is not expressed (Soriano, 1999). In the presence of Cre recombinase, the neomycin cassette is removed, allowing for expression of the reporter transgene. Tissue from the various cohorts produced in this mating were

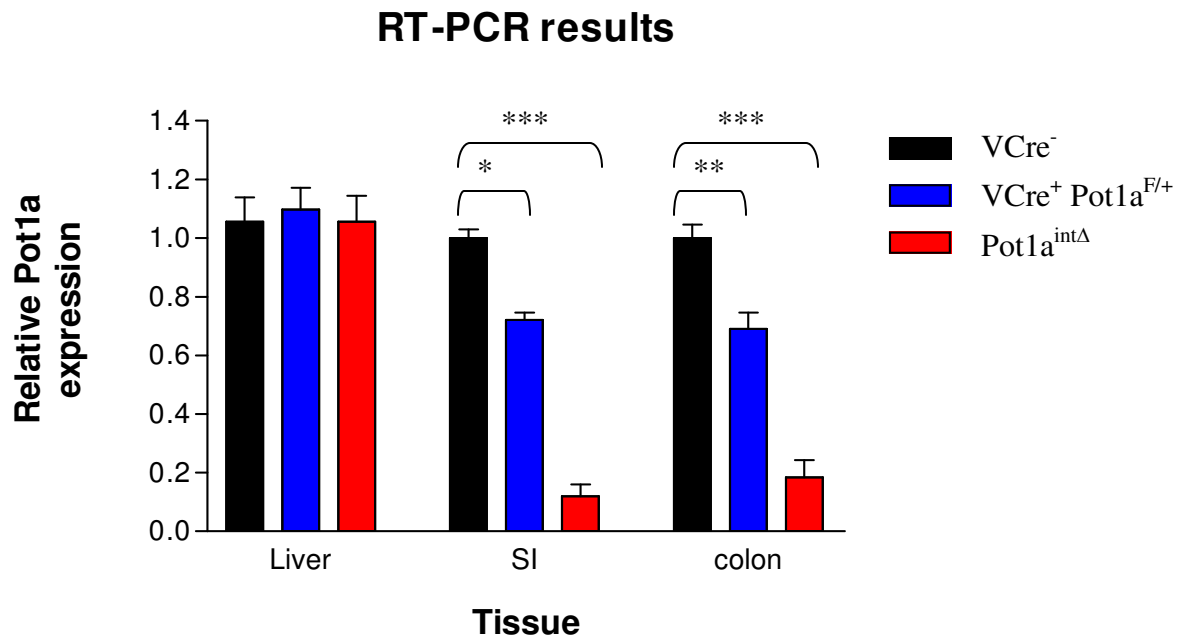


Figure 6: Villin-Cre expression leads to decreased expression of Pot1a mRNA in the intestines. RNA was extracted from liver tissue and intestinal scrapings from animals in the three cohorts. mRNA expression was analyzed through RT-PCR using Taqman probes specific for a region in exon 4 of the Pot1a gene. The above results show that animals with no VCre transgene (VCre⁻) did not show any changes in Pot1a expression. The VCre transgene in a Pot1a^{F/+} animal leads to a slight decrease in Pot1a expression in both the small intestine and the colon, but not in the liver. The expression of Pot1a is drastically decreased when both copies of Pot1a are deleted (Pot1a^{intΔ}). (*: p-value = 0.022; **: p-value = 0.012; ***: p-value <0.001) Tissue samples from three animals for each genotype were analyzed. RT-PCR reactions were performed in triplicate and normalized to GAPDH expression.

harvested and assayed for X-gal staining, which is an indicator of the lacZ gene expression leading to β -galactosidase (β -gal) activity. X-gal staining was only observed in mice that contained both the reporter transgene (R26R⁺) and the Villin-Cre transgene (VCre⁺) (Figure 7). Furthermore, in VCre⁺ R26R⁺ animals, blue staining was only seen the small intestines and colon, while other tissues, such as the kidney, heart, liver and stomach remained unstained (Figure 8).

Closer inspection revealed that β -gal activity was restricted to the epithelial cells of the GI tract, leaving the supporting stroma and muscularis mucosa unstained (Figure 8). Interestingly, Pot1a^{int Δ} intestines showed a decrease in staining intensity in both the small intestines and colon when compared to VCre⁺ controls, with some crypts completely devoid of X-gal staining (Figure 8, arrows). This suggests that VCre activity and as a result Pot1a deletion may not be complete in Pot1a^{int Δ} intestines.

Pot1a^{int Δ} mice have normal intestinal morphology, but increased apoptosis and anaphase bridges

Mice in the VCre, Pot1a colony were followed for up to 2 years. The majority of these mice lived up to two years without overt signs of illness suggesting that loss of Pot1a in the intestinal epithelium does not affect overall survival. Accordingly, Kaplan-Meier analysis of survival showed that lifespan was not significantly affected by Pot1a deletion (Figure 9). Late generation telomerase null mice with critically shortened telomeres show degenerative phenotypes in the intestines, such as villous blunting and crypt atrophy, which lead to weight loss (Begus-Nahrman et al., 2009; Rudolph et al., 1999). To determine if loss of Pot1a also results in these features, intestines were harvested from three month old animals and

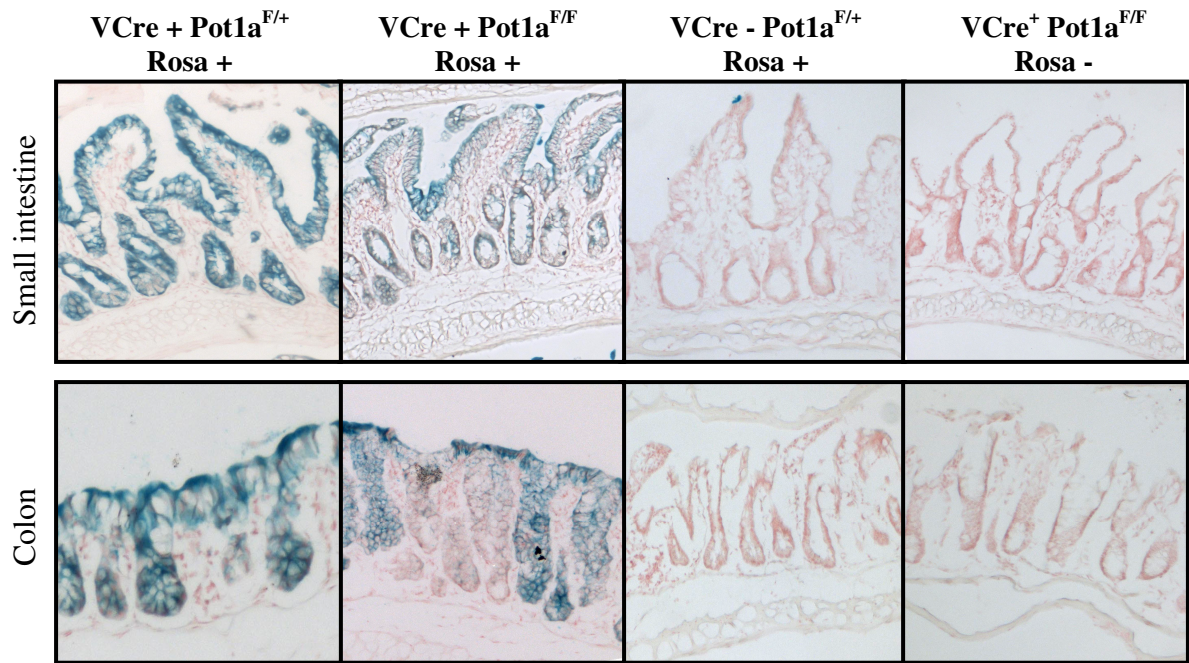


Figure 7: β -galactosidase activity is only detected in the intestines when both the Rosa26-LacZ (R26R) and the Villin-Cre (VCre) transgenes are present. To determine the distribution of Villin-Cre expression and indirectly determine where Pot1a is being deleted, mice from the VCre, Pot1a colony were crossed with the Rosa26-LacZ (R26R) reporter transgene. Cre recombinase activity activates the reporter gene, which can be detected through β -galactosidase (β -gal) activity. Intestines were collected from animals of various genotypes and assayed for β -gal activity. Positive activity is indicated by blue staining. Intestines that did not express the VCre transgene (VCre-) and mice that were R26R negative did not show any β gal activity. In contrast, VCre⁺ R26R⁺ mice showed β -gal activity in both the small intestines and colons. Two animals were examined per genotype.

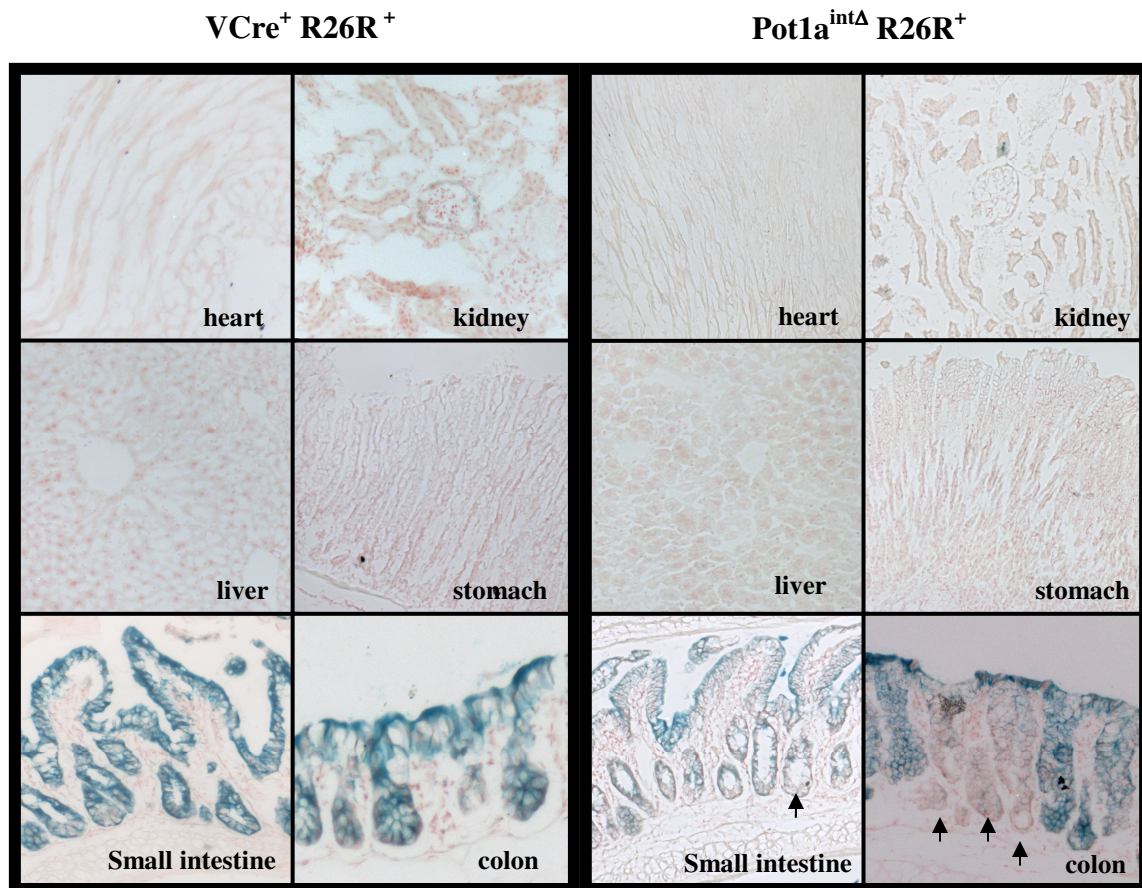


Figure 8: Villin-Cre activity is specific to the intestinal epithelium. β -gal activity was assayed in various organs of VCre⁺ Rosa⁺ mice. No activity was seen in the heart, kidney, liver or stomach of these animals. However, β -gal staining was readily visible in the small intestines and colon. Note that the staining in the Pot1a^{intΔ} Rosa26⁺ intestines is less intense than in the control samples. Furthermore, there seem to be entire crypts that do not stain for β -gal at all (arrow). These results suggest that intestinal deletion of Pot1a may not be complete in the Pot1a^{intΔ} animals. (Two animals for each genotype were examined.)

examined. Comparison of hematoxylin and eosin (H&E) stained sections from $Pot1a^{int\Delta}$ intestines to controls showed no villous blunting, no crypt atrophy, and no changes to the overall morphology of the intestines (Figure 10).

However, closer inspection revealed an increase in apoptotic cells in the crypts of Lieberkuhn (Figure 10), a characteristic that is seen in mice with telomere dysfunction (Begus-Nahrman et al., 2009; Cosme-Blanco et al., 2007; Wong et al., 2000). Examination of 500 crypts per sample, comparing four animals per genotype, showed that there was an 8-fold increase in apoptotic bodies in the $Pot1a^{int\Delta}$ animals compared to the $VCre^{-}$ controls (control: 0.076 ± 0.057 vs. $Pot1a^{int\Delta}$: 0.598 ± 0.119 , $p = 0.001$) (Figure 10). There was no significant difference between the $VCre^{-}$ and $VCre^{+}$ controls, suggesting that the phenotype is due to $Pot1a$ deficiency and not Villin-Cre expression. TUNEL staining was also performed to assay for apoptosis. Four animals per genotype were tested and 500 crypts per animal were examined. Quantification of TUNEL positive cells in the crypts revealed a 15-fold increase in the intestines of $Pot1a^{int\Delta}$ animals compared to the $VCre^{-}$ controls (control: 0.076 ± 0.072 vs. $Pot1a^{int\Delta}$: 1.22 ± 0.08 , $p = 0.001$) (Figure 11).

Dysfunctional telomeres can be improperly repaired by the generation of random fusions through the non-homologous ending joining (NHEJ) or homologous recombination (HR) pathway forming dicentric chromosomes. During anaphase, migration of the dicentric chromosomes to opposite poles can be seen as an anaphase bridge. These are readily visible in H&E sections and are used as an indication of telomere dysfunction in highly proliferative compartments, including the intestinal epithelium (Cosme-Blanco et al., 2007; Rudolph et al., 2001). To determine if $Pot1a$ deletion leads to telomere dysfunction in our model, H&E sections were examined for anaphase bridges (Figure 12). The number anaphase bridges

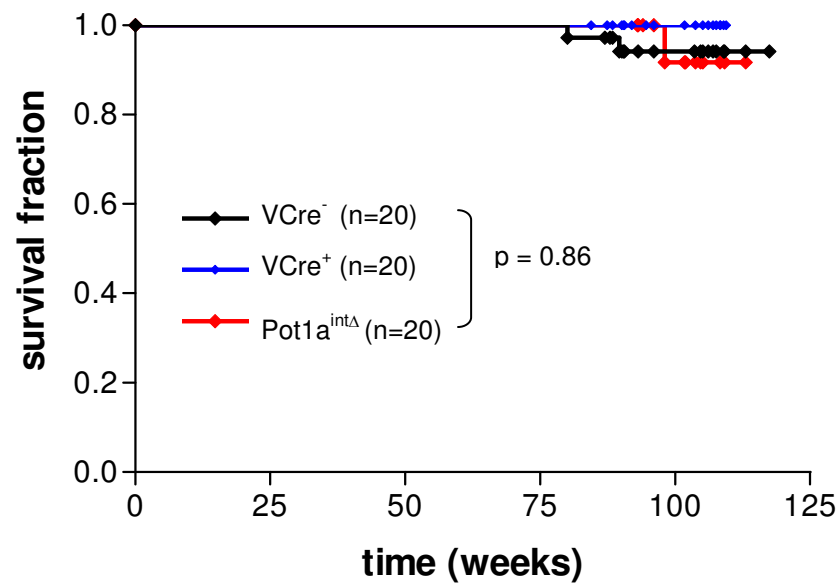


Figure 9: Intestinal deficiency of Pot1a does not affect overall survival. Mice in the VCre, Pot1a colony were followed for up to 2 years. Kaplan-Meier analysis of the cohorts show that Pot1a^{intΔ} mice survived at a rate comparable to controls.

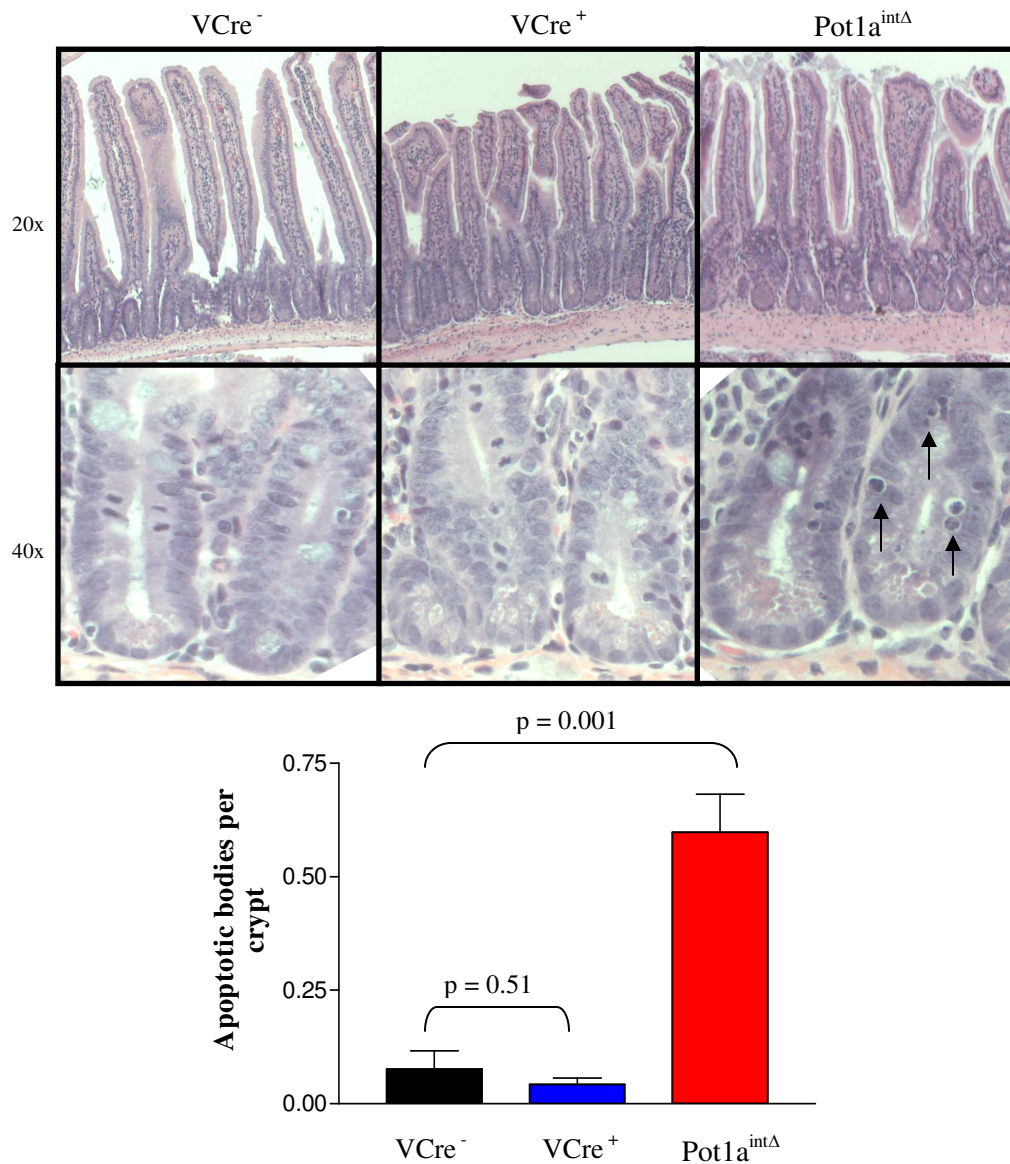


Figure 10: Loss of Pot1a does not affect the gross morphology of the intestinal epithelial, but increases apoptosis in crypts. Examination of H&E staining of intestines from 1-year old VCre, Pot1a animals showed that there is no appreciable difference in gross morphology. Closer examination of the intestinal crypts revealed that Pot1a^{intΔ} animals have an increase in apoptotic bodies. Quantification showed that there is 8-fold increase in apoptotic bodies in the Pot1a^{intΔ} compared to the VCre⁻ controls (0.076 ± 0.057 vs. 0.598 ± 0.119 , $p = 0.001$). Intestines from four animals per genotype were examined, and 500 crypts per animal were analyzed.

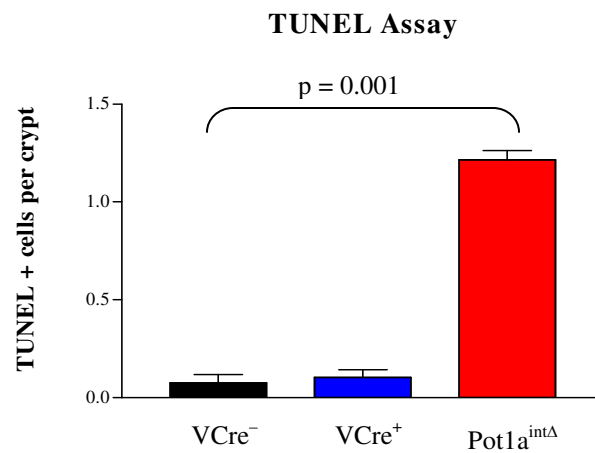
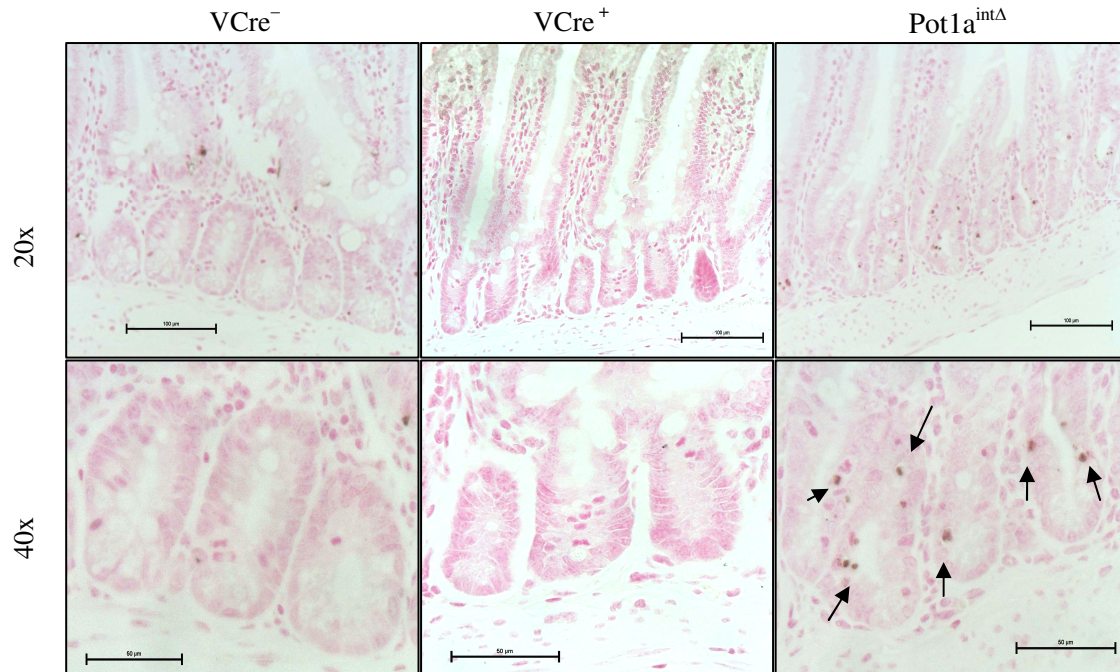


Figure 11: Pot1a deficiency leads to increased TUNEL positive cells in the intestinal crypts. TUNEL was performed on intestinal samples to detect apoptosis. TUNEL positive cells (arrows) were only detected in the intestines of Pot1a^{intΔ} animals. Furthermore, the increase in TUNEL positive cells was restricted to the crypts. No appreciable increase was seen in the villi. Intestines from four animals per genotype were examined, and 500 crypts per animal were analyzed.

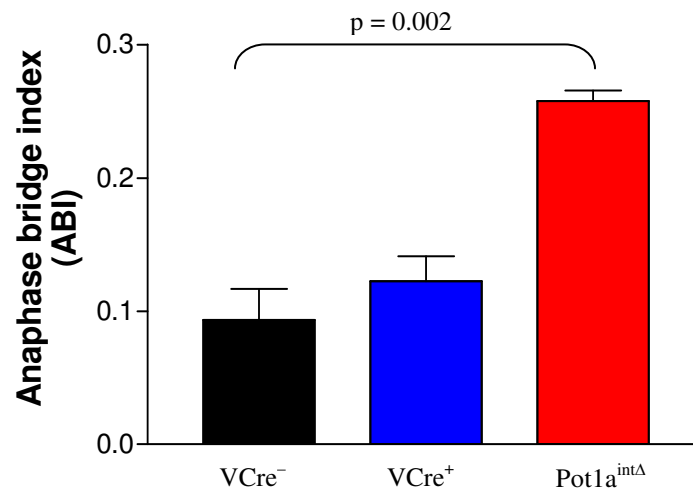
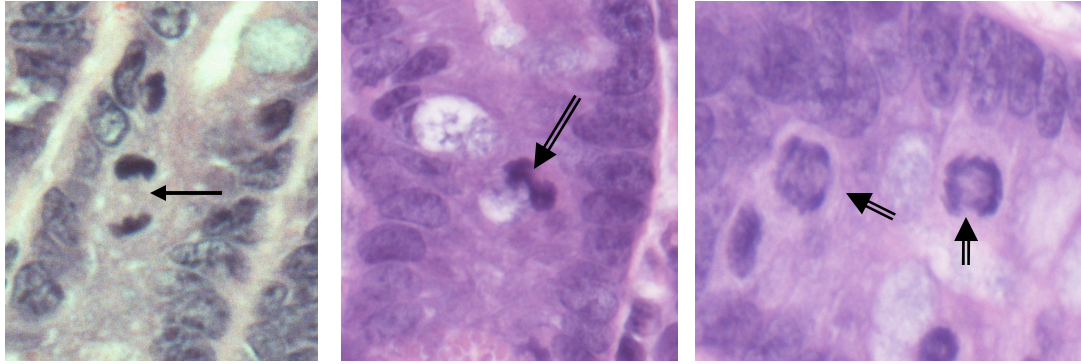


Figure 12: Anaphase bridges are a hallmark of telomere dysfunction. Dysfunctional telomeres can lead to chromosomal fusions that can be visualized as anaphase bridges. The upper panel shows a normal anaphase (single arrow) and several examples of anaphase bridging (double-line arrows). Quantification of the anaphase bridges in Pot1a^{intΔ} mice show a 2.5 fold increase in ABI as compared to VCre⁻ (0.258±0.008 vs. 0.093±0.023). Intestines from four animals per genotype were examined, and 500 crypts per animal were analyzed.

observed was divided by the total number of anaphase seen to determine the anaphase bridge index (ABI). Quantification of the anaphase bridges in $Pot1a^{int\Delta}$ mice show a 2.5 fold increase in ABI as compared to $VCre^-$ (0.258 ± 0.008 vs. 0.093 ± 0.023 , respectively; $p=0.002$) (Figure 12).

Taken together, these results indicate that while $Pot1a^{int\Delta}$ mice do not show the same overt intestinal degeneration, $Pot1a$ deficiency leads to phenotypes in the crypts of Lieberkuhn that recapitulate those observed in telomerase null animals with critically shortened telomeres, including increased apoptosis and anaphase bridges.

Pot1a deficiency leads to increased activation of p53 and p21

Similar to severe telomere attrition, loss of $Pot1a$ activates a potent DNA damage response that triggers p53-dependent cellular senescence in cell culture (Wu et al., 2006). p53 is also a potent inducer of apoptosis in mouse models of telomere shortening (Chin et al., 1999). To determine if loss of $Pot1a$ also activates p53 in our model, IHC was performed on paraffin-embedded intestine sections (Figure 13). Comparison of four animals per genotype and 500 crypts per animal revealed that intestines from $Pot1a^{int\Delta}$ mice show a 10-fold increase in p53 positive cells as compared to $VCre^-$ controls ($Pot1a^{int\Delta}$, 0.362 ± 0.068 ; $VCre^-$: 0.003 ± 0.0008 ; t-test, $p=0.006$). In fact, little to no p53 staining was seen in either $VCre^-$ or $VCre^+$ controls, again confirming that these phenotypes are due to loss of $Pot1a$ instead of Villin-Cre expression.

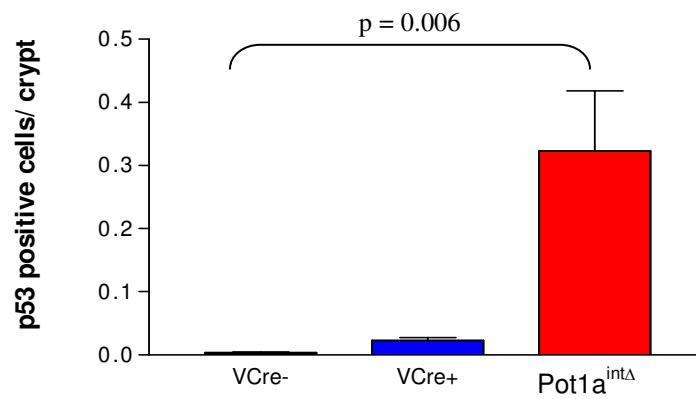
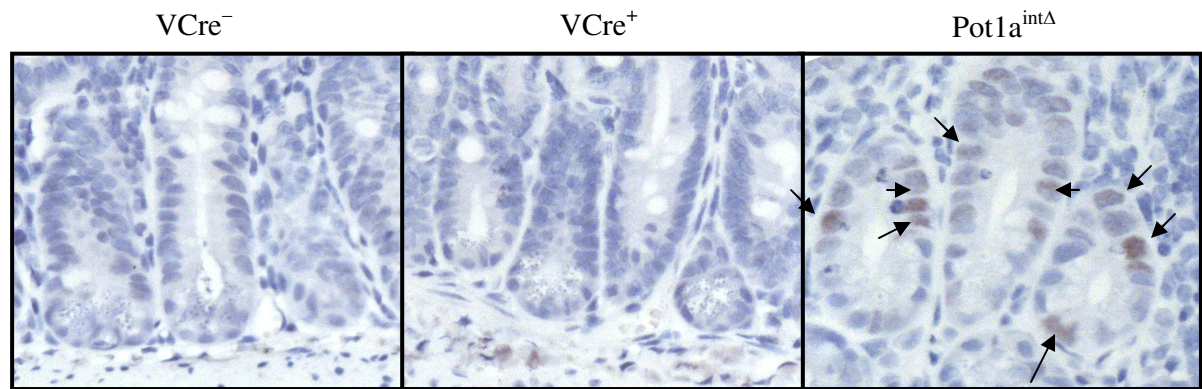


Figure 13: Loss of Pot1a activates p53 in the intestinal crypts. p53 is a major mediator of apoptosis that is also activated in response to telomere dysfunction. IHC staining for p53 was performed to determine if this response could be observed. Cells staining positively for p53 (arrows) were seen almost exclusively in the intestinal crypts of the Pot1a^{intΔ} mice. Intestines from four animals per genotype were examined, and 500 crypts per animal were analyzed.

p21 is potent inducer of cell cycle arrest during cellular senescence triggered by telomere attrition (Herbig et al., 2004) and Pot1a loss in cultured cells (Wu et al., 2006). p21 is also a downstream target of p53 that is also activated in response to telomere dysfunction in late generation telomerase null mice (Choudhury et al., 2007). IHC to assay for p21 expression was performed to determine if the increased expression of p53 seen above also leads to upregulation of p21 (Figure 14). Indeed, intestines from Pot1a^{intΔ} mice show an 8-fold increase in p21 expression over VCre⁻ controls (3.98±1.08 vs. 0.54±0.15, respectively; t-test; p = 0.006). Four mice from each cohort were examined and 500 crypts from each sample were analyzed.

These results indicate that Pot1a deficiency leads to the activation of p53 and its downstream effector, p21. Taken together with the previous section, these data suggest that loss of Pot1a activates p53 leading to apoptosis or p21 activation and senescence, similar to cells and mice with severe telomere attrition or Pot1a deficient cells (Figure 4).

Loss of Pot1a leads to activation of a telomere-induced DNA damage response

Pot1a binds to the single-stranded G-rich telomeric overhang to protect it from activating a DNA damage response mediated by ATR (Denchi and de Lange, 2007; Guo et al., 2007). Loss of Pot1a is thought to expose the overhang to RPA binding, which recruits ATR/ATRIP. These proteins trigger the DDR pathway by phosphorylating and recruiting factors like the phosphorylated histone variant H2AX (γ -H2AX), the mediator of DNA damage checkpoint1 (MDC1), and p53 binding protein 1 (53BP1) (Shiloh, 2003). These proteins accumulate at the sites of damage and along the surrounding chromatin, and can be readily visualized through fluorescence microscopy as DNA damage foci. To assess damage

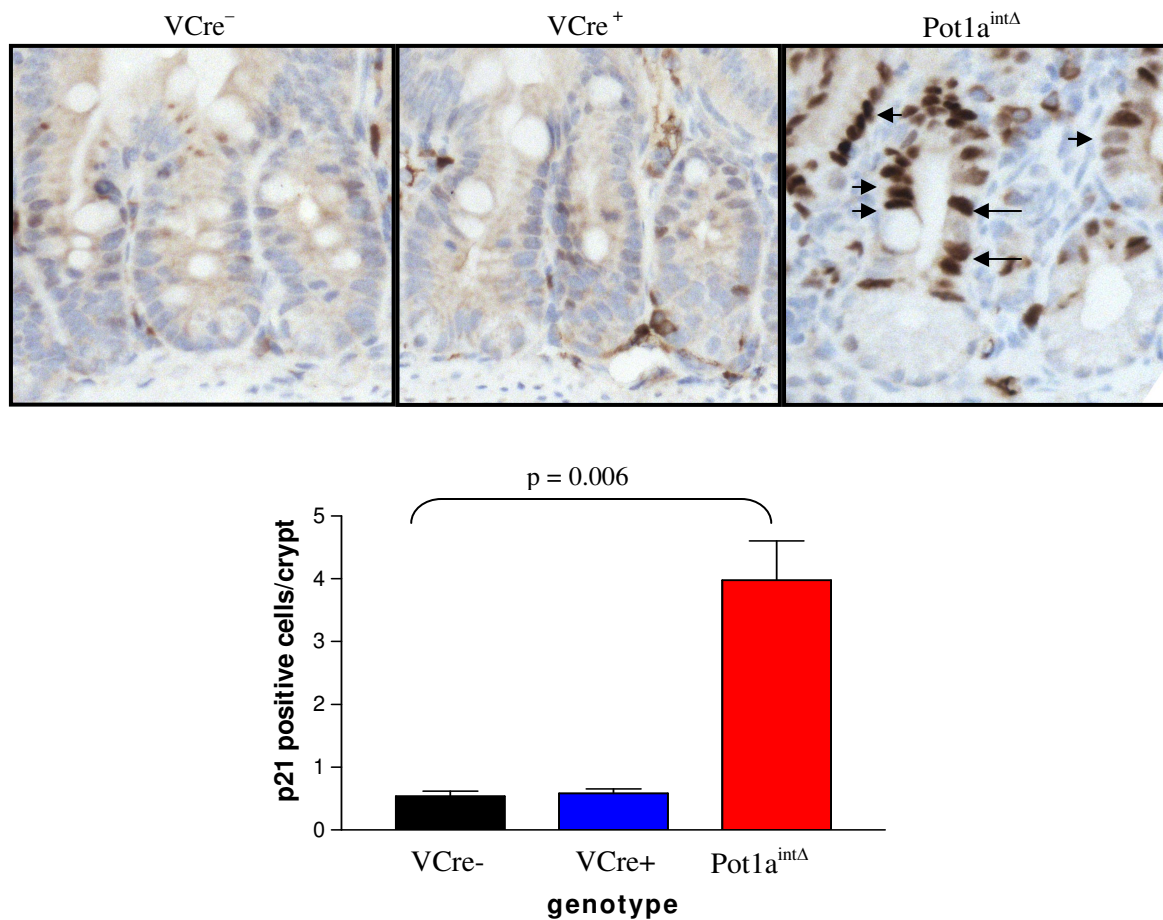


Figure 14: Loss of Pot1a leads to upregulated p21 expression in the intestines. p21 is a downstream target of p53 and is thought to be involved in triggering senescence in response to telomere dysfunction. IHC of intestinal sections show an increase in p21 positive nuclei (arrows) in $\text{Pot1a}^{\text{int}\Delta}$ crypts. Quantification (graph) reveals almost an 8-fold increase in p21 expression in mice that have lost Pot1a. Intestines from four animals per genotype were examined, and 500 crypts per animal were analyzed.

signaling at telomeres, an invaluable experimental tool based on this property has been used extensively. Telomere-induced damage foci (TIFs)(Takai et al., 2003) are fluorescently-labeled DNA damage protein markers, such as γ -H2AX or 53BP1, that co-localize to dysfunctional telomeres, which are also marked by fluorescently-labeled telomeric nucleotide probes or shelterin proteins. We assayed for TIFs in paraffin-embedded tissues through double immunofluorescent staining for γ -H2AX (green) and the telomere binding protein, mTRF2 (red) (Figure 15). Sections were examined through fluorescence or confocal microscopy. Nuclei with three or more co-localized foci were scored as TIF positive. Examination of intestinal sectionals revealed that TIF positive cells were found exclusively in the crypts of Lieberkuhn; no TIFs were seen in the villi (Figure 16). Comparison of the different cohorts showed that TIF positive cells were found mostly in Pot1a^{intΔ} crypts, which had 10-fold more TIF positive cells than VCre- controls (26.4 ± 7.4 vs. 2.2 ± 0.8 TIF positive cells per 100 nuclei, respectively; t-test; $p=0.005$). These results indicate that deletion of Pot1a elicits a DNA damage response in the intestinal crypts.

Intestinal Pot1a deficiency does not affect response to gamma-irradiation

The results above have shown that loss of Pot1a induces a DNA damage response in the intestinal epithelium leading to increased cell cycle arrest and apoptosis. Although these features do not appear to lead to degenerative phenotypes, we postulated that chronic DNA damage may have an effect on the stem cell reserve of the intestines. To determine whether this mechanism of telomere dysfunction has an effect on the regenerative capacity of the intestines, we subjected mice in the Villin-Cre, Pot1a colony to whole body gamma irradiation (IR), which would deplete the epithelial layer.

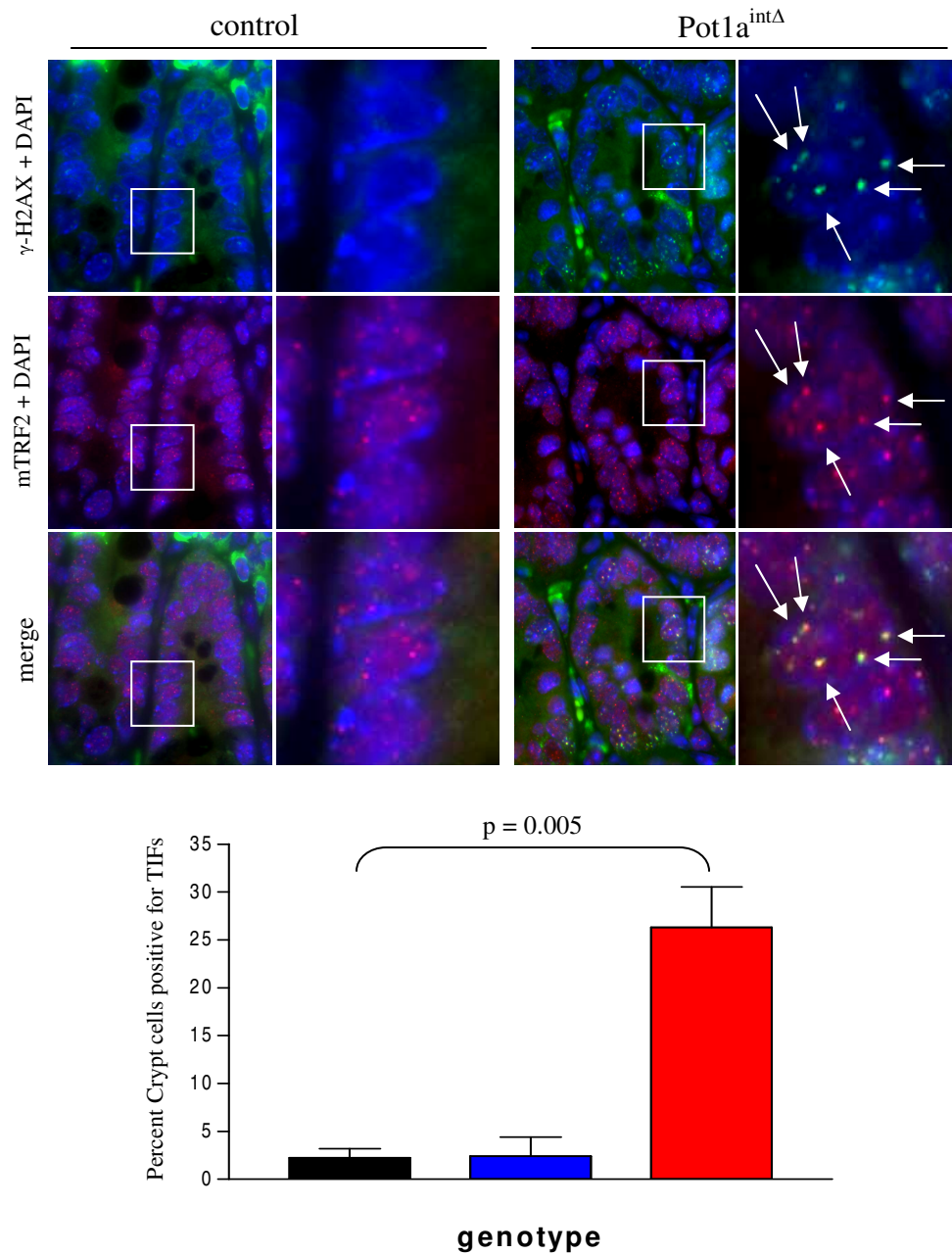


Figure 15: Loss of Pot1a activates a DNA damage response in the intestines. Telomere-induced damage foci (TIFs) are formed when markers of DNA damage, such as γ -H2AX (green) colocalize to sites of dysfunctional telomeres (marked by mTRF2 (red)). Cells with three or more foci are considered TIF positive. Double IF staining of intestinal sections demonstrate that Pot1a^{intΔ} crypts contain ten-fold more TIF positive cells than controls. Intestinal crypts from four animals per genotype were examined, and 1000 nuclei per animal were analyzed.

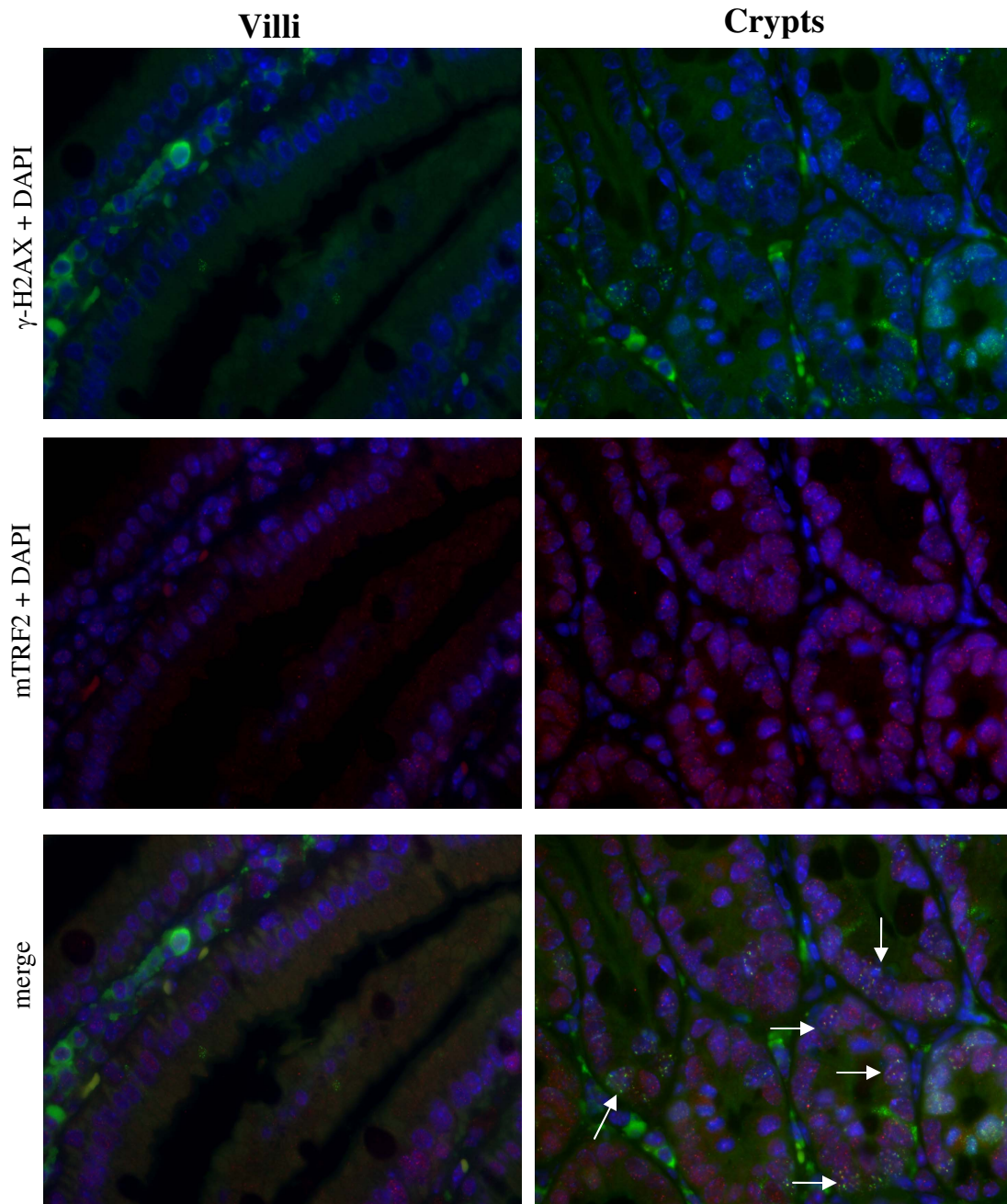


Figure 16: DNA damage is only observed in cells of the crypts. Double IF staining of intestinal sections to assay for telomere-induced damage foci (TIFs). γ -H2AX serves as a marker of DNA damage (green), while mTRF2 serves as a marker for telomeres (red). The left panel shows pictures of a villus, while the right panel shows crypts. Several TIF positive cells are indicated by white arrow.

In the first experiment, two groups of 10-week old mice were subjected to whole body IR. At a dose 4Gy, there seemed to be no difference between the responses of the two genotypes as all the animals survived more than 40 days (Figure 17, solid lines). Next, we increased the dose and exposed a second set of 10-week old animals to a higher dose of radiation (8Gy). This dose proved to be lethal as animals in both cohorts did not survive for more than three weeks after exposure. A comparison of the survival curves showed that there was no significant difference between survival among animals that were deficient in Pot1a compared to wild-type (Figure 17, dashed lines).

One possible reason for the lack of difference may be the age of the mice. Despite the increased apoptosis that would put a strain on stem cell reserve, perhaps the intestines of 10-week old animals have not been challenged enough by the telomere dysfunction to significantly deplete the reserve of such a proliferative organ. The experiment was repeated in animals that were aged to one year. These mice were exposed to a 6Gy dose of radiation. Similar to previous results with a 4Gy dose, all the animals survived longer than 40 days (Figure 18A). Surprisingly, comparison of the intestinal morphology of animals at one and four days after radiation exposure also did not show any significant difference (Figure 18B). These results suggest that the Pot1a^{intΔ} mice responded to radiation in a similar fashion as the wild-type controls.

Discussion

We sought to create a mouse model of telomere dysfunction in the gastrointestinal tract through the targeted deletion of Pot1a. To achieve this, we crossed a conditional Pot1a knockout mouse with the Villin-Cre transgenic mouse that only expresses the Cre

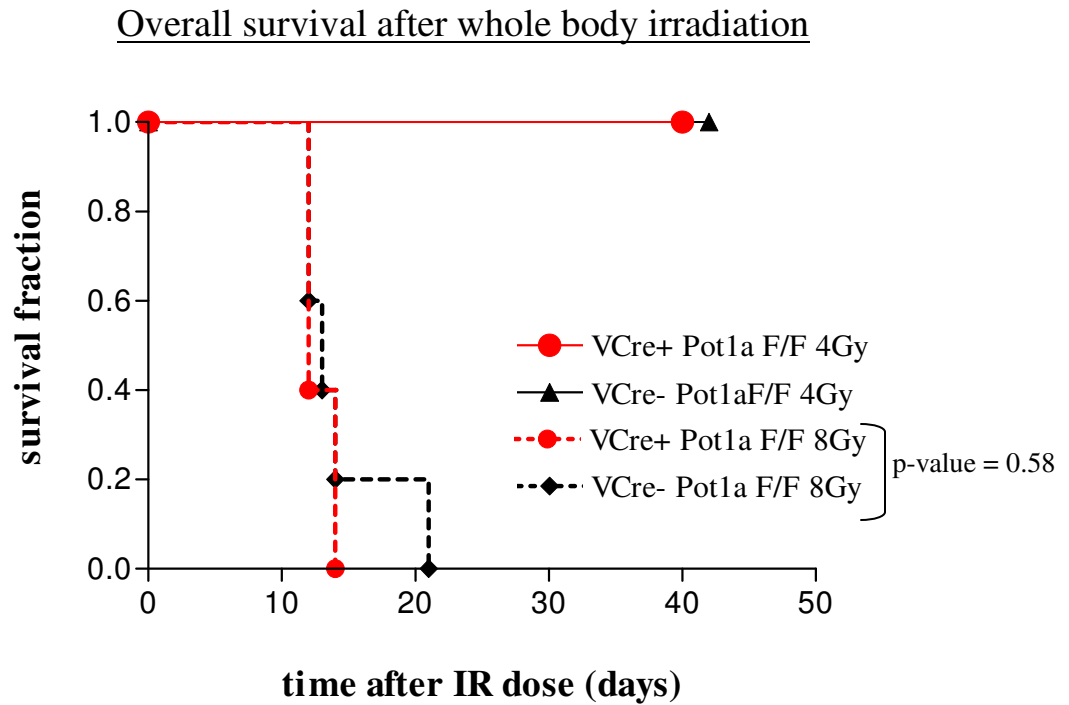


Figure 17: Pot1a deficiency in the intestines does not affect survival of 3-month old animals after irradiation. Whole body irradiation was given at a dose of 4Gy to 3-month old animals. The treatment did not affect survival of control or Pot1a^{intΔ} mice (solid lines) as they all survived for over 40 days. When the dose was increased to 8Gy, none of the irradiated animals survived longer than 3 weeks. However, there was no significant difference between the survival of the Pot1a^{intΔ} mice as compared to control mice (dashed lines).

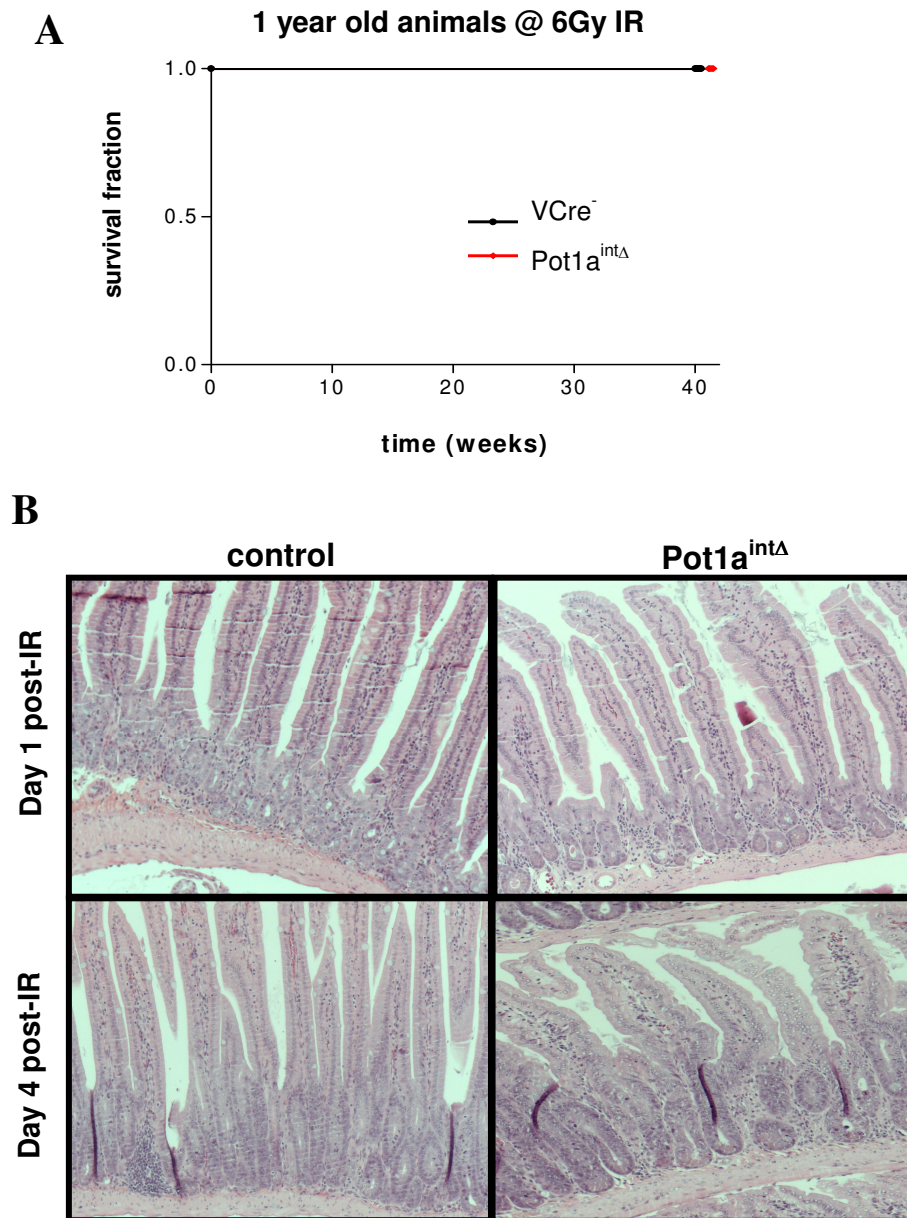


Figure 18: Pot1a deficiency does not affect intestinal response to irradiation. One year old animals were exposed to 6Gy of γ -irradiation (n=6 for both groups). All animals survived at least 40 weeks (Panel A). Intestines of one year old mice exposed to 6Gy doses of irradiation were examined one and four days after treatment (Panel B). Surprisingly, analysis of H&E staining shows little effect on the intestines at both time points, irrespective of Pot1a status.

recombinase in the GI tract. Our data show that despite the fact that loss of Pot1a in cell culture is toxic, leading to cellular senescence, mice with homozygous loss of Pot1a in the intestines (Pot1a^{intΔ}) were viable and born at expected the expected Mendelian ratios. Pot1a deletion was verified indirectly through genomic PCR. However, the appearance of the delta band did not correlate with the disappearance of the floxed band. This result may be explained by the fact that Villin-Cre is only expressed in the epithelial layer, as demonstrated by the X-gal staining. There are many different cell types in the intestines in addition to the epithelial layer, including the surrounding stromal cells that support the epithelium, endothelial cells that make up the capillaries and lymphatic vessel in each villus, and lymphocytes. Although intestinal scrapings were performed to enrich epithelial cells from the supporting submucosa and muscle wall, these other cells could not be separated and may contribute to the amplification of the flox band.

Interestingly, X-gal staining in VCre, Pot1a, R26R⁺ mice demonstrated that Cre activity was restricted to intestinal epithelial cells. However, qualitative comparisons of staining suggested that β -gal activity was not equal in Pot1a^{intΔ} R26R⁺ mice as compared to VCre⁺ R26R⁺ controls. The staining was in fact weaker throughout the crypt-villus axis in Pot1a^{intΔ} intestines, and some crypts did not stain for X-gal at all. This result may prove to be significant as it suggests that Pot1a may not be completely deleted in these intestines.

The VCre, Pot1a colony was followed for over two years, and there was no difference in overall survival between mice with Pot1a loss and controls. Comparison of intestinal morphology also revealed no appreciable difference in gross morphology. However, closer examination revealed that loss of Pot1a leads to various microscopic changes in the intestinal epithelium. Pot1a deletion leads to increased apoptotic cells in the crypts, as well as

upregulation of p53 and p21 expression. Finally, Pot1a deletion leads to increased cells with TIFs, an indicator of activation of the DDR in response to dysfunctional telomeres. These data correspond to previous work in cell culture, which has shown that deletion of Pot1a leads to a DNA damage response, which activates p53 to trigger cell cycle arrest through p21 or apoptosis(Wu et al., 2006). Late generation telomerase null animals with critically short telomeres have also shown the same features in intestinal crypts(Choudhury et al., 2007; Rudolph et al., 1999). Taken together, we have generated a model of telomere dysfunction through Pot1a disruption in the gastrointestinal tract that has similar microscopic features as mouse models of telomere attrition.

However, our model does not show the overall morphological features of critical telomere shortening, such as blunting or atrophy of villi(Rudolph et al., 1999). The β -gal staining result on the reporter mice may provide some insight to this result. Given the apoptosis results, one possible explanation is that Pot1a deficient cells are being culled from the crypts through p53-dependent apoptosis, while the cells that have retained some Pot1a expression due to incomplete deletion of the two conditional alleles or complete inactivation of the Cre recombinase are populating the villi. This phenotype has been described previously in mice that have intestinal specific Mdm2-deficiency(Valentin-Vega et al., 2008). Mdm2 is a potent inhibitor of p53, and its loss in mice leads to p53-dependent apoptosis and consequently embryonic lethality(Montes de Oca Luna et al., 1995). Even conditional deletion of Mdm2 in tissues, such as the heart and nerve cells, cannot produce viable animals(Grier et al., 2006; Xiong et al., 2006). However, the intestine is able to compensate for such toxic insults by selecting for cells that have lost the VCre transgene and have intact Mdm2 activity(Valentin-Vega et al., 2008). It is possible that our model is

behaving similarly to the Mdm2, with the cells that have lost or reduced Cre expression surviving to populate the villi and prevent degenerative phenotypes.

THE EFFECT OF POT1A DEFICIENCY ON ESTABLISHED MOUSE MODELS OF GI TUMORS

Because of the potent DNA damage response that is elicited in response to Pot1a deficiency and the subsequent activation of p53, p21 and apoptosis in the intestines of the VCre, Pot1a animals, we postulate that loss of Pot1a will be tumor suppressive *in vivo*. The mTerc null mouse has been used in multiple cancer models to show that critically short telomeres are tumor suppressive (Cosme-Blanco et al., 2007; Farazi et al., 2003; Feldser and Greider, 2007; Gonzalez-Suarez et al., 2000; Greenberg et al., 1999; Khoo et al., 2007; Rudolph et al., 2001; Wong et al., 2003) (Table 2). For example, late generation telomerase null mice are resistant to skin tumors induced by the DMBA/TPA chemical skin carcinogenesis model (Gonzalez-Suarez et al., 2000). Also, in the APC^{min} intestinal carcinoma mouse model, mice with critically short telomeres showed improved survival with a decrease in macroscopic adenoma formation compared to mice with intact telomeres (Rudolph et al., 2001). To determine if loss of Pot1a in the intestines is also tumor suppressive, we combined our Villin-Cre, Pot1a mouse with two separate models of intestinal cancer: the APC^{min} mouse or the chemical colitis-induced model of colorectal cancer.

The effect of Pot1a-induced telomere dysfunction on the APC^{min} genetic model of intestinal tumorigenesis

Mutations in the adenomatous polyposis coli (APC) gene are responsible for intestinal tumor syndrome called familial adenomatous polyposis (FAP) and found in 34-

Table 2: Shortened telomeres (*Terc*^{-/-}) reduce tumor incidence in mouse models of cancer

Gene or treatment	Tumor phenotypes	Effect of dysfunctional telomeres	Ref.
<i>APC^{min}</i>	Multiple intestinal neoplasia (MIN).	<u>increase</u> in (microadenomas) <u>decreased</u> size and number of macroadenomas	Rudolph, Millard et al. 2001
Alb-uPA	hepatocellular carcinoma (HCC)	<u>decreased number and size</u> of liver nodules.	Farazi, Glickman et al. 2003
<i>PMS2</i>	Lymphomas, sarcomas, and colon carcinomas	<u>reduced</u> the incidence of all three tumors types.	Siegl-Cachedenier, Munoz et al. 2007
<i>Em-myc</i>	Burkitt's lymphoma.	Formation of lymphoma was almost completely suppressed for two years in mice with dysfunctional telomeres (G5/G6)	Feldser and Greider 2007
<i>ATM</i>	Thymic lymphoma	<u>Delayed onset</u> and <u>decreased incidence</u> of thymic lymphomas	Qi, Strong et al. 2003; Wong, Maser et al. 2003
DMBA/TPA Treatment	Squamous cell carcinomas (SCC) of the skin	Decreased growth rate and size of papillomas, with a slight decrease in numbers. G5 mice with dysfunctional telomeres were almost completely Resistant to papilloma formation.	(Gonzalez-Suarez, Samper et al. 2000)
CCl₄ or DEN treatment	Hepatocellular carcinoma (HCC)	<u>Decreased number and size</u> of liver nodules.	(Farazi, Glickman et al. 2003)

72% of sporadic colorectal cancer(Takayama et al., 2006). In the APC^{min} mouse model, loss of the wildtype copy of the APC allele results in mice with multiple intestinal neoplasia, at 100% penetrance. Previous results from the mTerc^{-/-}, APC^{min} mouse, showed that critically short telomeres improved overall survival of these mice by suppressing the progression of microadenoma to macroadenoma, and impairment of macroadenoma growth(Rudolph et al., 2001). This is thought to be due to telomere-induced p53-dependent apoptosis or senescence, as the anaphase bridge index, p53 staining and apoptotic index is all increased in the late generation mutant mice(Rudolph et al., 2001). To determine if telomere dysfunction due to loss of Pot1a will have the same effect, the Villin-Cre, Pot1a mice were crossed with the APC^{min} mice to produce the following three cohorts: VCre⁻ APC^{min}, VCre⁺ APC^{min}, and Pot1a^{intΔ} APC^{min}.

These mice were followed and monitored for signs of intestinal tumor burden, including abdominal distention, anemia, cachexia and rectal prolapse. Moribund animals were euthanized and intestines were harvested and examined. Tumors were mostly round sessile adenomas, and the size (longest dimension) and number were noted. Animals developed between 29 and 76 tumors, and ranged in size from 1mm to 6mm. To simplify quantitation, tumors were divided into three size categories: less than 2mm, 2-4mm, and greater than 4 mm. Comparison of the three cohorts revealed that there was no significant difference in the number of tumors formed in each size category, nor in the total number of found (Figure 19, Table 3). These results suggest that unlike late generation telomerase null mice, Pot1a deficiency is not tumor suppressive.

Since telomere dysfunction due to Pot1a loss did not affect tumor formation, we examined the histological features of the tumors formed in each cohort to determine if there

Tumor distribution in VCre, Pot1a, APC cohorts

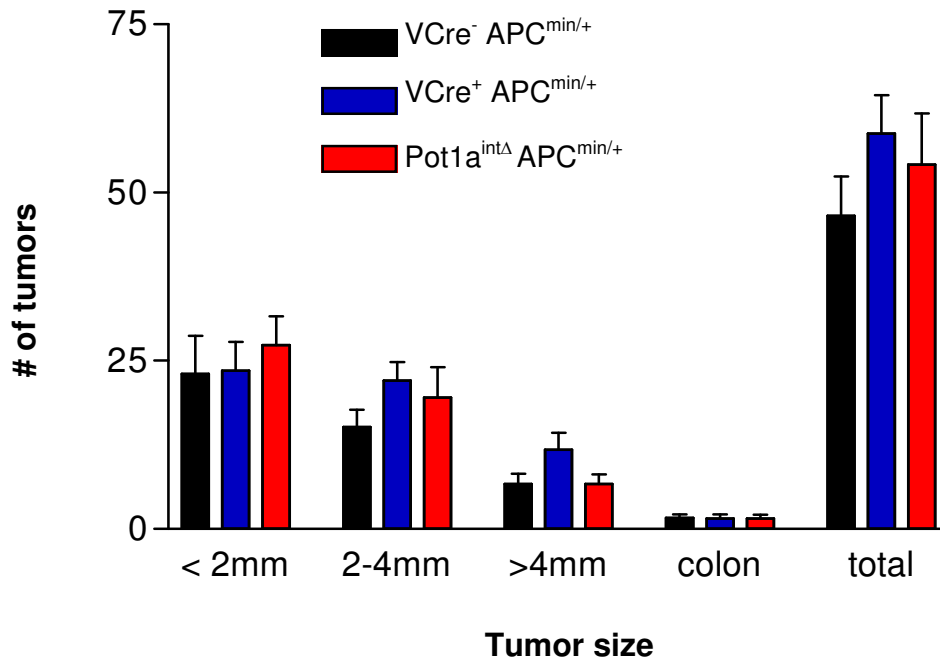


Figure 19: Loss of Pot1a does not affect the number or size of tumors in APC^{min}. The number and size of tumors found in the intestines of mice from the various Pot1a, APC cohorts were recorded on dissection of moribund animals. Tumors from the small intestine were divided into three size categories, while the few colon tumors that formed were lumped together. Comparison of the cohorts revealed no significant difference between the total number or predominant sizes of tumors found in each cohort.

Table 3: Summary of average tumors burdens for each cohort

Cohort/ Tumor size	VCre⁻ APC^{min/+}	VCre⁺ APC^{min/+}	Pot1a^{intΔ} APC^{min/+}
< 2mm	23.0 ± 14.0	23.5 ± 8.6	27.3 ± 10.4
2 – 4mm	15.2 ± 6.2	22.0 ± 5.6	19.5 ± 11.1
> 4mm	6.7 ± 3.8	11.8 ± 5.1	6.7 ± 3.5
Colon	1.7 ± 1.2	1.5 ± 1.3	1.5 ± 1.5
total	46.5 ± 14.4	58.8 ± 11.4	54.2 ± 18.7

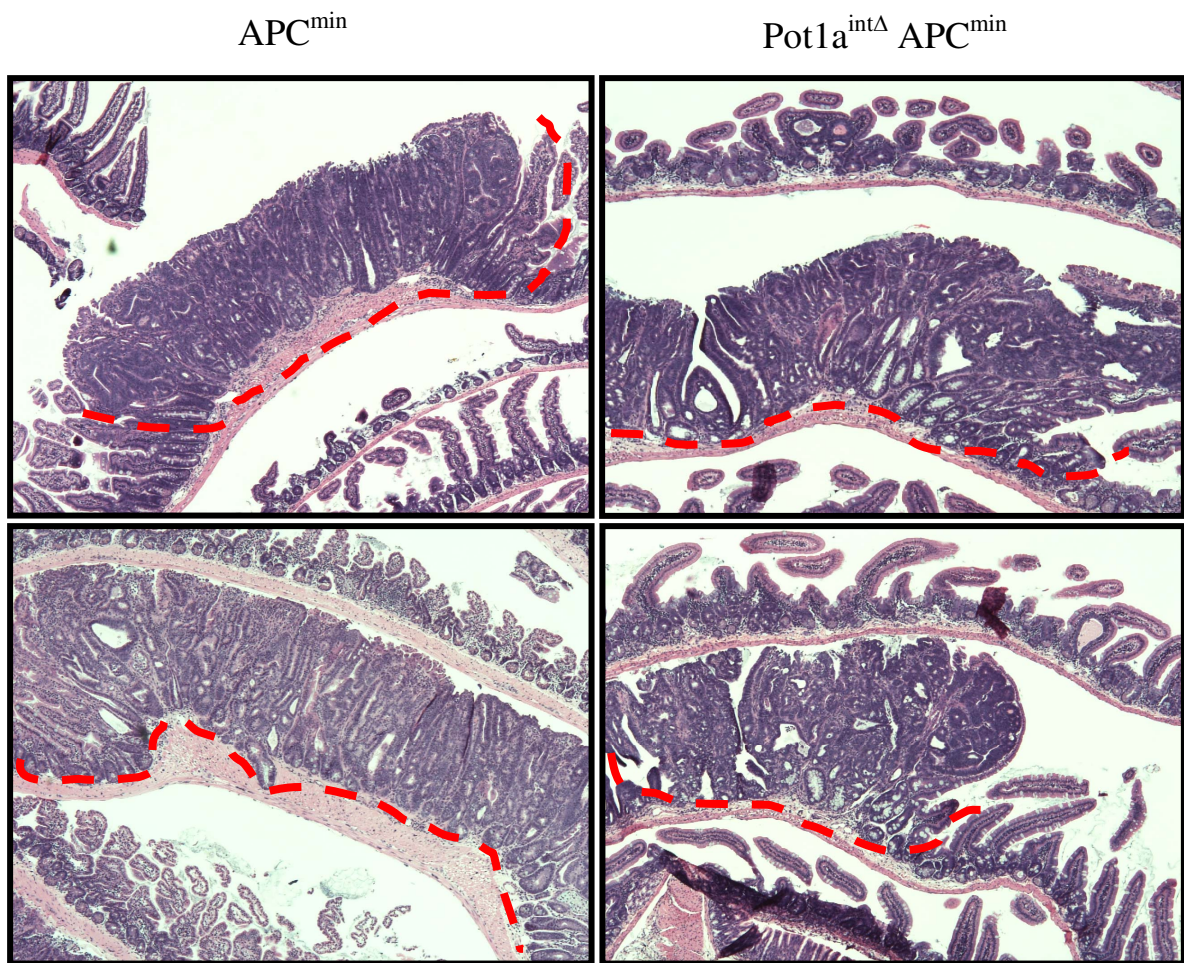


Figure 20: $Pot1a$ loss does not affect the tumor type or grade in APC^{min} mice. Comparison of H&E staining of intestinal sections from $Pot1a^{int\Delta} APC^{min}$ and APC^{min} mice reveal no histological differences between the two groups. Both develop well-differentiated adenomas with no invasion. Areas of tumors are outlined by red-dashed line.

was a difference in the type or grade of tumor formed. H&E staining of paraffin embedded sections revealed that mice from all three cohorts developed benign well-differentiated adenomas. There were no signs of invasion or metastasis, and overall no significant histological difference appreciated between tumors from $Pot1a^{int\Delta} APC^{min}$ mice and controls (Figure 20). This result suggests that $Pot1a$ deficiency does not affect the grade of tumor that is formed in the APC^{min} background.

While $Pot1a$ deficiency did not affect the type and grade of tumor formed, it appeared to have an effect on overall survival. Kaplan-Meier analysis of overall survival was performed (Figure 21) and $Pot1a^{int\Delta} APC^{min}$ mice showed a significant reduction in lifespan, with a median survival of 16.3 weeks and compared to 25 weeks in control $VCre^{-} APC^{min}$ mice (t-test, $p = 0.0012$). This result suggests that loss of $Pot1a$ leads to decreased survival in the APC^{min} colony.

Since there was no appreciable difference between the tumor burden for each cohort at death, we hypothesized that perhaps tumor formation was occurring earlier in $Pot1a^{int\Delta} APC^{min/+}$ mice. To determine if this was the case, we surveyed five mice from the $VCre^{-} APC^{min/+}$ and the $Pot1a^{int\Delta} APC^{min/+}$ cohorts at an early timepoint (12 weeks) for tumor formation. The number of tumors visualized on dissection was noted and categorized by size for each animal as described above (Figure 22A). Statistical analysis of each size category revealed that while the total number of tumors was not significantly increased in $Pot1a^{int\Delta} APC^{min/+}$ mice, these mice did have larger tumors at earlier timepoints (Figure 22B). These data suggest that the reason for decreased survival in $Pot1a^{int\Delta} APC^{min/+}$ mice is that $Pot1a$ deficiency accelerates tumor formation in the APC^{min} background.

Overall survival of VCre, Pot1a, APC^{min} animals

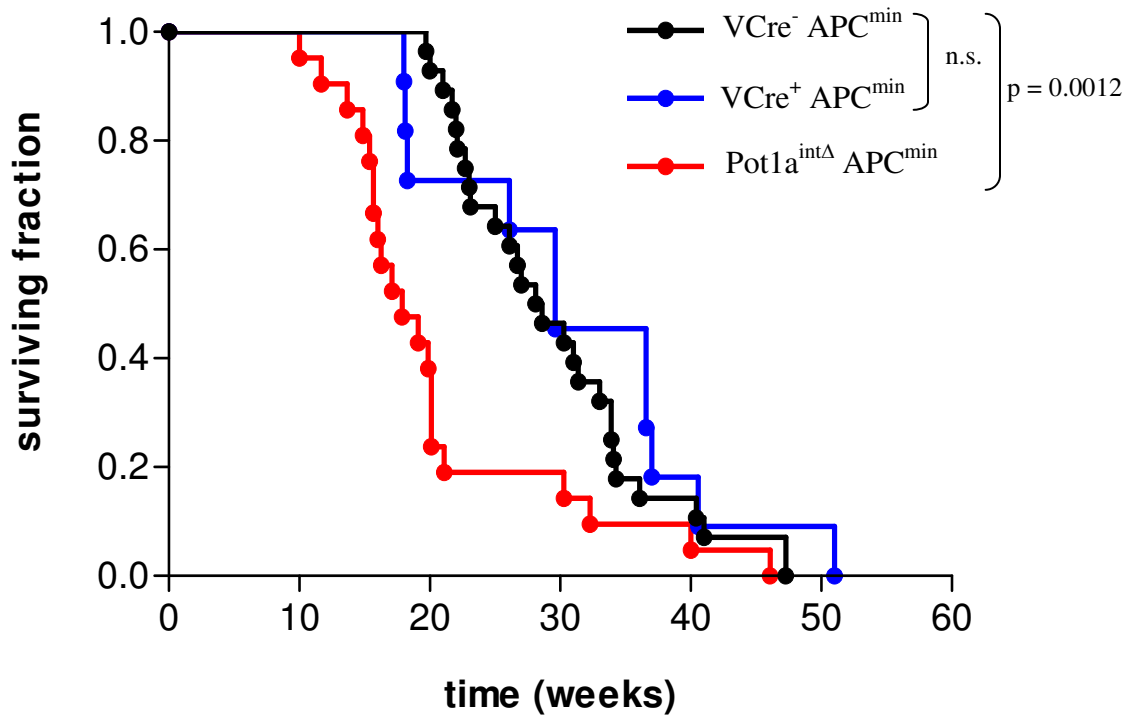


Figure 21: Intestinal depletion of Pot1a leads to decreased overall survival in APC^{min} mice. The VCre, Pot1a mice were crossed with APC^{min} mice to determine the affect of loss of Pot1a on this mouse model of intestinal tumorigenesis. Surprisingly, Pot1a^{intΔ} APC^{min} (red line) leads to earlier death than VCre⁻ APC^{min} controls (black line), with a median life span of 16.3 weeks vs. 25.0 weeks, respectively. VCre⁺ controls (blue line) showed no significant difference when compared to VCre⁻ controls. (n=27 animals for VCre⁻ APC^{min}; n=12 for VCre⁺; and n=20 for Pot1a^{intΔ} APC^{min}.)

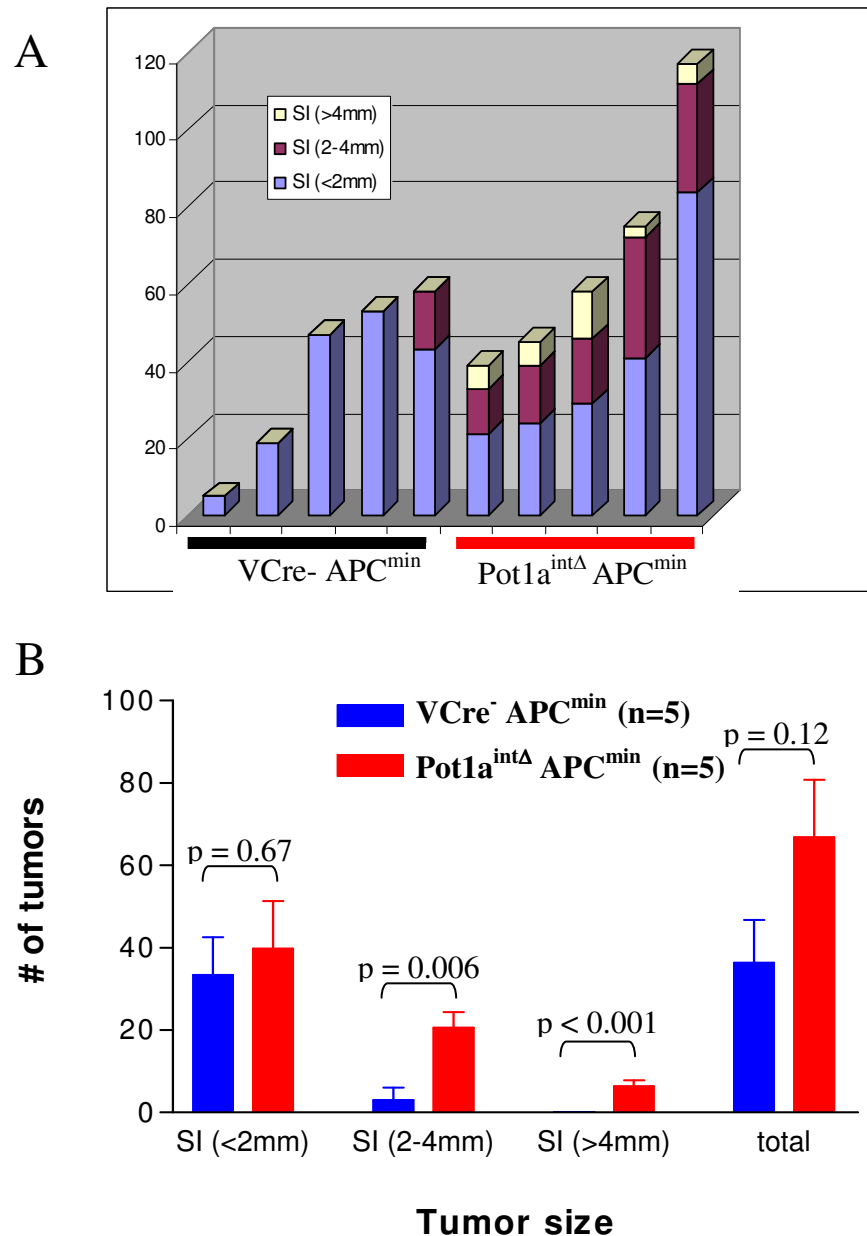


Figure 22: Pot1a^{intΔ} APC^{min} animals form large tumors earlier than control mice. To determine why Pot1a^{intΔ} APC^{min} animals died earlier than control mice, five mice from each cohort were examined for tumor formation at 12 weeks of age. Panel A shows the number and size of tumors found in each mouse that was examined. Tumors were mostly round sessile polyps and size was determined by longest dimension. A statistical comparison of the number of tumors stratified by size showed that Pot1a^{intΔ} APC^{min} mice had more medium (2-4mm) and large (>4mm) tumors at 13-weeks than control.

To gain some insight as to why tumor formation was accelerated, we examined the histological features of the 12 week old mice through H&E staining. Comparison of apoptotic bodies in VCre⁻, VCre⁺ and Pot1a^{intΔ} APC^{min/+} mice revealed a 7.5-fold increase in apoptosis in the intestinal crypts of Pot1a^{intΔ} APC^{min/+} mice as compared to VCre⁻ APC^{min/+} controls (0.75±0.11 vs. 0.10±0.05, respectively; t-test, p>0.001) (Figure 23A). We further examined the intestines for the presence of anaphase bridges. There was a modest 1.5 fold increase in anaphase bridge index in the Pot1a^{intΔ} APC^{min/+} crypts as compared to controls (Pot1a^{intΔ}: 0.017±0.02; VCre⁻: 0.08±0.02; t-test; p = 0.002) (Figure 23B). The increased anaphase bridges suggest that there may be increased genomic instability in APC^{min} intestines that are deficient in Pot1a, possibly contributing to increased apoptosis.

Discussion

The data described above indicate that our model of Pot1a deficiency is not tumor suppressive. Instead, telomere dysfunction caused by uncapping appears to accelerate tumor initiation as evident by the heavier tumor burden in young animals and decreased survival of the Pot1a^{intΔ} APC^{min/+} cohort as compared to VCre⁻ and VCre⁺ APC^{min/+} controls. These results are in contrast to what was seen in late generation telomerase null mice, where telomere dysfunction from severely shortened telomeres acted to suppress tumor formation (Rudolph et al., 2001). This may be due to telomere-induced genomic instability driving LOH of the APC allele faster than in wild-type controls, as the mutant intestines show an increase in anaphase bridging. While the concurrent increase in apoptosis may suggest that tumor suppression should occur, perhaps this increased turnover combined with

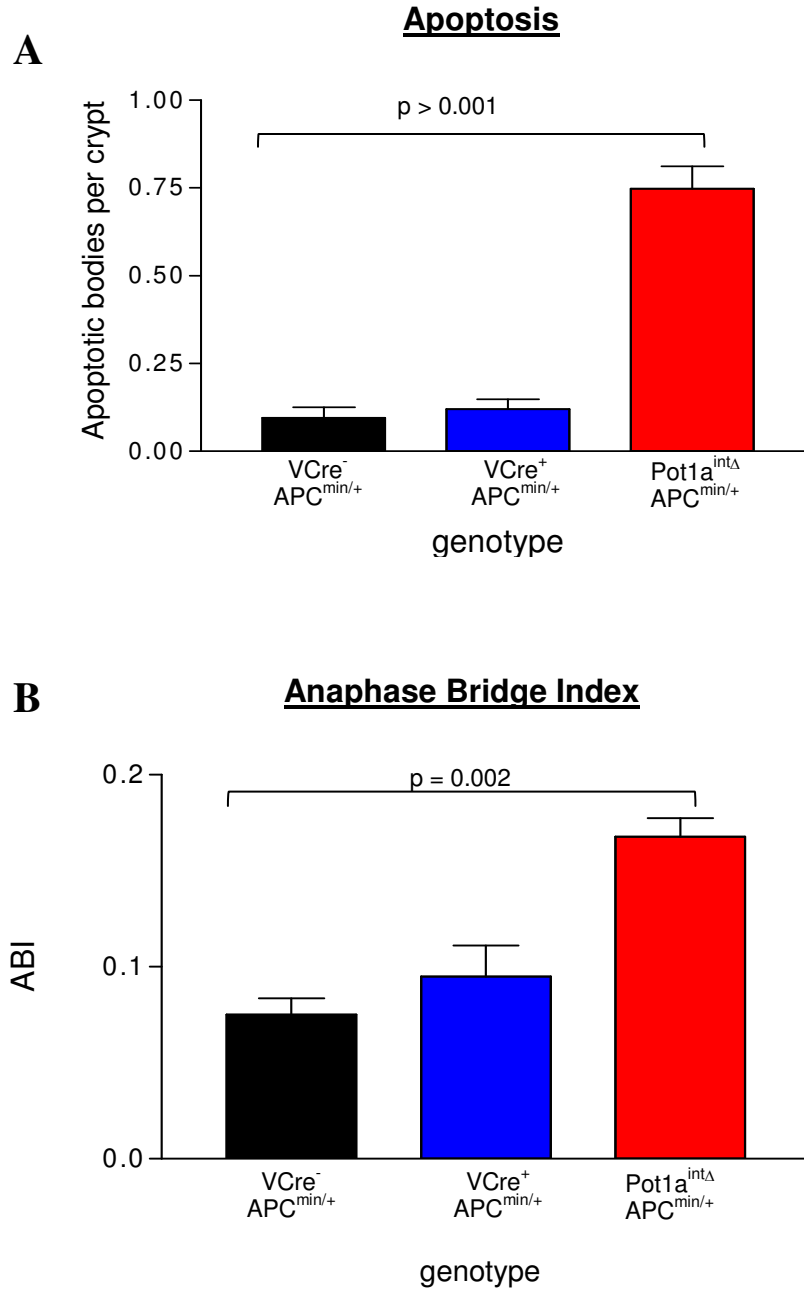


Figure 23: Pot1a^{intΔ} APC^{min} have increased apoptosis and anaphase bridges. Five mice from each cohort were examined at 12 weeks of age (500 crypts per animals). (A) Quantification of apoptotic bodies. (B) Quantification of the number of anaphase bridge index (# anaphase bridges over total anaphases).

genomic instability shortens the time needed for generation and selection of cells with cancer-promoting genomes.

The combination of telomere-induced genomic instability with the tumor-initiating power of the APC^{min} mutation in the intestinal epithelium, suggests that it might be a good model for promoting tumor progression. Unfortunately, the accumulation of the appropriate genetic alterations to promote progression is a stochastic process that requires time. The overwhelming tumor burden of this model prevented the animals from surviving long enough to determine if that process could occur.

The effect of loss of Pot1a on a colitis-induced model of colorectal cancer

The APC^{min} model mainly produces tumors in the small intestine. To examine the effect of loss of Pot1a in the colon, we used a model of chemically induced colon cancer that combines the chemical carcinogen azoxymethane (AOM) and dextran sodium sulfate (DSS) induced colitis (Neufert et al., 2007). While there are different versions of this protocol with varying doses of AOM and DSS (Suzuki et al., 2006; Tanaka et al., 2003), we chose to follow the protocol outlined in Figure 24 (Neufert et al., 2007). Briefly, 10-15 week old VCre, Pot1a animals from each cohort were treated with a single injection of AOM (10mg/kg body weight). Immediately after the injection, the mice were fed a one week course of 3% DSS water, followed by two weeks of regular water. This was repeated two more times for a total of three cycles.

Under this protocol, we expected VCre⁻ wild-type animals to develop multiple large tumors in the colon by 10 weeks (Becker et al., 2005), therefore tumor evaluation was performed at this timepoint. However, our cohorts showed very little tumor formation,

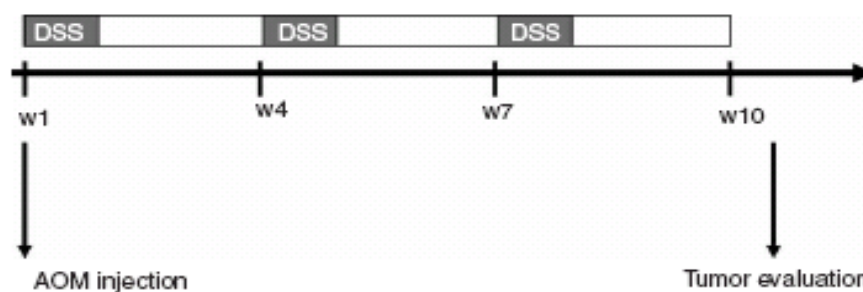


Figure 24: Protocol for AOM/DSS experiment. The protocol for the chemically induced colon carcinogenesis model is outlined in the figure above. At Day 0, mice are injected with azoxymethane (AOM) at a concentration of 10mg/kg. A regular diet was supplemented with 3% dextran sodium sulfate (DSS) water instead of tap water for a period of one week. Mice were fed regular tap water for two weeks following DSS treatment. This 3-week cycle was repeated for a total of three times. Mice were euthanized at 10 weeks to evaluate tumor formation.

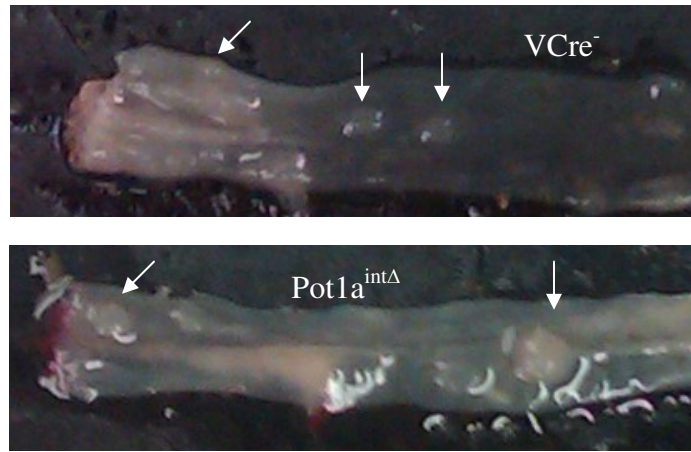
Table 4: Tumor formation in mice treated with AOM/DSS at 10-weeks

Genotype	# animals	# tumors
VCre-	26	3
VCre ⁺	14	0
Pot1a ^{intΔ}	16	0

including the VCre⁻ control cohort in which only three tumors were found, one macroscopically on dissection and two additionally upon histological analysis (Table 4). The lack of tumor formation in the control mice led us to consider this a failed experiment. Previous studies have demonstrated the strain differences can affect the susceptibility of mice to this protocol(Suzuki et al., 2006). Our mice have a mixed background of C57Bl/6 and 129Sv. C57Bl/6 strain is not very susceptible to AOM treatment alone, moderately susceptible to the combined treatment(Suzuki et al., 2006). We considered the possibility that the genetic background of our mice was a barrier to tumor formation using this model.

Another possible explanation is that because of the inherent strain resistance to the treatment, tumor formation occurs after a longer latency in our mice than other strains. To test this theory, the protocol was repeated with another cohort of mice. In this experiment, tumor evaluation was performed at 15 weeks instead of 10 weeks. Tumors were seen in mice from this experimental cohort, but they were still few in numbers and most were very small (<2mm) (Figure 25A). Quantification of tumor number showed no significant difference in tumor formation in the VCre⁻ control mice as compared to Pot1a^{intΔ} mice (4.75±3.4 vs. 5.13±2.7, respectively; t-test; p=0.81)(Figure 25B). Therefore, Pot1a deletion does not appear to suppress tumor formation in this model. However, future experiments may include delaying tumor evaluation for a longer period (greater than 20weeks) to determine if telomere dysfunction has an effect on tumor growth and progression in this model. The low multiplicity makes the tumor burden easier for the mice to bear, and longer timepoints that cannot be achieved in the APC^{min} model may be studied in the AOM/DSS model.

A



B

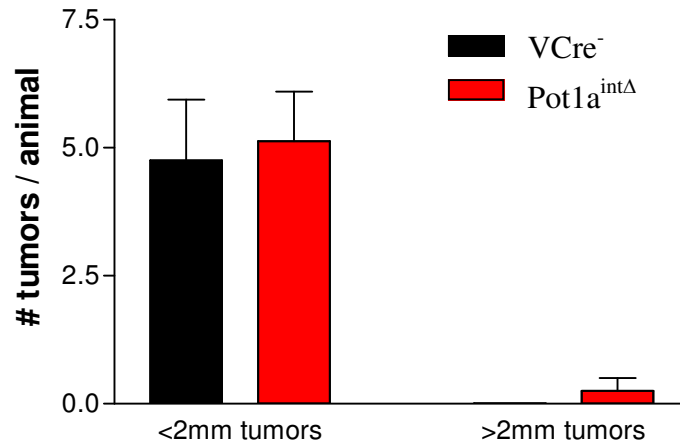


Figure 25: Tumor formation in mice treated with AOM/DSS at 15 weeks. The AOM/DSS protocol for chemically inducing colon carcinogenesis was repeated. Eight animals of each genotype were treated with the same protocol, but tumor evaluation was conducted at 15 weeks, instead of the previous endpoint of 10 weeks. At this later time point, more tumors were visualized in the colons of the treated animals (Panel A; white arrows). Most of these tumors were less than 2mm in size. A comparison of the tumors found in the two cohorts (Panel B) showed that there was no significant difference in the number of tumors formed in the control vs. the Pot1a^{intΔ} mice ($p=0.81$).

COMBINED LOSS OF POT1A AND P53 LEADS TO TUMOR FORMATION

p53-dependent activation of p21 and apoptosis serves as a potent checkpoint to stop propagation of cells with dysfunctional telomeres. Therefore, p53 activity is a key barrier that keeps dysfunctional telomeres acting in a tumor suppressive fashion and prevents the transition to telomere dysfunction driving genomic instability and tumor formation. The importance of this checkpoint was demonstrated in the telomerase null mouse model (Chin et al., 1999), where p53 deficiency rescued or delayed many of the degenerative phenotypes seen in late generation *mTerc*^{-/-} mice, such as testicular atrophy and bone marrow failure. Telomerase null animals that are deficient in p53 develop tumors (Artandi et al., 2000), further confirming the importance of this checkpoint for tumor suppression. In fact, dysfunctional telomeres in this case cooperate with p53 loss to form tumors, and interestingly, the combination shifts the tumor spectrum from lymphomas and sarcomas to carcinomas of the breast and gastrointestinal tract (Artandi et al., 2000). p53 deficiency also allows Pot1a null cells to bypass senescence (Wu et al., 2006). Furthermore, injection of immortalized Pot1a and p53 double deficient cells into SCID mice produces tumors (Wu et al., 2006). Based on these data, we hypothesized that abrogation of p53 in our Villin-Cre, Pot1a mice would allow tumor formation in the gastrointestinal tract.

To generate mice with intestinally deleted Pot1a and p53, we crossed the Villin-Cre, Pot1a mice with a mouse that contains conditional p53 alleles that are also flanked by loxP sites (Jonkers et al., 2001). The following cohorts were created for analysis: *Pot1a*^{intΔ} *p53*^{+/+}; *Pot1a*^{intΔ} *p53*^{F/+}; *Pot1a*^{intΔ} *p53*^{F/F}; and finally *p53*^{F/F}, which represents mice with only p53 deleted in the intestines. To determine p53 deletion, we employed a PCR strategy developed by the Berns lab for this allele (Jonkers et al., 2001). Analysis of DNA from several tissues

demonstrated that deletion of Pot1a and p53 were both still restricted to the small intestines and colon (Figure 26).

Apoptosis and p21 activation in Pot1a intestines is p53-dependent

Two of the main microscopic features seen in Pot1a^{intΔ} mice are upregulation of p21 and increased apoptotic cells in the crypts. Concurrent upregulation of p53 and the importance of the p53 checkpoint in the response to dysfunctional telomeres suggest that these phenotypes are p53-dependent. Comparison of the presence of apoptotic bodies (Figure 27A) in the intestines of the various cohorts revealed that loss of one allele of p53 lead to a slight but significant decrease in apoptosis (Pot1a^{intΔ} p53^{+/-}: 0.559±0.042 vs. Pot1a^{intΔ} p53^{F/+}: 0.399 ± 0.033, t-test, p = 0.006). Loss of both p53 alleles led to almost complete rescue of the phenotype with a 4.5-fold decrease in apoptosis (0.123 ± 0.04; t-test, p = 0.0002). Similarly, upregulation of p21 was also completely abrogated in the setting of p53 deficiency (Figure 27B). These results confirm that the activation of p21 and apoptosis in response to Pot1a loss are p53-dependent processes.

p53 deficiency allows for more cells with telomere dysfunction to persist

With cell cycle arrest and apoptosis abrogated in p53 deficient animals, we sought to determine how this affects the cells with telomere dysfunction. Double IF staining to assay for TIFs in the intestines revealed that p53 deficiency leads to an increase of TIF positive nuclei in the crypts (Pot1^{intΔ}p53^{+/-}: 0.27±0.05 vs. Pot1^{intΔ}p53^{F/F}: 0.57±0.13; t-test; p=0.02) (Figure 28). These results suggest that in the absence of a clearing mechanism, such as

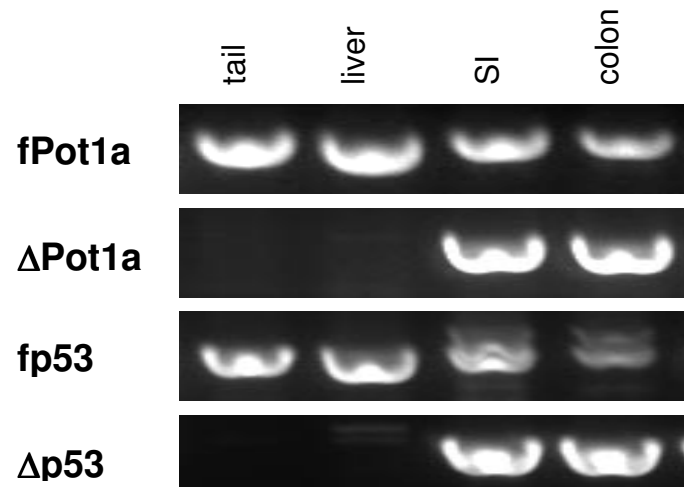


Figure 26: Verification of Pot1a and p53 deletion in $Pot1a^{int\Delta} p53^{F/F}$ mice. Using primers can detect deletion of the Pot1a and p53 alleles, PCR analysis of genomic DNA isolated from various organs of $Pot1a^{int\Delta} p53^{F/F}$ mice show that both genes are indeed being deleted only in the intestines.

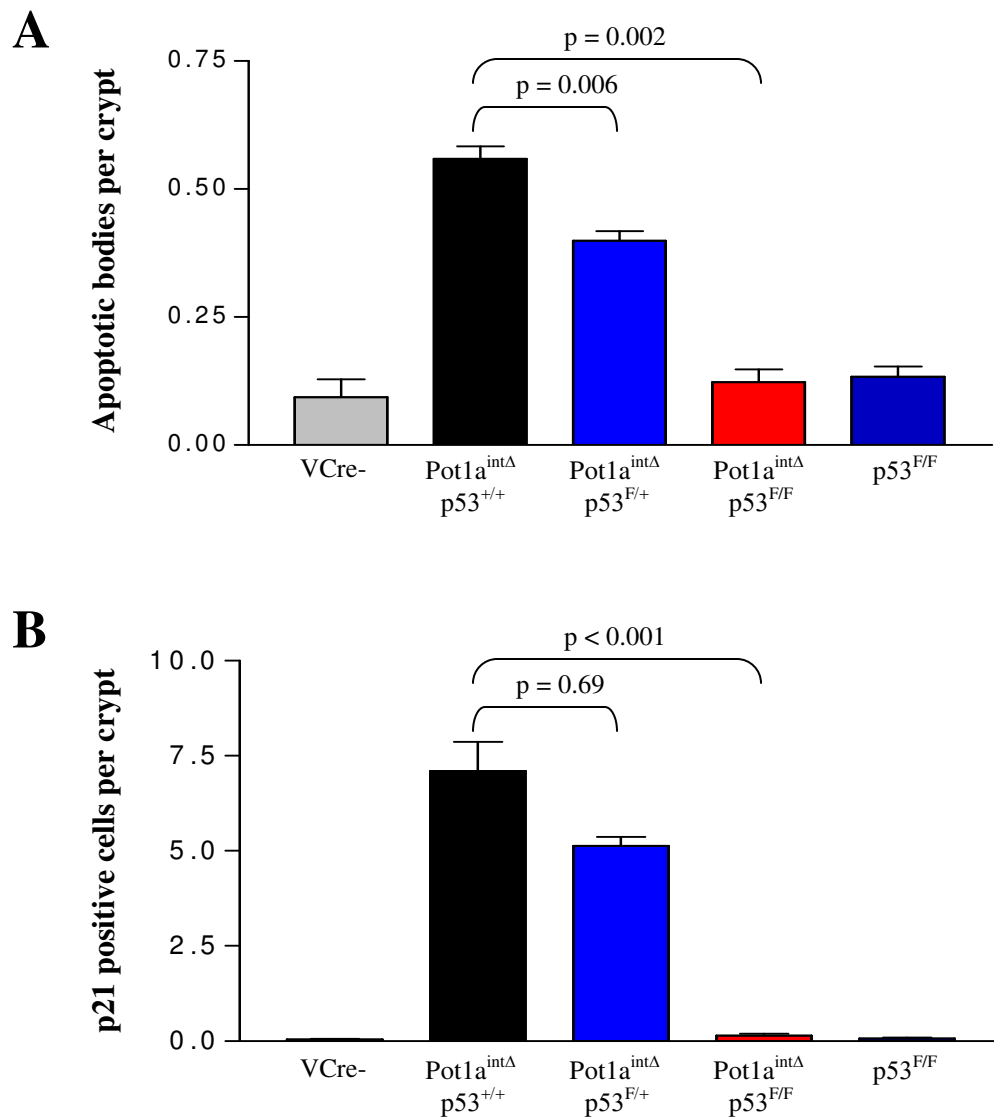


Figure 27: Apoptosis and p21 activation in Pot1a^{intΔ} intestines is p53-dependent. Comparison on apoptotic bodies on H&E sections of mice from the VCre, Pot1a, p53 mouse colony show that while p53 haploinsufficiency partially decreases the apoptosis in Pot1a^{intΔ} mice, complete p53 deficiency rescues the phenotype to control levels (Panel A). Similarly, p21 IHC reveals that p53 deficiency abrogates activation of this pathway in Pot1a^{intΔ} mice (Panel B). Intestines from four animals per genotype were examined, and 500 crypts per animal were analyzed.

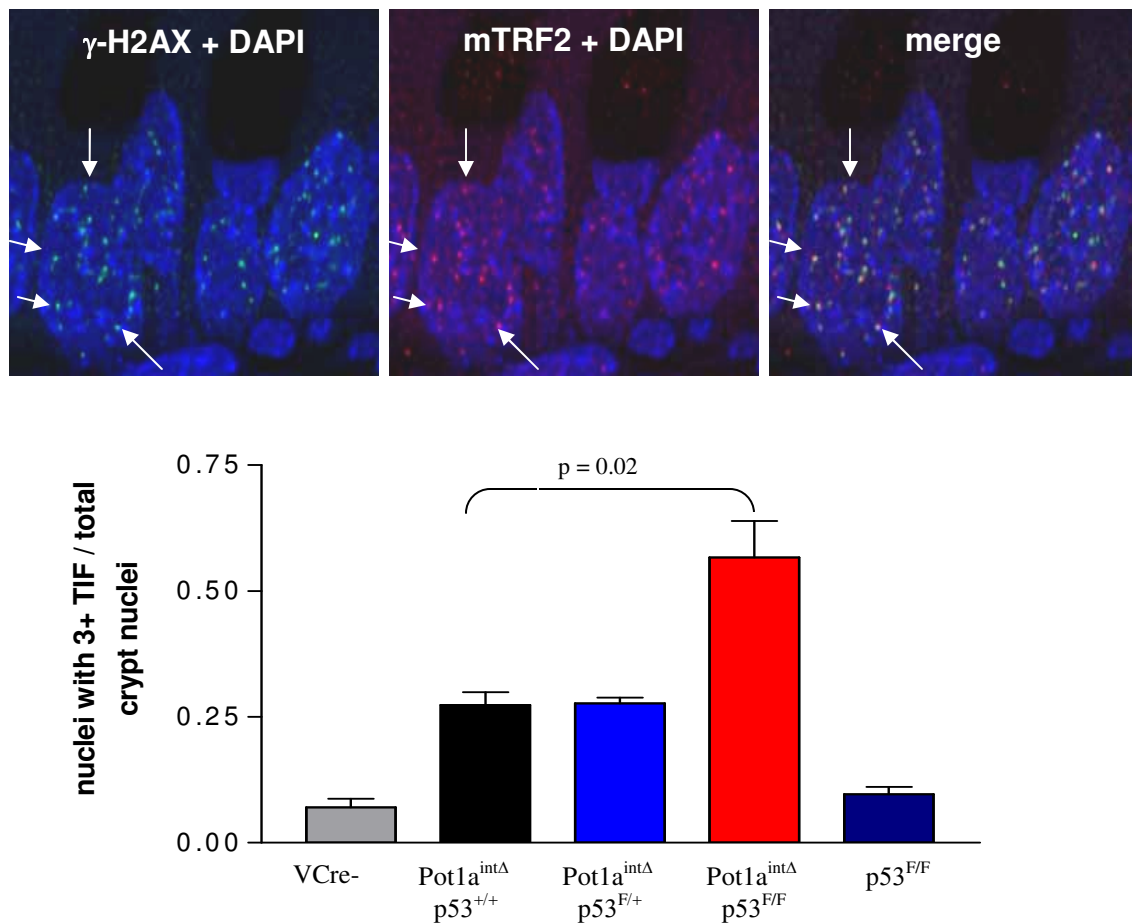


Figure 28: p53 deficiency leads to increased numbers of cells with telomere dysfunction. A tissue TIF assay was performed through double IF, using γ -H2AX (green) as a marker for DNA damage, and mTRF2 as a marker for telomeres (red). Nuclei with three or more foci of colocalization were counted as TIF positive. The top panel contains representative images of TIF positive nuclei from Pot1a^{intΔ} p53^{F/F} mice. Quantification of intestines from the different cohorts show that loss of p53 leads to an increase in cells with dysfunctional telomeres in the intestinal crypts. Three mice for each genotype were examined, and 1000 nuclei from each sample were analyzed.

apoptosis, cells with telomere dysfunction are allowed to persist and accumulate in the crypts of the mutant mice.

Mice with combined Pot1a and p53 loss develop invasive adenocarcinomas

Villin-Cre, Pot1a, p53 mice that were allowed to age developed intestinal tumors. Pot1a^{intΔ} p53^{F/F} mice form tumors in the gastrointestinal tract with almost 100% penetrance (Table 5). Tumor formation had a long latency, mostly appearing after 15 months of age. Tumors formed in low multiplicity, with most mice bearing only 1-4 tumors. Pot1a^{intΔ} p53^{F/+} mice also developed tumors but longer latency and lower penetrance. This is presumably due to spontaneous LOH of p53. Meanwhile, p53^{F/F} only animals did not form any tumors in the gastrointestinal tract, suggesting that this process is driven by the combination of p53 deficiency and telomere dysfunction; and loss of p53 is not enough to drive tumorigenesis in the intestines.

Tumors had two different appearances: cecal masses were rounded polypoid masses that protrude into the lumen of the cecum (Figure 29A), while tumors found in the small intestine and colon tended to be flat annular rings, with beaded up borders and depressed centers (Figure 29B). The flat tumors were difficult to distinguish between irregular epithelium overlying lymphocytic aggregates (Peyer's patches) in the intestinal walls, which looked similar. All tissue taken for further analysis was first confirmed histologically. Examination of the tumors revealed lesions that ranged from microscopic benign adenomas to well-differentiated adenocarcinomas that invaded into the submucosa, with some as far as the muscular wall (Figure 29C). While there was deep invasion into the muscle wall, no metastasis was observed in any of the animals.

Table 5: Combined Pot1a and p53 deficiency leads to tumor formation

Genotype	Age range	Animals with tumors	Multiplicity	Size range (longest dimension)
Pot1a ^{intΔ} p53 ^{+/+}	12-24 months	0/15	na	Na
Pot1a ^{intΔ} p53 ^{F/+}	12-15 months	1/7	4	micro
	15-18 months	1/6	2	2mm
	18-24 months	3/8	1	3mm
Pot1a ^{intΔ} p53 ^{F/F}	12-15 months	3/8	1-2	2-6mm
	15-18 months	7/8	1-3	4-15mm
	18-24 months	3/3	1-3	3-6mm
p53 ^{F/F}	12-15 months	0/5	na	n.a.
	15-18 months	0/6		
	18-24 months	0/3		

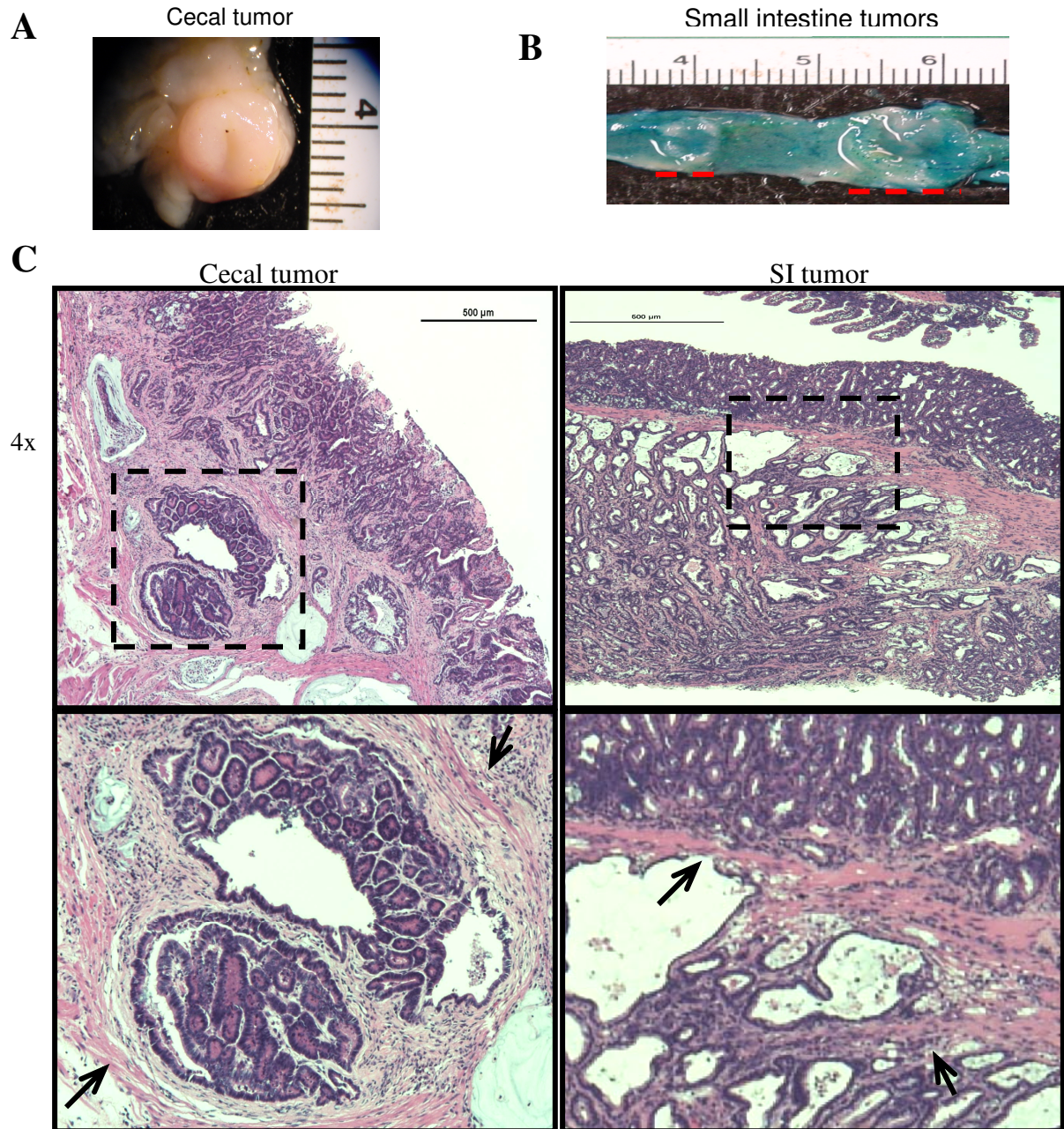


Figure 29: Combined loss of Pot1a and p53 leads to formation of invasive cancers in the GI tract. (A) Gross photo of round polypoid cecal tumor. (B) Gross picture of two small intestine tumors that are flat with raised borders and depressed centers (red dashed lines). (C) H&E staining of SI and cecal tumors. Regions of invasion (black dashed box) are shown under higher magnification. Invasion into the submucosa and muscle wall (dark pink staining, arrows) can be seen.

Pot1a, p53 intestinal tumors shows signs of genomic instability

DNA was isolated from thirteen tumors grossly dissected from VCre, Pot1a, p53 animals and assayed for genetic alterations through array comparative genomic hybridization (aCGH) analysis. The genotypes, tumor location and description are listed in Table 6. Tumor genomes were assayed against DNA pooled from the kidneys of five wild-type females using the Nimblegen Mouse 385K Whole Genome Tiling Arrays. Whole genome profiles were generated for each individual tumor (Figures 30 & 31). A few recurrent peaks and large areas of change are noted with asterisks. Tumors 3 and 6 appear to have the most regions of CNV with variations in large regions of several chromosomes.

A more detailed analysis of genetic alterations was performed using Biodiscovery's Nexus 5 software. The tumors used for array CGH were dissected from the GI tract at the time of necropsy, and though tumor margins were approximated using a dissection microscope, there is likely to be normal tissue in the samples. Attempts were also made to separate some of the muscle wall from the tumors, but H&E staining clearly shows that tumor cells invaded deep in to the muscle wall and the tumor tissue was mixed with many other cells types including stromal cells, lymphocytes, submucosal cells and even muscle wall (Figure 29C). The thresholds were set using the copy number losses of in the X chromosome of samples from males to determine the baseline setting. This occurred at approximately -0.2 on the log2 ratio scale. The thresholds were further lowered to -0.1 for a loss and 0.1 for a gain in an attempt to account for the non-tumor tissue DNA was mixed into the sample that was analyzed.

Table 6: Description of tumors used for aCGH experiments

Sample	Genotype	Age (weeks)	Location	Tumor grade
1	Pot1a ^{intΔ} p53 ^{F/+}	87	Small intestine	Low-grade adenoma
2	Pot1a ^{intΔ} p53 ^{F/+}	87	Small intestine	High-grade adenoma
3	Pot1a ^{intΔ} p53 ^{F/F}	78	Small intestine	Invasive adenocarcinoma
4	Pot1a ^{intΔ} p53 ^{F/F}	63	Small intestine	Invasive adenocarcinoma
5	Pot1a ^{intΔ} p53 ^{F/F}	63	Colon	High-grade adenoma
6	Pot1a ^{intΔ} p53 ^{F/F}	76	Small intestine	Invasive adenocarcinoma
7	Pot1a ^{intΔ} p53 ^{F/F}	76	Small intestine	Invasive adenocarcinoma
8	Pot1a ^{intΔ} p53 ^{F/F}	76	Cecum	Invasive adenocarcinoma
9	Pot1a ^{intΔ} p53 ^{F/F}	76	Colon	Invasive adenocarcinoma
10	Pot1a ^{intΔ} p53 ^{F/F}	65	Cecum	Invasive adenocarcinoma
11	Pot1a ^{intΔ} p53 ^{F/F}	67	Cecum	Invasive adenocarcinoma
12	Pot1a ^{intΔ} p53 ^{F/F}	83	Small intestine	Invasive adenocarcinoma
13	Pot1a ^{intΔ} p53 ^{F/F}	83	Cecum	Invasive adenocarcinoma

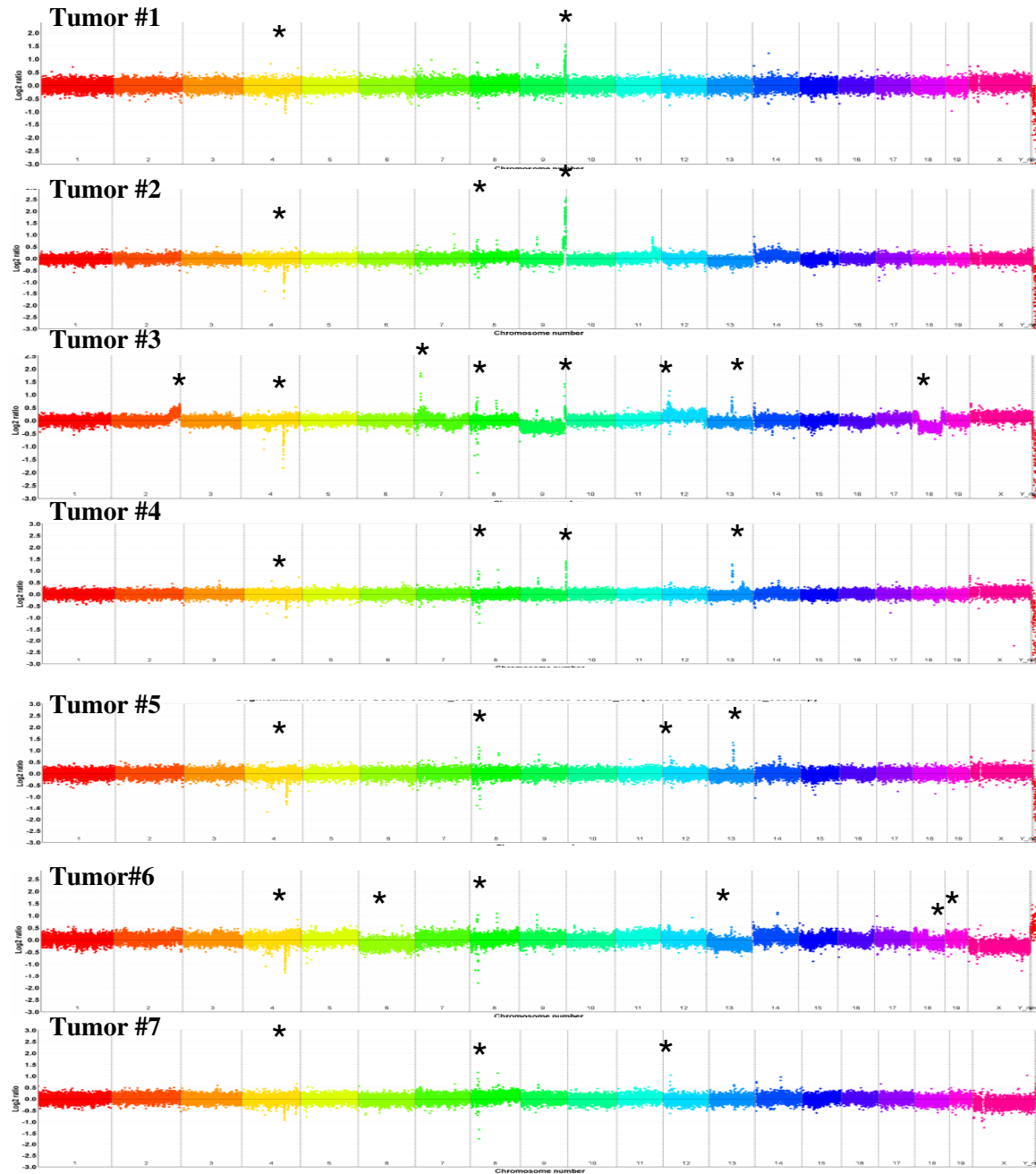


Figure 30. Tumors from *Pot1^{intΔ} p53^{F/F}* mice show genomic alterations. Whole genome profiles for Tumors #1-7. The x-axis is divided by chromosomes and the results for each chromosome are color coded. The y-axis represents the copy number change on a log₂ ratio scale, where the baseline (no change) is set to zero. A few recurrent peaks and large areas of change are noted with asterisks (*).

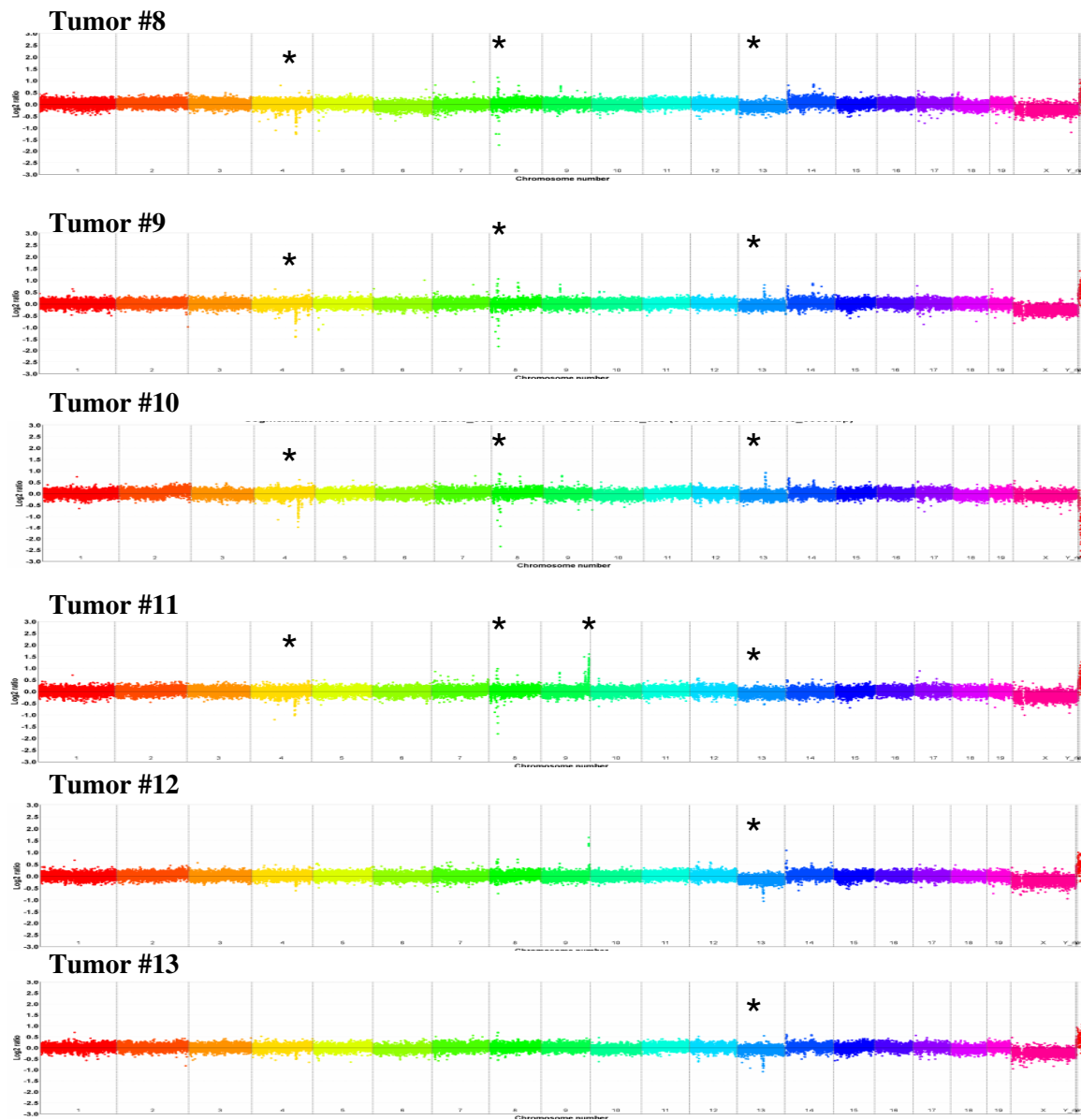


Figure 31. Tumors from $Pot1^{int\Delta}$ $p53^{F/F}$ mice show genomic alterations. Whole genome profiles for Tumors #8-13. The x-axis is divided by chromosomes and the results for each chromosome are color coded. The y-axis represents the copy number change on a log₂ ratio scale, where the baseline (no change) is set to zero. A few recurrent peaks and large areas of change are noted with asterisks (*).

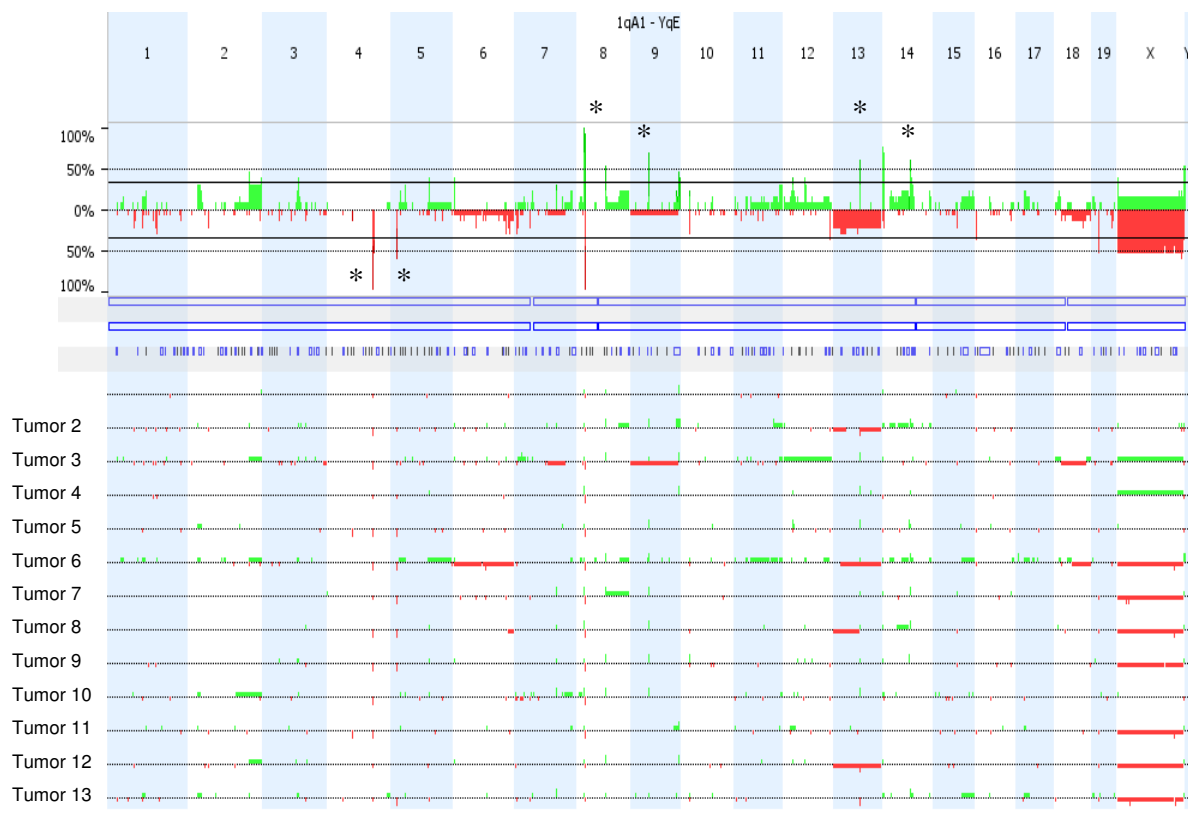


Figure 32: Summary of aCGH results for thirteen intestinal tumors. The top panel represents a summary of genetic alterations seen within the tumor set. The x-axis is divided by chromosomes, from chromosome 1 on the far left, ascending to chromosome 19 on the right, ending with the X and Y chromosomes on the far right. The y-axis represents the percent recurrence of each alteration in the tumor set. Green bars represent copy number gains, while red bars represent copy losses. The bottom half of the figure displays the changes seen in each individual tumor. Each horizontal line represents an individual tumor and the variations in each sample can be seen.

Using these settings, the set of thirteen tumors were analyzed and a summary of the distribution of changes along the whole genome was generated (Figure 32). Of notes are several small regions of highly recurrent (present in >50% of tumors) gains and losses on chromosomes 4, 5, 8, 9, 13, 14 and 19(Figure 32, asterisks).

The total number of regions with copy number variations was determined for each individual sample (Figure 33). The number of changes per sample ranged from 16 to 97 regions, with a mean of 47.8 changes per tumor. Interestingly, the number of changes does not seem to correlate with tumor grade as an invasive cecal adenomcarcinoma (tumor #8) had as few as 27 changes, while a high grade adenoma with no invasion (tumor #2) had as many as 70 changes. There also seemed to be no correlation between age and copy number change: an invasive tumor from an 83-week old animal (#12) harbored only 34 regions of CNV, while a tumor from a 65-week old animal (#10) had 63 changes. This distribution suggests that each tumor harbors variable numbers of genetic alterations and serves as evidence that tumors generated by combined Pot1a and p53 deficiency are genomically unstable. The variation also suggested that the process is stochastic and telomere dysfunction with p53 deficiency is permissive for the formation of random genome changes.

DISCUSSION

The results above describe the generation of a novel mouse model of intestinal tumorigenesis that is driven by telomere dysfunction. Our model of combined Pot1a and p53 deficiency proved to be permissive to cancer formation as aging Pot1a^{intΔ} p53^{F/F} mice developed tumors throughout gastrointestinal tract, including the small intestine, cecum and colon. These tumors were well-differentiated but showed frequent invasion into the submucosa, with some

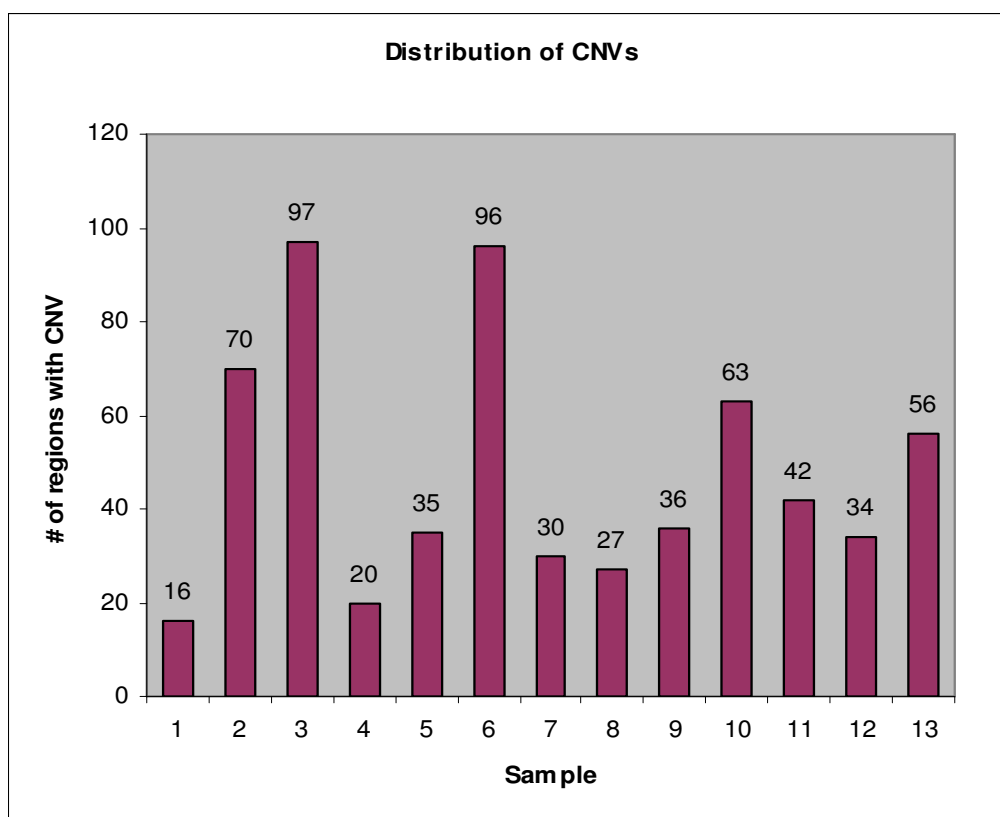


Figure 33: Distribution of copy number changes. The total number of regions with copy number variations was determined for each sample and plotted above. The numeric value is listed above the bars. The number of changes per sample ranged from 16 to 97 regions, with a mean of 47.8 changes per tumor.

extending as deep as the muscle wall. These tumors resemble the GI tumors found in a small subset of late generation telomerase null mice with p53 haploinsufficiency (Artandi et al., 2000). Similar to that model, our mice developed tumors with low multiplicity and a latency of 15 months. However, G5-G7 mTerc^{-/-} p53^{+/-} mice often succumb to other tumor types, such as lymphomas, breast and squamous cell, and a variety of sarcomas (Artandi et al., 2000). Additionally, it requires five to seven rounds of intergenerational breeding to develop severely shortened telomeres. Our model is superior for studying telomere dysfunction in the GI tract because our phenotypes are limited to the intestines and we do not require intergenerational breeding to induce telomere dysfunction.

Genomic profiling of the tumors revealed frequent copy number variation and heterogeneous profiles, also similar to tumors harvested from telomerase null p53 heterozygous mice (O'Hagan et al., 2002), suggesting that telomere dysfunction was indeed driving genomic instability. These genomic alterations are currently being worked up to determine if there are any changes common to what is seen in human cancers and to determine if there are any new recurrent changes to explore.

It is interesting to note that another group also tried to create a mouse model of telomere dysfunction in the setting of p53 deficiency in the intestine. This model paired conditional deletion of p53 in the intestines with late generation telomerase null mice (Begus-Nahrman et al., 2009). While they also concluded that p53 deficiency impairs the clearance of chromosomally unstable cells from intestines with severe telomere erosion, their model did not develop tumors. They postulated that although their model allowed them to bypass p53-dependent checkpoints, a second p53-independent checkpoint called crisis prevented tumor formation in their mice as progressive accumulation of cells with dysfunctional

telomeres lead to increased apoptosis(Begus-Nahrman et al., 2009). The crisis checkpoint is thought to be bypassed in human cancers with the reactivation of telomerase(Maser and DePinho, 2002), a step that cannot occur in the telomerase null mice. Our model leaves telomerase activity intact, and may allow for bypass of crisis and possible progression to metastasis.

Some of the limitations of this model may provide directions that can be pursued in the future work towards improvement. The long latency of the tumor formation can possibly be decreased combining the conditional p53 knockout allele with a conventional p53 knockout allele to form p53^{F/-} mice. This would increase the probability of cells with homozygous deletion of p53 in the intestines because only one additional allele would need to be deleted conditionally, which may be helpful given the decreased X-gal staining and presumably decreased Villin-Cre activity in Pot1a^{intΔ} mice. However, this system will only be beneficial if tumor latency is significantly shortened, as p53 haploinsufficiency throughout the organism also leads to lymphoma or sarcoma development.

Shortened tumor latency may also prevent the animals from succumbing to environmental contaminants. Many of our mice were euthanized without any symptoms of tumor formation. Unfortunately, there was an outbreak of fur mites in our mouse colony forcing us to euthanize the mice to relieve severe ulcerative dermatitis that was unresponsive to treatment. Given the invasive nature of the tumors seen on histology and the chromosomal instability seen on genomic profiling, we postulate that if the mice are allowed to live longer, we may be able to see more progression.

Another major limitation was the inability to monitor tumor formation. Our mutant mice developed tumors at a very low multiplicity, only one to four tumors per animal. While

this is an improvement over the APC^{min} models, which develops dozens of tumors but leads to early death due to the overwhelming load, low multiplicity means mice could bear the small tumor burden with few symptoms. In fact, tumor formation was quite insidious and most of the mice euthanized in this experiment were for symptoms not related to colon cancer formation. Some techniques that might be used for detection of tumor formation include *in vivo* imaging of mice. We attempted several protocols for computed tomography (CT) scanning and magnetic resonance imaging (MRI), however, the results were not robust enough to warrant the cost (data not shown). Because the tumors that develop in our Pot1a^{intΔ} p53^{F/F} mice were usually flat and thin, they were difficult to detect using these modalities. Furthermore, tumors often developed in the small intestines and the tortuous nature of this organ made it difficult to visualize on scans. We finally settled on using fecal occult blood testing (FOBT) to look for signs of occult GI bleeding due to tumor formation. The results from this test showed that positive results on this assay usually required tumors of at least 4mm in size (data not shown). However, results could easily be false positive if the animals had cuts or sores on its skin that it may have groomed. Future developments in animal imaging, such as endoscopy, may provide a better method of monitoring tumor formation and possibly progression.

Another major limitation that prevented further analysis of the tumors was the lack of material to work with. Several factors contributed to this problem. First, the low multiplicity of tumor formation in this model limits the number tumors that can be harvested. Second, while some of the tumors stretched as long as 15mm at its longest dimension, most ranged between 2-4mm. Furthermore, most tumors fell in the category of flat lesions with raised edges, so that there was very little volume of tissue to work with. Finally, because this

morphology mimics irregular epithelium overlying lymphoid aggregates, half of the tumor was taken tissue sectioning to verify that it was indeed a tumor and determine its grade through H&E staining. Therefore, we used all of the material harvested from the thirteen tumors for aCGH was extracted for DNA.

One technique that might help to expand the amount of material available from each tumor for future experiments is cell culture. Creating cell cultures from tumor tissue would solve several problems. First, there would be plenty of cells to harvest DNA, RNA and protein from to perform further validation experiment, especially cytogenetics. Cytogenetic techniques such as spectral karyotyping (SKY), have been used previously in verifying genomic instability and picking up chromosomal translocation induced by telomere dysfunction (Artandi et al., 2000; Maser et al., 2007). Furthermore, general karyotyping of genomes could pick up details such as aneuploidy and whole chromosome gains and losses on a single cell level. Second, cell cultures would help enrich for the colon cancer cells, as the normal stromal cells surrounding should not grow. We attempted to make cell lines through several different protocols from intestinal tumors, using the APC^{min} mice for pilot studies because of the abundance of lesions in these mice. Unfortunately, we were unable to produce a culture of growing cells, and there were many incidents of contamination. Although a lot of antibiotics were used, it was difficult to completely wash away the large quantities of bacteria that normally inhabit the gut to obtain a sterile culture.

An alternative to cell culture to enrich for tumor cells is laser capture microdissection (LCM) of tumors from frozen sample. This method would also allow for the isolation of tumor cells, while limiting contamination from surrounding stromal cells. While this technique is used at MD Anderson, the aCGH platform we used for our experiments could

not support materials harvested in this fashion. Perhaps future experiments with different platforms will be able to take advantage of this technique.

THE EFFECT OF ATM ON POT1A-INDUCED TELOMERE DYSFUNCTION IN THE GI TRACT

Animals with combined loss of Pot1a and ATR in the intestinal tract are not viable

Pot1a contributes to the protection of telomeres by suppressing ATR-mediated DNA damage responses to the G-rich overhang(Denchi and de Lange, 2007; Guo et al., 2007). We sought to determine the affect of the ATR deficiency in our Pot1a^{intΔ} mouse model by crossing it to a mouse harboring a conditional knockout allele of ATR (Brown and Baltimore, 2003). However, we were unable to generate mice with deletion of both genes (Table 7).

This is not a surprising result as loss of ATR is very toxic to cells in culture as it leads to massive chromosomal fragmentation(Brown and Baltimore, 2003). Also, ATR deficient mice are not viable due to very early embryonic lethality(Brown and Baltimore, 2000). Previous experiments using a tamoxifen-inducible Cre system to conditionally knockout ATR in a grown mouse showed that deletion of ATR leads to transient but severe degenerative phenotypes in the intestines(Ruzankina et al., 2007). Therefore, it is not surprising that we were unable to generate many animals with chronic loss of ATR. Because ATR^{+/-} mice occasionally developed tumors(Brown and Baltimore, 2000), we followed a small cohort of VCre⁺, Pot1a^{F/F}, ATR^{F/+} mice for two years, but no tumor formation or intestinal abnormalities were detected (data not shown).

Table 7: Results of VCre⁺ Pot1a^{F/F} ATR^{F/+} x VCre⁻ Pot1a^{F/F} ATR^{F/+}

Genotypes	Expected	# Observed	% observed
VCre ⁻ Pot1a ^{F/F} ATR ^{+/+}	1/8 (12.5%)	14	17.3%
VCre ⁻ Pot1a ^{F/F} ATR ^{F/+}	1/4 (25%)	22	27.2%
VCre ⁻ Pot1a ^{F/F} ATR ^{F/F}	1/8 (12.5%)	12	14.8%
VCre ⁺ Pot1a ^{F/F} ATR ^{+/+}	1/8 (12.5%)	15	18.5%
VCre ⁺ Pot1a ^{F/F} ATR ^{F/+}	1/4 (25%)	25	30.9%
VCre ⁺ Pot1a ^{F/F} ATR ^{F/F}	1/8 (12.5%)	*1	1.2%
	Total:	89 mice	

* Mouse survived for 4 weeks.

ATM loss results in decreased overall survival

While Pot1a mainly suppresses ATR-mediated DNA damage responses, deletion of Pot1a has been shown to also activate ATM(Wu et al., 2006). Furthermore, stable disruption of TPP1, whose main function is to facilitate Pot1a binding to telomeres, also leads to activation of the ATM pathway(Guo et al., 2007). It is postulated that while the immediate response to Pot1a loss is ATR-activation, ATM may also plays a role in a later response. Since *in vivo* deletion of Pot1a represents a chronic process, we sought to determine if loss of this checkpoint affected the phenotypes of our Pot1a mutants. To achieve this, we crossed our VCre, Pot1a mice with an ATM knockout mouse(Borghesani et al., 2000). This mouse was a straight knockout, so that ATM loss occurs throughout the entire organism. As seen in ATM^{-/-} mice, these animals showed in shortened lifespan due to formation of thymic lymphoma (Figure 34), regardless of Pot1a status in the intestines.

ATM deficiency rescues p21 activation and apoptosis

A few mice were sacrificed at early timepoints (10 weeks) to examine the intestines for the microscopic characteristics seen in Pot1a^{intΔ} crypts. Interestingly, in the setting of ATM deficiency, Pot1a loss does not manifest in increased apoptosis in the intestinal crypts (Pot1a^{intΔ} ATM^{+/+}: 0.60±0.12 vs. Pot1a^{intΔ} ATM^{-/-}: 0.17±0.08; t-test; p=0.05) (Figure 35A). Furthermore, examination of p21 IHC staining revealed that activation of p21 is also abrogated in Pot1a and ATM deficient intestines (Pot1a^{intΔ} ATM^{+/+}: 3.71±0.54 vs. Pot1a^{intΔ} ATM^{-/-}: 0.23±0.07; t-test; p<0.001) (Figure 35B&C). These results suggest that p53 activation is not occurring in the absence of ATM. We postulate that loss of ATM may be

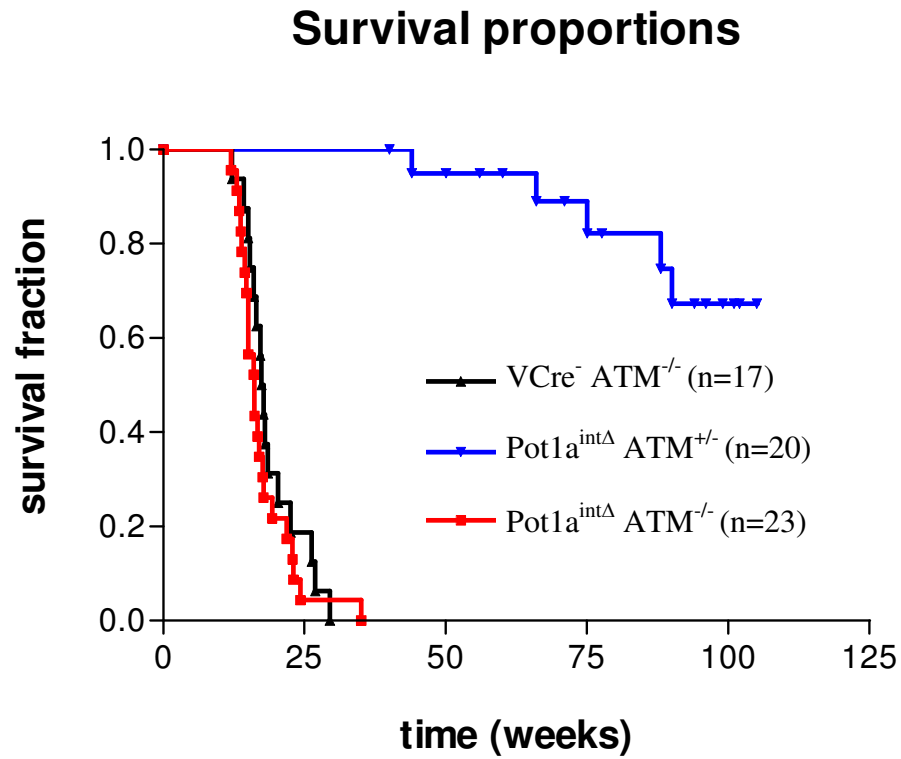


Figure 34: ATM deficiency leads to early death in Pot1a deficient mice. Kaplan-Meier analysis showed that ATM deficiency lead to decreased overall survival, regardless of Pot1a status.

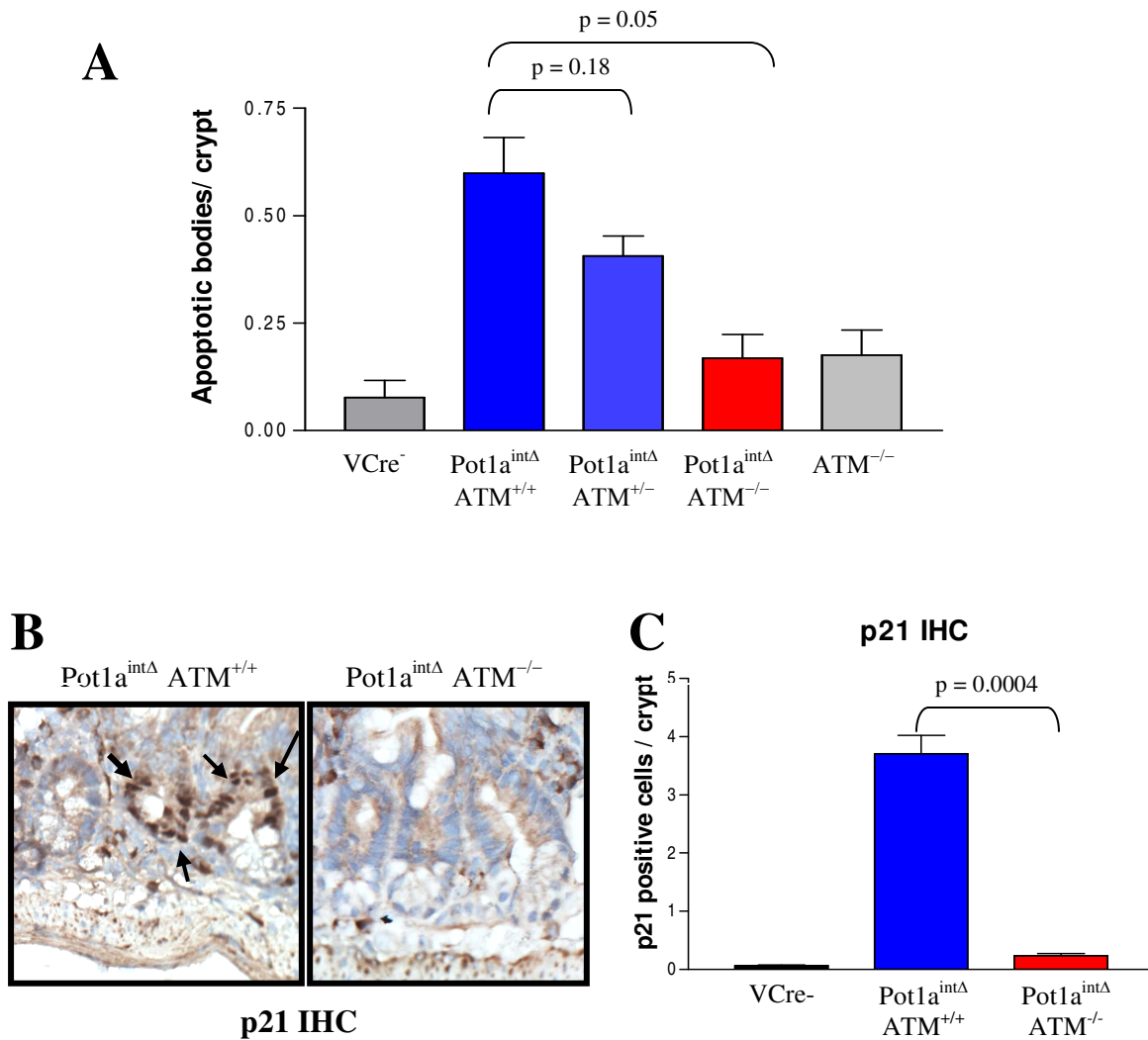


Figure 35: ATM deficiency rescues apoptosis and p21 activation in Pot1^{intΔ} crypts. (A) H&E staining of intestines harvested from various cohorts were examined for apoptosis. Quantification of apoptotic bodies per crypt demonstrated that ATM deficiency leads to decreased apoptosis in Pot1^{intΔ} intestines as compared to Pot1^{intΔ} ATM^{+/+}. (B) Representative p21 IHC staining in Pot1a^{intΔ} ATM^{+/+} and Pot1^{intΔ} ATM^{-/-} intestines. p21 positive nuclei are indicated by the arrows. (C) Quantification of IHC staining shows a decrease in p21 activation in Pot1a deleted intestines when ATM is also deficient.

interfering with the DNA damage response to dysfunctional telomeres but recent attempts to assay for TIFs have been unsuccessful.

Pot1a^{intΔ} ATM^{+/-} mice occasionally develop intestinal tumor formation in the aged mice

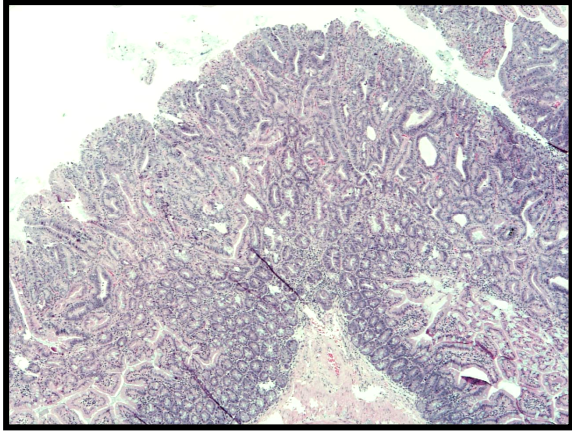
While ATM^{-/-} mice did not survive very long, we followed a cohort of Pot1a^{intΔ} ATM^{+/-} mice for a period of two years. Routine euthanasia of these mice revealed occasional tumor formation in aged mice (Table 8). Of the sixteen mice older than 18 months that we examined, only four mice were observed to have tumors. These tumors were mostly well-differentiated adenomas, with one tumor showing signs of invasion. We postulated that loss of the wild-type ATM allele was necessary for tumor formation, but PCR experiments to verify this have been inconclusive. Taken together, these results suggest that loss of the ATM barrier may also be permissive to driving tumor formation in the setting of telomere dysfunction, possibly through the prevention of p53 activation in response to telomere dysfunction secondary to Pot1a loss.

Discussion

Pot1a binds specifically to the 3' G-rich overhang of telomeres. It has been shown contribute to the protection of telomeres from the DNA damage response by preventing the activation of an ATR-dependent DDR (Denchi and de Lange, 2007; Guo et al., 2007). We sought to determine the effect of losing this checkpoint in our in vivo model of Pot1a deficiency by generating a VCre⁺ Pot1a^{F/F} ATR^{F/F} mouse. However, we were unable to produce this mouse. This result is not surprising given that ATR is an essential gene for cell survival (Brown and Baltimore, 2003). Deletion of ATR from cells in culture lead to rapid

Table 8: Pot1a^{intΔ} ATM^{+/-} mice occasionally form tumors

Age range	Animals with tumors	multiplicity	Size range (diameter)
12-15 months	0/4	n.a	n.a.
15-18 months	0/5	n.a.	n.a.
18-21 months	1/4	1	3mm
21-24 months	3/12	1-2	3-8mm



Non-invasive Pot1a^{intΔ} ATM^{+/-} adenocarcinoma

chromosomal instability and cell death(Brown and Baltimore, 2003). Conditional deletion of the ATR in mice using an inducible Cre system resulted in massive cell death in highly proliferative compartments, especially in the intestinal tract(Ruzankina et al., 2007).

Since we were unable to remove the ATR checkpoint, we decided to target ATM, which is also a potent transducer of the DNA damage response. In response to telomere dysfunction, ATM activation is typically associated with severe telomere erosion or loss of the TRF2 protein(Karlseder et al., 1999), both of which are thought to resemble double strand breaks. However, there is some evidence that ATM activation may play a role in the response to Pot1a loss. Western blots performed on cells that have lost Pot1a(Wu et al., 2006) or stably express a TPP1-mutant that prevents Pot1a from binding to telomeres (TPP1^{ARD})(Guo et al., 2007) show activation of ATM. Those results suggest that ATM-mediated DDR may play a role in chronic loss of Pot1a.

These results from this model suggest that ATM is necessary for activation of p53 in response to Pot1a loss, as Pot1a^{intΔ} ATM^{-/-} intestines fail to activate apoptosis and p21. These results are surprising because ATM deficiency does not affect the DDR to shortened telomeres in late generation telomerase null mice(Wong et al., 2003). This may suggest that ATM response to telomere uncapping due to Pot1a deletion triggers a different ATM response than critically short telomeres.

A small subset of aging Pot1a^{intΔ} ATM^{+/-} produce tumors in the gastrointestinal tract, suggesting that abrogation of the ATM DNA damage checkpoint may also be a good model for telomere driven intestinal tumorigenesis. If this model is to be pursued further, I would recommend using a conditional ATM knockout allele to restrict ATM deletion to the

intestinal. This would bypass the early death caused by thymic lymphoma to allow the $Pot1a^{int\Delta} ATM^{-/-}$ GI phenotype time to manifest, possibly shortening tumor latency.

Finally, future work may combine $Pot1a$ deletion with both p53 and ATM deficiency. Loss of both barriers to genomic stability may provide a model with shorter tumor latency and more chromosomal changes. Previous experiments have combined p53 and ATM deficiency with the telomerase knockout mouse to generate a model of lymphoma with unstable genomes (Maser et al., 2007). Work from this model has suggested that genetic changes seen in tumors with unstable genomes driven by telomere dysfunction, p53 and ATM deficiency, are similar to those seen in a variety of human tumors (Maser et al., 2007). These results suggest that genetic information found in tumors from these mouse models can be used as a filter for deciphering important genetic changes in human tumors. Perhaps future work with our $Pot1a$ conditional model can yield such information to facilitate new gene discoveries based on telomere dysfunction in gastrointestinal tumors or other organ systems.

CONCLUSIONS AND FUTURE DIRECTIONS

The results of this manuscript describe the generation of a novel mouse model of intestinal tumorigenesis that is driven by telomere dysfunction. Taking advantage of the similar effects of telomere uncapping due to loss of the Pot1a telomere binding protein, we first created a mouse model of telomere dysfunction in the gastrointestinal tract that does not require multiple rounds of intergenerational matings necessary in the telomerase knockout models. First, we created a novel mouse model of telomere dysfunction in the gastrointestinal tract through the targeted deletion of the telomere binding protein, Pot1a. While our model does not show the overall morphological features of critical telomere shortening, such as blunting or atrophy of villi (Rudolph et al., 1999), the VCre, Pot1a mice developed various microscopic changes in the intestinal epithelium that are similar to late generation telomerase null animals with critically short telomeres (Choudhury et al., 2007; Rudolph et al., 1999). Pot1a deletion led to increased apoptotic cells in the crypts, as well as upregulation of p53 and p21 expression. Finally, Pot1a deletion leads to increased cells with TIFs, an indicator of activation of the DDR in response to dysfunctional telomeres. These data correspond to previous work in cell culture, which has shown that deletion of Pot1a leads to a DNA damage response, which activates p53 to trigger cell cycle arrest through p21 or apoptosis (Wu et al., 2006), supporting the conclusion that *in vivo* consequences of Pot1a deficiency is similar to those seen *in vitro*.

Our second mouse model featuring combined Pot1a and p53 deficiency proved to be permissive to cancer formation as aging Pot1a^{intΔ} p53^{F/F} mice developed tumors throughout gastrointestinal tract, including the small intestine, cecum and colon. These tumors were

well-differentiated but showed frequent invasion into the submucosa, with some extending as deep as the muscle wall. These tumors resemble the GI tumors found in a small subset of late generation telomerase null mice with p53 haploinsufficiency (Artandi et al., 2000). Similar to that model, our mice developed tumors with low multiplicity and a latency of 15 months. However, G5-G7 mTerc^{-/-} p53^{+/-} mice often succumb to other tumor types, such as lymphomas, breast and squamous cell, and a variety of sarcomas (Artandi et al., 2000). Additionally, it requires five to seven rounds of intergenerational breeding to develop severely shortened telomeres. Our model is superior for studying telomere dysfunction in the GI tract because our phenotypes are limited to the intestines and we do not require intergenerational breeding to induce telomere dysfunction.

It is interesting to note that another group also tried to create a mouse model of telomere dysfunction in the setting of p53 deficiency in the intestine. This model paired conditional deletion of p53 in the intestines with late generation telomerase null mice (Begus-Nahrman et al., 2009). While they also concluded that p53 deficiency impairs the clearance of chromosomally unstable cells from intestines with severe telomere erosion, their model did not develop tumors. They postulated that although their model allowed them to bypass p53-dependent checkpoints, a second p53-independent checkpoint called crisis prevented tumor formation in their mice as progressive accumulation of cells with dysfunctional telomeres lead to increased apoptosis (Begus-Nahrman et al., 2009). The crisis checkpoint is thought to be bypassed in human cancers with the reactivation of telomerase (Maser and DePinho, 2002), a step that cannot occur in the telomerase null mice. Our model leaves telomerase activity intact, and may allow for bypass of crisis and possible progression to metastasis.

Our final mouse model paired loss of Pot1a with ATM deficiency. In response to telomere dysfunction, ATM activation is typically associated with severe telomere erosion or loss of the TRF2 protein(Karlseder et al., 1999), both of which are thought to resemble double strand breaks. However, there is some evidence that ATM activation may play a role in the response to Pot1a loss. Cell culture experiments with cells deficient in Pot1a(Wu et al., 2006) or cells with mutant TPP1(Guo et al., 2007) can lead to ATM activation, suggesting that ATM-mediated DDR may play a role in chronic loss of Pot1a. The phenotypes seen in our VCre, Pot1a, ATM mouse models support this theory and further suggest that ATM is necessary for activation of p53 in response to telomere uncapping, as Pot1a^{intΔ} ATM^{-/-} intestines fail to activate apoptosis and p21. These results are surprising because ATM deficiency does not affect the DDR to shortened telomeres in late generation telomerase null mice(Wong et al., 2003). This may suggest that ATM response to telomere uncapping due to Pot1a deletion triggers a different ATM response than critically short telomeres. Furthermore, a small subset of aging Pot1a^{intΔ} ATM^{+/-} produce tumors in the gastrointestinal tract, suggesting that abrogation of the ATM DNA damage checkpoint may also be a good model for telomere driven intestinal tumorigenesis.

The phenotypes seen in the p53 and ATM colonies suggest that a combination of Pot1a loss with both p53 and ATM deficiency may possibly result in a model with even more pronounced phenotypes. Loss of both barriers to genomic stability may provide a model with shorter tumor latency and more chromosomal changes. Previous experiments have combined p53 and ATM deficiency with the telomerase knockout mouse to generate a model of lymphoma with unstable genomes (Maser et al., 2007). Work from this model has suggested that genetic changes seen in tumors with unstable genomes driven by telomere dysfunction,

p53 and ATM deficiency, are similar to those seen in a variety of human tumors(Maser et al., 2007). These results suggest that genetic information found in tumors from these mouse models can be used as a filter for deciphering important genetic changes in human tumors. Perhaps future work with our Pot1a conditional model can yield such information to facilitate new gene discoveries based on telomere dysfunction in gastrointestinal tumors or other organ systems.

Genomic profiling of the VCre, Pot1a, p53 tumors revealed frequent copy number variation and heterogeneous profiles, which is similar to tumors harvested from telomerase null p53 heterozygous mice(O'Hagan et al., 2002), suggesting that telomere dysfunction was indeed driving genomic instability. Genetic diversity and the wide variation of tumor genomes is one of the barriers to development of effective treatments for solid tumors, such as colorectal cancer. It is the reason why one patient treated with a particular drug can go into remission, while that same therapy will have no effect on another patient's tumor. Future work with this model may also elucidate new gene mutations and genetic pathways to target with therapeutics.

One major limitation of this model was the inability to monitor tumor formation. However, there are new techniques for *in vivo* imaging of mouse models that are currently being developed and used at other institutions. For instance, it is now possible to perform endoscopic imaging of mouse intestines using fiber optic technologies (Becker et al., 2005). If these techniques can be applied to our model, one could imagine even more questions that these mice can be use to answer. For instance, if endoscopic techniques for the mouse GI tract can be modified to take biopsies early and late during tumor develop, we could compare the genetic make-up or protein expression to look for targets involved in cancer progression.

This technique could also open up the possibility of using this mouse model for testing therapeutics. It would allow for monitoring of tumors for treatment effect as growth or regression could be monitored while sparing the animal from early euthanasia. Also, profiling pre-treatment biopsies may allow us to determine which genomic changes make a tumor more susceptible or more resistant to a particular type of treatment. For these applications, the variable genetic profiles of tumors from one animal to another more closely recapitulate the diversity of human tumors, making it a unique model for studying these phenomena.

Advances in cancer genomics are fueling the push towards personalized medicine, the idea that treatment regimens can be individualized to each person's tumor according to its genetic make-up. The unique nature of this mouse model of sporadic colon cancer driven by telomere dysfunction may provide a valuable tool for preclinical trials of therapeutics based on this concept.

MATERIALS AND METHODS

DNA extraction from tissue

Tissue was harvested from animals at autopsy and rinsed immediately with ice cold phosphate buffered saline (PBS). Intestinal samples were obtained by scraping epithelial cells with a scalpel. Tissue was digested using 450µl Cell Lysis Solution (Qiagen) and 10µl Proteinase K (20mg/ml) at 55°C overnight. Samples were then treated with RNase A for 30 min – 1 hour at 37°C. After addition of Protein Precipitation Solution (Qiagen), samples were spun for 30 minutes at 13,000 rpm. The DNA was precipitated from the supernatant with isopropanol and spun down. After washing with 70% ethanol, DNA pellets were air dried and the resuspended in 1X TE. Purity of samples was determined through Nanodrop and 1% agarose gels. If further purification was necessary, the samples were mixed with an equal volume of phenol-chloroform and spun down. The top aqueous layer was transferred to a new tube and the process was repeated. Then the top layer was transferred to a new tube, mixed with an equal volume of chloroform and spun down. DNA was precipitated with the top aqueous layer with 1/10 volume of 3M NaOAc, 3 times volume of 100% ethanol and incubated at -20°C for 2 hours. After spinning down, the pellet was air dried and then resuspended in 1xTE.

Genotyping of animals and tissue

Genotyping of animals was accomplished through PCR of tail or tissue DNA using primers and protocols previously described for each mouse line (Table 9).

Paraffin-embedding and H&E staining of tissue

Tissues harvest from animals at autopsy was rinsed with ice cold PBS immediately. Non-intestinal tissues were placed into cassettes and fixed in 10% formalin (Fisher) at room temperature for 24-48hrs. Cassettes were then transferred to 70% ethanol for storage before further processing. Intestines were dissected from the animal and washed in ice-cold PBS. They were further cleaning by flushing the lumen with ice cold PBS using a 10ml syringe and an 18g-feeding needle. The tissue was then fixed in 10% formalin for 24-48hrs at room temperature. The intestines were then cut open longitudinally and rolled with forceps. The Swiss rolls were pinned with a 26-gauge needle and stored in 1xPBS for 24-48hrs. The intestinal rolls were then sliced in half, placed in cassettes, and stored in 70% ethanol until further processing. The samples were then submitted to the MD Anderson Histology CORE, where the tissue were embedded in paraffin and cut into 5 micron section. Hematoxylin and eosin (H&E) staining was also performed at the Histology CORE according to standard protocols.

TUNEL assay

TUNEL assay was performed on paraffin embedded tissue using the Apoptag Kit (Millipore) according to the instructions. Briefly, paraffin-embedded tissue sections were run through a xylene to alcohol gradient and rinsed with 1x PBS. The sections were pretreated with a Proteinase K solution (20 μ g/ml) for 15 minutes at room temperature. After washing with ddH₂O, the slides were then quenched with 3% H₂O₂ for 5 minutes at room temperature. Slides were rinsed with 1xPBS and then incubated briefly with Equilibration buffer. The slides were treated with TdT enzyme for one hour at 37°C. The reaction was stopped

STOP/wash buffer for 10 minutes at room temperature. Anti-digoxigenin solution was applied for 30 minutes at room temperature, followed by washes with 1x PBS. The DAB solution (Vector) was prepared with 2 drops, buffer, 4 drops reagent, 2 drops H₂O₂, and 2 drops nickel in 5ml H₂O, and applied to the specimen for 3-6 minutes. The slides were washed with water before counterstaining with Nuclear Fast Red (H-3403, Vector) for 45 seconds to 1 minute, followed by more washing. The sections were through a reverse alcohol to xylene gradient and a glass coverslip was mounted with Permount. Analysis of TUNEL slides were performed on the Nikon 80i Upright Microscope using the NIS-Elements AR 3.1 software.

Immunohistochemical (IHC) staining

IHC staining on paraffin embedded tissue sections was performed at the Histology and Tissue Processing Facility Core at MDACC Science Park – Research Division in Smithville, Texas. Tissue sections were stained for p53 and p21 according to their standardized protocols. Slides were analyzed through brightfield microscopy on a Nikon 80i Upright Microscope and pictures were taken using NIS-Elements AR 3.1 software.

Immunofluorescence (IF) staining

Sections of paraffin embedded tissue were run through a xylene to alcohol gradient and rinsed with ddH₂O. Epitope retrieval was performed with Antigen Unmasking Solution (Vector) diluted 1:100 in ddH₂O, steamed for 45 minutes, and cooled for 25 minutes. Slides were rinsed with ddH₂O and then 1xPBS. Slides were blocked with 10% goat serum/PBS for 30 minutes to 1 hour at room temperature. Sections were incubated with primary antibodies

diluted in 10% goat serum/PBS at 4°C overnight. For double staining, both primaries were added at the same time. The primary antibodies were diluted in the following manner: mouse monoclonal γ -H2AX (Millipore #05-636; 1:200), rabbit polyclonal γ -H2AX (Millipore #07-164; 1:200), mTRF2 (1:200), BrdU (BD #347580; 1:100), beta-catenin (BD #610153; 1:100), Cox-2 (Cayman #160162; 1:100). After washing with PBS, Alexa-conjugated fluorochromes (see below) were diluted 1:200 in 10% goat serum/PBS and incubated at room temperature for 1 hour. Slides were rinsed with PBS, and then samples for fluorescent microscope analysis were mounted with Vector Shield mounting media with DAPI. Samples for confocal analysis were counterstained with TO-PRO-3 (Invitrogen #T3605), diluted 1:1000 at room temperature for 20 minutes. After another rinse with PBS, the coverslip was mounted on with Slowfade Gold (Invitrogen #S36936). Fluorescence microscopy was performed on a Nikon Eclipse 80i microscope using MetaMorph software. Confocal imaging was performed on a Zeiss LSM 510 Confocal microscope.

Secondary antibodies used included: Alexa Fluor 568 goat anti-rabbit (Molecular Probes #A11011), Alexa Fluor 568 goat anti-mouse (Molecular Probes #11004), Alexa Fluor 488 goat anti-rabbit (Molecular Probes #A11070) and Alexa Fluor 488 goat anti-mouse (Molecular Probes #A11001).

β -galactosidase activity assay

Tissues were dissected from animals at the time of autopsy, washed with ice cold PBS, and fixed in 4% paraformaldehyde on ice for 20 minutes. Tissues were then embedded in OCT and flash frozen. 10 micron frozen tissue sections were cut in a cryostat and immediately fixed with 0.2% glutaraldehyde for 2 minutes and then immersed in X-gal staining solution

(1mg/ml X-gal, 5mM potassium ferricyanide, 5mM potassium ferrocyanide, 0.2% NP-40, 0.1% sodium deoxycholate, 2mM MgCl₂) overnight at 37°C. Slides were then washed in PBS before going through an alcohol to xylene gradient. Coverslip was mounted with Permount. Slides were analyzed through brightfield microscopy on a Nikon 80i Upright Microscope and pictures were taken using NIS-Elements AR 3.1 software.

RT-PCR

Tissue was harvested from animals at autopsy and flash frozen. RNA isolation was accomplished using Trizol as outlined by the product guide. Briefly, tissue was homogenized in 1ml Trizol and then incubated at room temperature for 5 min. 200µL of chloroform was added and the sample was incubated for an additional 3 minutes at room temperature. Centrifuge at 13,000 rpm for 15min at 4°C. The top aqueous layer was transferred to a new tube. 500µl of isopropanol was added and the sample was then incubated at room temperature for 5 min. Centrifuge 13,000 rpm for 10min at 4°C. Discard supernatant and wash with 70% ethanol. Spin down and air dry the pellet. Resuspend in RNase/DNase free water.

RT-PCR was performed directly with RNA using the Taqman One Step RT-PCR Mastermix (Applied Biosystems/Roche). Pot1a was assayed using Taqman Custom Gene Expression Assay probes for exon 4. Results were normalized to GAPDH expression, which was determined with Taqman murine GAPDH primers. All samples were run in triplicate.

Chemical induction of colon tumors (AOM-DSS model)

10-15 week old VCre, Pot1a animals from each cohort were treated with a single injection of AOM (10mg/kg body weight). Immediately after the injection, the mice were fed a one week course of 3% DSS water, followed by two weeks of regular water. This was repeated two more times for a total of three cycles. Tumor evaluation was performed at 10 weeks or 15 weeks after the AOM injection.

Irradiation experiments

Mice were dosed in the Mark I25 irradiator which has a ^{137}Cs line source. The mice were first placed in a plastic CD contained with ventilation holes punched in. The time of exposure was calculated by the following equation:

$$\text{Time} = \frac{\text{desired dose (cGy)}}{0.98 \times 315 \text{ cGy} \cdot \text{min}^{-1}} - 0.005 \text{ min}$$

Array comparative genomic hybridization (aCGH)

Array CGH was performed by the MD Anderson Genomics CORE on a Nimblegen 385K Whole genome tiling array (Roche). DNA was extracted from tumors as described above. Control DNA was pooled from the kidneys of five wild-type female mice. Raw data was processed with Imagene by the Core. Analysis was performed using the Nexus 5 software with the following settings: High gain = 0.5, gain = 0.1, loss = 0.1, big loss = -0.5.

Table 9: Genotyping primers and conditions

Genotype	Primer sequence	Conditions
Pot1a (WT/ floxed)	EcoRI-21196: 5'- CTC GAA TTC CAT CTC CTC CCA GTA CTC TCT CAG Confirm_20560: 5'- GGA ACT GGT ACG TAT CAG TGT GTG TGG	94°C 0:30 60°C 0:30 72°C 1:00 x 30 cycles
Pot1a (delta)	EcoRI_21196: 5'- CTC GAA TTC CAT CTC CTC CCA GTA CTC TCT CAG Delta: 5'- ACA CGG ATC CTG AGC CAT AAA CAT GCC ACA CAA AGG	94°C 0:30 60°C 0:30 72°C 1:00 x 30 cycles
P53 (WT/ floxed)	p53loxFWB 5'- AAG GGG TAT GAG GGA CAA GG p53loxRVB 5'- GAA GAC AGA AAA GGG GAG GG	94°C 1:00 60°C 1:00 72°C 1:00 x 35 cycles
P53 (delta)	p53-1F: 5'- CAC AAA AAC AGG TTA AAC CCA G p53loxRVB 5'- GAA GAC AGA AAA GGG GAG GG	94°C 1:00 60°C 1:00 72°C 1:00 x 35 cycles
P53 (KO)	P53X7: 5'- TAT ACT CAG AGC CGG CCT P53X6-5: 5'- ACA GCG TGG TGG TAC CTT AT neoP53: 5'- TCC TCG TGC TTT ACG GTA TC	94°C 1:00 62°C 1:00 72°C 1:00 x 30 cycles
ATM	CZ514: 5'- GTA GTA ACT ATT AGT TTC GTG CA CZ513: 5'- TAG GGT GTA CTA GTG GAG GA CZ054: 5'- GCT GGA CGT AAA CTC CTC TTC AGA C	94°C 0:40 55°C 0:40 72°C 0:45 x 30 cycles
Villin-Cre	MVP+5498: 5'- ACA GGC ACT AAG GGA GCC AATG MVP+6378: 5'- GAT TCA GGT CAG AAA GAG GTC ACA G CreORF: 5'- CAT GTC CAT CAG GTT CTT GCG	94°C 1:00 59°C 1:00 72°C 1:30 x 35 cycles
APC ^{min}	IMR0033: 5'- GCC ATC CCT TCA CGT TAG IMR0034: 5'- TTC CAC TTT GGC ATA AGG C IMR0758: 5'- TTC TGA GAA AGA CAG AAG TTA	94°C 0:30 55°C 1:00 72°C 1:30 x 35 cycles
Rosa26-LacZ (R26R)	IMR0315: 5'- GCG AAG AGT TTG TCC TCA ACC IMR0316: 5'- GGA GCG GGA GAA ATG GAT ATG IMR0883: 5'- AAA GTC GCT CTG AGT TGT TAT	94°C 0:30 65°C 0:45 72°C 1:00 x 35 cycles
ATR	GATR-I#5: 5'-TAC ATT TTA GTC ATA GTT GCA TAA CAC GATR-I#15: 5'- CTT CTA ATC TTC CTC CAG AAT TGT AAA AGG	Ramp 1.5°C/s to 94°C 94°C 1:00 Ramp 1.5°C/s to 62°C 62°C 2:30 Ramp 1.5°C/s to 72°C 72°C 2:30 x 35 cycles

BIBLIOGRAPHY

ACS (2010). Colorectal Cancer: Facts & Figure 2008-2010. In.

Artandi, S. E., Chang, S., Lee, S. L., Alson, S., Gottlieb, G. J., Chin, L., and DePinho, R. A. (2000). Telomere dysfunction promotes non-reciprocal translocations and epithelial cancers in mice. *Nature* 406, 641-645.

Artandi, S. E., and DePinho, R. A. Telomeres and telomerase in cancer. *Carcinogenesis* 31, 9-18.

Bae, N. S., and Baumann, P. (2007). A RAP1/TRF2 complex inhibits nonhomologous end-joining at human telomeric DNA ends. *Mol Cell* 26, 323-334.

Bailey, S. M., and Murnane, J. P. (2006). Telomeres, chromosome instability and cancer. *Nucleic Acids Res* 34, 2408-2417.

Baumann, P., and Cech, T. R. (2001). Pot1, the putative telomere end-binding protein in fission yeast and humans. *Science* 292, 1171-1175.

Becker, C., Fantini, M. C., Wirtz, S., Nikolaev, A., Kiesslich, R., Lehr, H. A., Galle, P. R., and Neurath, M. F. (2005). In vivo imaging of colitis and colon cancer development in mice using high resolution chromoendoscopy. *Gut* 54, 950-954.

Begus-Nahrman, Y., Lechel, A., Obenaus, A. C., Nalapareddy, K., Peit, E., Hoffmann, E., Schlaudraff, F., Liss, B., Schirmacher, P., Kestler, H., *et al.* (2009). p53 deletion impairs clearance of chromosomal-unstable stem cells in aging telomere-dysfunctional mice. *Nat Genet* 41, 1138-1143.

Blasco, M. A. (2007). Telomere length, stem cells and aging. *Nat Chem Biol* 3, 640-649.

Borghesani, P. R., Alt, F. W., Bottaro, A., Davidson, L., Aksoy, S., Rathbun, G. A., Roberts, T. M., Swat, W., Segal, R. A., and Gu, Y. (2000). Abnormal development of Purkinje cells and lymphocytes in *Atm* mutant mice. *Proc Natl Acad Sci U S A* 97, 3336-3341.

Broccoli, D., Smogorzewska, A., Chong, L., and de Lange, T. (1997). Human telomeres contain two distinct Myb-related proteins, TRF1 and TRF2. *Nat Genet* 17, 231-235.

Brown, E. J., and Baltimore, D. (2000). ATR disruption leads to chromosomal fragmentation and early embryonic lethality. *Genes Dev* 14, 397-402.

Brown, E. J., and Baltimore, D. (2003). Essential and dispensable roles of ATR in cell cycle arrest and genome maintenance. *Genes Dev* 17, 615-628.

Chen, Y., Yang, Y., van Overbeek, M., Donigian, J. R., Baciú, P., de Lange, T., and Lei, M. (2008). A shared docking motif in TRF1 and TRF2 used for differential recruitment of telomeric proteins. *Science* 319, 1092-1096.

Chin, L., Artandi, S. E., Shen, Q., Tam, A., Lee, S. L., Gottlieb, G. J., Greider, C. W., and DePinho, R. A. (1999). p53 deficiency rescues the adverse effects of telomere loss and cooperates with telomere dysfunction to accelerate carcinogenesis. *Cell* 97, 527-538.

Choudhury, A. R., Ju, Z., Djojotubroto, M. W., Schienke, A., Lechel, A., Schaetzlein, S., Jiang, H., Stepczynska, A., Wang, C., Buer, J., *et al.* (2007). *Cdkn1a* deletion improves stem cell function and lifespan of mice with dysfunctional telomeres without accelerating cancer formation. *Nat Genet* 39, 99-105.

Churikov, D., and Price, C. M. (2008). Pot1 and cell cycle progression cooperate in telomere length regulation. *Nat Struct Mol Biol* 15, 79-84.

Cosme-Blanco, W., Shen, M. F., Lazar, A. J., Pathak, S., Lozano, G., Multani, A. S., and Chang, S. (2007). Telomere dysfunction suppresses spontaneous tumorigenesis in vivo by initiating p53-dependent cellular senescence. *EMBO Rep* 8, 497-503.

d'Adda di Fagagna, F., Reaper, P. M., Clay-Farrace, L., Fiegler, H., Carr, P., Von Zglinicki, T., Saretzki, G., Carter, N. P., and Jackson, S. P. (2003). A DNA damage checkpoint response in telomere-initiated senescence. *Nature* 426, 194-198.

de Lange, T. (2005). Shelterin: the protein complex that shapes and safeguards human telomeres. *Genes Dev* 19, 2100-2110.

de Lange, T. (2009). How telomeres solve the end-protection problem. *Science* 326, 948-952.

Denchi, E. L., and de Lange, T. (2007). Protection of telomeres through independent control of ATM and ATR by TRF2 and POT1. *Nature* 448, 1068-1071.

Deng, Y., Chan, S. S., and Chang, S. (2008). Telomere dysfunction and tumour suppression: the senescence connection. *Nat Rev Cancer* 8, 450-458.

Deng, Y., Guo, X., Ferguson, D. O., and Chang, S. (2009). Multiple roles for MRE11 at uncapped telomeres. *Nature* 460, 914-918.

DePinho, R. A. (2000). The age of cancer. *Nature* 408, 248-254.

DePinho, R. A., and Polyak, K. (2004). Cancer chromosomes in crisis. *Nat Genet* 36, 932-934.

Dimitrova, N., and de Lange, T. (2009). Cell cycle-dependent role of MRN at dysfunctional telomeres: ATM signaling-dependent induction of nonhomologous end joining (NHEJ) in G1 and resection-mediated inhibition of NHEJ in G2. *Mol Cell Biol* 29, 5552-5563.

Farazi, P. A., Glickman, J., Jiang, S., Yu, A., Rudolph, K. L., and DePinho, R. A. (2003). Differential impact of telomere dysfunction on initiation and progression of hepatocellular carcinoma. *Cancer Res* 63, 5021-5027.

Fearon, E. R., and Vogelstein, B. (1990). A genetic model for colorectal tumorigenesis. *Cell* 61, 759-767.

Feldser, D. M., and Greider, C. W. (2007). Short telomeres limit tumor progression in vivo by inducing senescence. *Cancer Cell* 11, 461-469.

Gire, V., Roux, P., Wynford-Thomas, D., Brondello, J. M., and Dulic, V. (2004). DNA damage checkpoint kinase Chk2 triggers replicative senescence. *Embo J* 23, 2554-2563.

Gonzalez-Suarez, E., Samper, E., Flores, J. M., and Blasco, M. A. (2000). Telomerase-deficient mice with short telomeres are resistant to skin tumorigenesis. *Nat Genet* 26, 114-117.

Goss, K. H., and Groden, J. (2000). Biology of the adenomatous polyposis coli tumor suppressor. *J Clin Oncol* 18, 1967-1979.

Greenberg, R. A., Chin, L., Femino, A., Lee, K. H., Gottlieb, G. J., Singer, R. H., Greider, C. W., and DePinho, R. A. (1999). Short dysfunctional telomeres impair tumorigenesis in the INK4a(Δ 2/3) cancer-prone mouse. *Cell* 97, 515-525.

Grier, J. D., Xiong, S., Elizondo-Fraire, A. C., Parant, J. M., and Lozano, G. (2006). Tissue-specific differences of p53 inhibition by Mdm2 and Mdm4. *Mol Cell Biol* 26, 192-198.

Griffith, J. D., Comeau, L., Rosenfield, S., Stansel, R. M., Bianchi, A., Moss, H., and de Lange, T. (1999). Mammalian telomeres end in a large duplex loop. *Cell* 97, 503-514.

Guo, X., Deng, Y., Lin, Y., Cosme-Blanco, W., Chan, S., He, H., Yuan, G., Brown, E. J., and Chang, S. (2007). Dysfunctional telomeres activate an ATM-ATR-dependent DNA damage response to suppress tumorigenesis. *Embo J* 26, 4709-4719.

Hara, E., Tsurui, H., Shinozaki, A., Nakada, S., and Oda, K. (1991). Cooperative effect of antisense-Rb and antisense-p53 oligomers on the extension of life span in human diploid fibroblasts, TIG-1. *Biochem Biophys Res Commun* 179, 528-534.

Hardy, C. F., Sussel, L., and Shore, D. (1992). A RAP1-interacting protein involved in transcriptional silencing and telomere length regulation. *Genes Dev* 6, 801-814.

Harrington, L., and Robinson, M. O. (2002). Telomere dysfunction: multiple paths to the same end. *Oncogene* 21, 592-597.

Hayflick, L., and Moorhead, P. S. (1961). The serial cultivation of human diploid cell strains. *Exp Cell Res* 25, 585-621.

He, H., Multani, A. S., Cosme-Blanco, W., Tahara, H., Ma, J., Pathak, S., Deng, Y., and Chang, S. (2006). POT1b protects telomeres from end-to-end chromosomal fusions and aberrant homologous recombination. *Embo J* 25, 5180-5190.

Herbig, U., Jobling, W. A., Chen, B. P., Chen, D. J., and Sedivy, J. M. (2004). Telomere shortening triggers senescence of human cells through a pathway involving ATM, p53, and p21(CIP1), but not p16(INK4a). *Mol Cell* 14, 501-513.

Hockemeyer, D., Daniels, J. P., Takai, H., and de Lange, T. (2006). Recent expansion of the telomeric complex in rodents: Two distinct POT1 proteins protect mouse telomeres. *Cell* 126, 63-77.

Hockemeyer, D., Palm, W., Else, T., Daniels, J. P., Takai, K. K., Ye, J. Z., Keegan, C. E., de Lange, T., and Hammer, G. D. (2007). Telomere protection by mammalian Pot1 requires interaction with Tpp1. *Nat Struct Mol Biol* 14, 754-761.

Hockemeyer, D., Palm, W., Wang, R. C., Couto, S. S., and de Lange, T. (2008). Engineered telomere degradation models dyskeratosis congenita. *Genes Dev* 22, 1773-1785.

Jacobs, J. J., and de Lange, T. (2004). Significant role for p16INK4a in p53-independent telomere-directed senescence. *Curr Biol* 14, 2302-2308.

Jiang, H., Ju, Z., and Rudolph, K. L. (2007). Telomere shortening and ageing. *Z Gerontol Geriatr* 40, 314-324.

Jonkers, J., Meuwissen, R., van der Gulden, H., Peterse, H., van der Valk, M., and Berns, A. (2001). Synergistic tumor suppressor activity of BRCA2 and p53 in a conditional mouse model for breast cancer. *Nat Genet* 29, 418-425.

Kaminker, P. G., Kim, S. H., Desprez, P. Y., and Campisi, J. (2009). A novel form of the telomere-associated protein TIN2 localizes to the nuclear matrix. *Cell Cycle* 8, 931-939.

Karlseder, J., Broccoli, D., Dai, Y., Hardy, S., and de Lange, T. (1999). p53- and ATM-dependent apoptosis induced by telomeres lacking TRF2. *Science* 283, 1321-1325.

Karlseder, J., Hoke, K., Mirzoeva, O. K., Bakkenist, C., Kastan, M. B., Petrini, J. H., and de Lange, T. (2004). The telomeric protein TRF2 binds the ATM kinase and can inhibit the ATM-dependent DNA damage response. *PLoS Biol* 2, E240.

Karlseder, J., Kachatrian, L., Takai, H., Mercer, K., Hingorani, S., Jacks, T., and de Lange, T. (2003). Targeted deletion reveals an essential function for the telomere length regulator Trf1. *Mol Cell Biol* 23, 6533-6541.

Khoo, C. M., Carrasco, D. R., Bosenberg, M. W., Paik, J. H., and Depinho, R. A. (2007). Ink4a/Arf tumor suppressor does not modulate the degenerative conditions or tumor spectrum of the telomerase-deficient mouse. *Proc Natl Acad Sci U S A* 104, 3931-3936.

Kibe, T., Osawa, G. A., Keegan, C. E., and de Lange, T. Telomere protection by TPP1 is mediated by POT1a and POT1b. *Mol Cell Biol* 30, 1059-1066.

Kim, W. Y., and Sharpless, N. E. (2006). The regulation of INK4/ARF in cancer and aging. *Cell* 127, 265-275.

Lee, H. W., Blasco, M. A., Gottlieb, G. J., Horner, J. W., 2nd, Greider, C. W., and DePinho, R. A. (1998). Essential role of mouse telomerase in highly proliferative organs. *Nature* 392, 569-574.

Lengauer, C., Kinzler, K. W., and Vogelstein, B. (1997). Genetic instability in colorectal cancers. *Nature* 386, 623-627.

Li, B., and de Lange, T. (2003). Rap1 affects the length and heterogeneity of human telomeres. *Mol Biol Cell* 14, 5060-5068.

Li, B., Oestreich, S., and de Lange, T. (2000). Identification of human Rap1: implications for telomere evolution. *Cell* 101, 471-483.

Loayza, D., and De Lange, T. (2003). POT1 as a terminal transducer of TRF1 telomere length control. *Nature* 423, 1013-1018.

Madison, B. B., Dunbar, L., Qiao, X. T., Braunstein, K., Braunstein, E., and Gumucio, D. L. (2002). Cis elements of the villin gene control expression in restricted domains of the vertical (crypt) and horizontal (duodenum, cecum) axes of the intestine. *J Biol Chem* 277, 33275-33283.

Markowitz, S. D., and Bertagnolli, M. M. (2009). Molecular origins of cancer: Molecular basis of colorectal cancer. *N Engl J Med* 361, 2449-2460.

Martinez, P., Thanasoula, M., Munoz, P., Liao, C., Tejera, A., McNees, C., Flores, J. M., Fernandez-Capetillo, O., Tarsounas, M., and Blasco, M. A. (2009). Increased telomere fragility and fusions resulting from TRF1 deficiency lead to degenerative pathologies and increased cancer in mice. *Genes Dev* 23, 2060-2075.

Maser, R. S., Choudhury, B., Campbell, P. J., Feng, B., Wong, K. K., Protopopov, A., O'Neil, J., Gutierrez, A., Ivanova, E., Perna, I., *et al.* (2007). Chromosomally unstable mouse tumours have genomic alterations similar to diverse human cancers. *Nature* 447, 966-971.

Maser, R. S., and DePinho, R. A. (2002). Connecting chromosomes, crisis, and cancer. *Science* 297, 565-569.

McClintock, B. (1941). The Stability of Broken Ends of Chromosomes in *Zea Mays*. *Genetics* 26, 234-282.

Montes de Oca Luna, R., Wagner, D. S., and Lozano, G. (1995). Rescue of early embryonic lethality in mdm2-deficient mice by deletion of p53. *Nature* 378, 203-206.

Neufert, C., Becker, C., and Neurath, M. F. (2007). An inducible mouse model of colon carcinogenesis for the analysis of sporadic and inflammation-driven tumor progression. *Nat Protoc* 2, 1998-2004.

O'Connor, M. S., Safari, A., Xin, H., Liu, D., and Songyang, Z. (2006). A critical role for TPP1 and TIN2 interaction in high-order telomeric complex assembly. *Proc Natl Acad Sci U S A* 103, 11874-11879.

O'Hagan, R. C., Chang, S., Maser, R. S., Mohan, R., Artandi, S. E., Chin, L., and DePinho, R. A. (2002). Telomere dysfunction provokes regional amplification and deletion in cancer genomes. *Cancer Cell* 2, 149-155.

Palm, W., and de Lange, T. (2008). How shelterin protects mammalian telomeres. *Annu Rev Genet* 42, 301-334.

Rajagopalan, H., Nowak, M. A., Vogelstein, B., and Lengauer, C. (2003). The significance of unstable chromosomes in colorectal cancer. *Nat Rev Cancer* 3, 695-701.

Rampazzo, E., Bertorelle, R., Serra, L., Terrin, L., Candiotto, C., Pucciarelli, S., Del Bianco, P., Nitti, D., and De Rossi, A. Relationship between telomere shortening, genetic instability, and site of tumour origin in colorectal cancers. *Br J Cancer* 102, 1300-1305.

Rudolph, K. L., Chang, S., Lee, H. W., Blasco, M., Gottlieb, G. J., Greider, C., and DePinho, R. A. (1999). Longevity, stress response, and cancer in aging telomerase-deficient mice. *Cell* 96, 701-712.

Rudolph, K. L., Millard, M., Bosenberg, M. W., and DePinho, R. A. (2001). Telomere dysfunction and evolution of intestinal carcinoma in mice and humans. *Nat Genet* 28, 155-159.

Ruzankina, Y., Pinzon-Guzman, C., Asare, A., Ong, T., Pontano, L., Cotsarelis, G., Zediak, V. P., Velez, M., Bhandoola, A., and Brown, E. J. (2007). Deletion of the developmentally essential gene ATR in adult mice leads to age-related phenotypes and stem cell loss. *Cell Stem Cell* 1, 113-126.

Sarthy, J., Bae, N. S., Scrafford, J., and Baumann, P. (2009). Human RAP1 inhibits non-homologous end joining at telomeres. *Embo J* 28, 3390-3399.

Sfeir, A., Kosiyatrakul, S. T., Hockemeyer, D., MacRae, S. L., Karlseder, J., Schildkraut, C. L., and de Lange, T. (2009). Mammalian telomeres resemble fragile sites and require TRF1 for efficient replication. *Cell* 138, 90-103.

Shay, J. W., Pereira-Smith, O. M., and Wright, W. E. (1991). A role for both RB and p53 in the regulation of human cellular senescence. *Exp Cell Res* 196, 33-39.

Shiloh, Y. (2003). ATM and related protein kinases: safeguarding genome integrity. *Nat Rev Cancer* 3, 155-168.

Smogorzewska, A., van Steensel, B., Bianchi, A., Oelmann, S., Schaefer, M. R., Schnapp, G., and de Lange, T. (2000). Control of human telomere length by TRF1 and TRF2. *Mol Cell Biol* 20, 1659-1668.

Soriano, P. (1999). Generalized lacZ expression with the ROSA26 Cre reporter strain. *Nat Genet* 21, 70-71.

Stansel, R. M., de Lange, T., and Griffith, J. D. (2001). T-loop assembly in vitro involves binding of TRF2 near the 3' telomeric overhang. *Embo J* 20, 5532-5540.

Suzuki, R., Kohno, H., Sugie, S., Nakagama, H., and Tanaka, T. (2006). Strain differences in the susceptibility to azoxymethane and dextran sodium sulfate-induced colon carcinogenesis in mice. *Carcinogenesis* 27, 162-169.

Takai, H., Smogorzewska, A., and de Lange, T. (2003). DNA damage foci at dysfunctional telomeres. *Curr Biol* 13, 1549-1556.

Takai, K. K., Hooper, S., Blackwood, S., Gandhi, R., and de Lange, T. In vivo stoichiometry of shelterin components. *J Biol Chem* 285, 1457-1467.

Takayama, T., Miyanishi, K., Hayashi, T., Sato, Y., and Niitsu, Y. (2006). Colorectal cancer: genetics of development and metastasis. *J Gastroenterol* 41, 185-192.

Tanaka, T., Kohno, H., Suzuki, R., Yamada, Y., Sugie, S., and Mori, H. (2003). A novel inflammation-related mouse colon carcinogenesis model induced by azoxymethane and dextran sodium sulfate. *Cancer Sci* 94, 965-973.

Valentin-Vega, Y. A., Okano, H., and Lozano, G. (2008). The intestinal epithelium compensates for p53-mediated cell death and guarantees organismal survival. *Cell Death Differ* 15, 1772-1781.

van Steensel, B., and de Lange, T. (1997). Control of telomere length by the human telomeric protein TRF1. *Nature* 385, 740-743.

van Steensel, B., Smogorzewska, A., and de Lange, T. (1998). TRF2 protects human telomeres from end-to-end fusions. *Cell* 92, 401-413.

Verdun, R. E., Crabbe, L., Haggblom, C., and Karlseder, J. (2005). Functional human telomeres are recognized as DNA damage in G2 of the cell cycle. *Mol Cell* 20, 551-561.

Verdun, R. E., and Karlseder, J. (2007). Replication and protection of telomeres. *Nature* 447, 924-931.

Wang, F., Podell, E. R., Zaug, A. J., Yang, Y., Baci, P., Cech, T. R., and Lei, M. (2007). The POT1-TPP1 telomere complex is a telomerase processivity factor. *Nature* 445, 506-510.

Wong, K. K., Chang, S., Weiler, S. R., Ganesan, S., Chaudhuri, J., Zhu, C., Artandi, S. E., Rudolph, K. L., Gottlieb, G. J., Chin, L., *et al.* (2000). Telomere dysfunction impairs DNA repair and enhances sensitivity to ionizing radiation. *Nat Genet* 26, 85-88.

Wong, K. K., Maser, R. S., Bachoo, R. M., Menon, J., Carrasco, D. R., Gu, Y., Alt, F. W., and DePinho, R. A. (2003). Telomere dysfunction and Atm deficiency compromises organ homeostasis and accelerates ageing. *Nature* *421*, 643-648.

Wu, L., Multani, A. S., He, H., Cosme-Blanco, W., Deng, Y., Deng, J. M., Bachilo, O., Pathak, S., Tahara, H., Bailey, S. M., *et al.* (2006). Pot1 deficiency initiates DNA damage checkpoint activation and aberrant homologous recombination at telomeres. *Cell* *126*, 49-62.

Xin, H., Liu, D., Wan, M., Safari, A., Kim, H., Sun, W., O'Connor, M. S., and Songyang, Z. (2007). TPP1 is a homologue of ciliate TEBP-beta and interacts with POT1 to recruit telomerase. *Nature* *445*, 559-562.

Xiong, S., Van Pelt, C. S., Elizondo-Fraire, A. C., Liu, G., and Lozano, G. (2006). Synergistic roles of Mdm2 and Mdm4 for p53 inhibition in central nervous system development. *Proc Natl Acad Sci U S A* *103*, 3226-3231.

Zou, L., and Elledge, S. J. (2003). Sensing DNA damage through ATRIP recognition of RPA-ssDNA complexes. *Science* *300*, 1542-1548.

VITA

Suzanne Sea-Wan Chan was born in Boston, Massachusetts on June 13, 1978, the Daughter of Anne K. Chan and Paul K. Chan. After completing her studies at Newton North High School, Newton, Massachusetts in 1996, she entered the School of Engineering at Tufts University in Medford, Massachusetts. She received a Bachelor of Science with a major in chemical engineering from Tufts in May of 2000. For the next three years, she worked as a research technician in the Department of Medical Oncology at the Dana Farber Cancer Center in Boston, Massachusetts. In May of 2003, she joined the M.D./Ph.D. program of the University of Texas Medical School at Houston and the University of Texas M.D. Anderson Cancer Center. After completing three years of medical coursework at the University of Texas Medical School at Houston, she entered The University of Texas Health Science Center at Houston Graduate School of Biomedical Sciences in September 2006.